



BERGISCHE
UNIVERSITÄT
WUPPERTAL

Investigation of Gaseous and Particulate Vehicle Emissions in Real-World Driving Conditions

Der Fakultät für Mathematik und Naturwissenschaften
der Bergischen Universität Wuppertal eingereichte

Dissertation

zur Erlangung des Doktorgrades der Naturwissenschaften

vorgelegt von

Dipl.-Phys. Jens Achim Gallus

im März 2017

Die Dissertation kann wie folgt zitiert werden:

urn:nbn:de:hbz:468-20171220-093940-7

[<http://nbn-resolving.de/urn/resolver.pl?urn=urn%3Anbn%3Ade%3Ahbz%3A468-20171220-093940-7>]

Die vorliegende Arbeit entstand am Ford Research and Innovation Center Aachen in Zusammenarbeit mit der Fakultät für Mathematik und Naturwissenschaften, Theoretische und Physikalische Chemie, der Bergischen Universität Wuppertal.

Referent: Prof. Dr. Thorsten Benter, Bergische Universität Wuppertal
Korreferent: PD Dr. Rainer Vogt, Ford Werke GmbH

„Alles Wissen und alle Vermehrung unseres Wissens endet nicht
mit einem Schlusspunkt, sondern mit Fragezeichen.“
- Hermann Hesse -

Danksagung

Nach vielen Jahren intensiver Arbeit ist meine Dissertation nun vollendet. Damit ist es an der Zeit, mich bei denjenigen zu bedanken, die mich in dieser herausfordernden, aber auch ungemein interessanten und lehrreichen Phase meiner Laufbahn begleitet haben.

Ich danke meinem Doktorvater Herrn Prof. Dr. Thorsten Benter, dass er mir diese Arbeit ermöglicht hat. Durch seine freundliche und unkomplizierte Art verlief die gesamte Betreuung seitens der Bergischen Universität Wuppertal reibungslos und zielführend.

Mein größter Dank gilt PD Dr. Rainer Vogt, der mir das nötige Vertrauen für die Überlassung dieser Arbeit entgegenbrachte. Durch seine qualifizierte Betreuung unterstützte er mich während der gesamten Entstehungsphase und trug einen großen Teil zum Gelingen dieser Arbeit bei.

Außerdem danke ich Dr. Ulf Kirchner für die vielen wertvollen Ratschläge und Diskussionen, für die Unterstützung bei der Durchführung der Versuche und für die kritischen Hinweise bei der Erstellung der Dissertation.

Für die freundliche Aufnahme in die Arbeitsgruppe und die freundschaftliche Zusammenarbeit danke ich zudem Volker Scheer, Dr. Marcel Mathissen sowie Ferdinand Farwick zum Hagen.

Im Verlauf meiner Doktorarbeit habe ich mit vielen Mitarbeitern des Ford Forschungszentrums ein freundschaftliches Verhältnis aufgebaut. Die daraus resultierende vertraute Arbeitsatmosphäre hat mich während meiner Arbeit stets motiviert und angetrieben. Im Speziellen seien hier Christoph Kessler und Norbert Schuster genannt, die mich vor allem in meiner Anfangszeit tatkräftig unterstützt haben. Ein Dankeschön geht zusätzlich auch an das gesamte Werkstatt-Team.

Ich danke der Ford Motor Company für die finanzielle Unterstützung.

Für ihre geduldige und liebevolle Art danke ich vor allem meiner Freundin Maren Polzin. Sie stand stets als motivierende Kraft an meiner Seite und verstand es, mich auch in schlechten Zeiten immer wieder aufzubauen.

Ich möchte mich auch ganz besonders bei meiner gesamten Familie bedanken, die seit so langer Zeit zu mir hält und an mich glaubt. Ich widme diese Arbeit meiner Mutter, die den Abschluss dieser Arbeit leider nicht mehr miterleben durfte. Ohne die wegweisende Unterstützung, die ich durch sie und meinen Vater erfahren habe, wäre dies alles nicht möglich gewesen. Meine Eltern und auch meine Schwester haben den Grundstein für meinen Werdegang und diese Arbeit gelegt.

List of Acronyms

CAG	Cumulated Altitude Gain
CLA	Chemiluminescence Analyzer
CO	Carbon monoxide
CO₂	Carbon dioxide
CoV	Coefficient of Variance
CPC	Condensation Particle Counter
CSEE	Cold Start Excess Emissions
CVS	Constant Volume Sampler
DC	Diffusion Charger
DPF	Diesel Particulate Filter
DI	Direct Injection
ECU	Engine Control Unit
EEA	European Environment Agency
EFM	Exhaust Flow Meter
EPA	Environment Protection Agency
ET	Evaporation Tube
EU	European Union
EUDC	Extra Urban Driving Cycle
FID	Flame Ionisation Detector
FOT	Field Operational Test
FTIR	Fourier Transform Infra-Red spectroscopy
GPS	Global Positioning System
HC	Hydrocarbons

LNT	Lean NO _x Trap
MPA	Mean Positive Acceleration
NEDC	New European Driving Cycle
NDIR	Non-Dispersive Infra-Red
NDUV	Non-Dispersive Ultra-Violet
NMHC	Non-Methane Hydrocarbons
NO	Nitrogen oxide
NO₂	Nitrogen dioxide
NO_x	Nitrogen oxides
OBD	On-Board Diagnostic
PASS	Photo Acoustic Soot Sensor
PCF	Pre-Classifier
PEMS	Portable Emission Measurement System
PM	Particulate Matter
PMP	Particle Measurement Program
PN	Particle Number
PNC	Particle Number Counter
PND	Particle Number Diluter
RDE	Real Driving Emissions
RPA	Relative Positive Acceleration
SPCS	Solid Particle Counting System
UDC	Urban Driving Cycle
UFP	Ultrafine Particles
VPR	Volatile Particle Remover
WLTC	World harmonized Light-Duty Test Cycle
WLTP	World harmonized Light-Duty Test Procedure

Abstract

In the European Union (EU), the upcoming Euro-6d regulation will include Real Driving Emissions (RDE), measured by a Portable Emission Measurement System (PEMS). The regulation will comprise the on-road measurement of Diesel NO_x and Particle Number (PN) emissions on an RDE compliant test route. Chassis dynamometer tests, such as the New European Driving Cycle (NEDC), are not able to cover the entire spectrum of driving situations that occur during on-road driving. On-road exhaust measurements depend on numerous conditions, such as ambient temperature, driving style and road grade that can hardly be accounted for in the test cell.

The present study addresses the impact of different driving conditions on on-road exhaust emissions. The focus is on the characterisation of different driving styles, the fraction of cold start emissions and the correlation with road grade along a route profile, which are all expected to have a high impact on exhaust emissions. Gaseous emission results for three Diesel vehicles (Euro-4, Euro-5 and Euro-6.1) and PN measurements with a prototype PN PEMS for two gasoline vehicles (Euro-5, Euro-6.1) are presented.

Correlation measurements of CO_2 and NO_x emissions were conducted between the PEMS and the test cell which proved the PEMS results within a deviation of 4 to 15% from the test cell. The PN PEMS showed a good agreement with an established Particle Measurement Program (PMP) set-up down to emissions of $1 \cdot 10^{10} \text{ km}^{-1}$. A PM PEMS was used in parallel for soot measurements as an independent technique. PN-to-soot ratios were determined for both test cell and on-road measurements, and appeared to be comparable at $1.3 \cdot 10^{12} \text{ mg}^{-1}$ indicating a constant performance of the PN PEMS.

Different driving styles (soft, normal, severe) were characterized by several driving parameters. Especially acceleration based driving parameters Relative Positive Acceleration (RPA), Mean Positive Acceleration (MPA) and $v \cdot a_{pos95}$ were found to show a good separation of different driving styles. Most notably, elevated

RPA and MPA could explain increases of CO₂, NO_x and PN emissions during severe driving. The comparison to reference data obtained from the World harmonized Light-duty Test Cycle (WLTC, version 5.3) and from Field Operational Tests (FOT) proved that the normal PEMS trips can be attributed to normal driving.

The cold start effect was investigated down to ambient temperatures below 0°C. A large cold start peak was observed, especially for CO, HC and PN emissions, which constituted to a large fraction of the corresponding total emissions. Several methods were applied to quantify cold start emissions during on-road driving and define Cold Start Excess Emissions (CSEE).

Based on different altitude data sources, the route characteristics of four routes were investigated applying the parameter Cumulated Altitude Gain (CAG). One route had more than 100% as much CAG, leading to almost 100% higher distance specific NO_x emissions at similar driving dynamics. A filtering and a subsequent smoothing process, as implemented in the RDE regulation draft, lowered the cumulated altitude gain values by 40 to 50%. Based on repetitive measurements, the road grades for two routes were calculated within 100m segments with an average precision of 0.29% and 0.12%. CO₂ and NO_x emissions showed a linear increase with road grade for all urban, rural and motorway parts. Larger emissions at higher road grades could be explained by more frequent high engine load points.

Contents

Abbreviations	vi
Abstract	ix
1 Introduction	1
2 Experimental Methods and Preparation	7
2.1 Laboratory Chassis Dynamometer	7
2.1.1 Emission Test Cycles	8
2.1.2 Gaseous Emission Analytics	9
2.1.3 PMP-Setup	10
2.2 On-road Emission Measurement Setup	11
2.2.1 Gaseous Measurements	11
2.2.2 Additional Particulate Equipment	14
2.3 Test Vehicles	18
2.4 Route Selection	20
3 Validation of PEMS Instrumentation	25
3.1 Gaseous Emissions	26
3.1.1 Repeatability	26
3.1.2 Correlation of PEMS with Test Cell	28
3.2 Particulate Emissions	28
3.2.1 Correlation of PN PEMS with PMP	30
3.2.2 Soot Measurements	34
4 Results of On-road Emission Measurements	37
4.1 Impact of Driving Style and Repeatability	37
4.1.1 Characterization of PEMS Trips	38
4.1.1.1 RDE Compliant Route	38
4.1.1.2 Cold and Hot Start Comparison	42

4.1.2	Effect on Emissions	44
4.1.2.1	Gaseous Emissions of Diesel Vehicles	44
4.1.2.2	Gasoline PN Emissions	48
4.1.2.3	PN-PM-Correlation	51
4.2	Cold Start Effect	53
4.2.1	Definition of Cold Start Phase	54
4.2.2	Methodology	57
4.2.3	Determination of Cold Start Emissions	58
4.2.3.1	Difference of Cold and Hot Start	58
4.2.3.2	Comparison of Cold Start and Post Cold Start Phase	60
4.3	Impact of Road Grade	65
4.3.1	Data Acquisition	67
4.3.1.1	GPS	67
4.3.1.2	Google	68
4.3.1.3	In-car Accelerometer	68
4.3.1.4	Barometer	70
4.3.2	Road Grade Measurements on Test Track	71
4.3.3	On-Road Methodologies	73
4.3.3.1	Route Comparison	73
4.3.3.2	Segment Method	76
4.3.3.3	Correlation with Exhaust Emissions	78
5	Summary and Conclusions	89
	List of Figures	97
	List of Tables	99
	Bibliography	112

Chapter 1

Introduction

Global air pollution due to elevated Carbon dioxide (CO_2) concentrations has captured public attention, especially considering global warming and the generation of greenhouse gases. Additionally, local air pollution due to Nitrogen dioxide (NO_2) and Particulate Matter (PM) is a major problem in many urban areas [Viana2014]. According to epidemiological studies, exposure to NO_2 or PM are attributed to a wide range of health effects including respiratory problems and cancer [WHO2013; EEA2015AQ]. Particle size is a major factor for PM health effects. Especially smaller particles with diameters in the nanometre range tend to penetrate deep into the alveoli and cause additional diseases [Sehlstedt2007; WHO2013PM].

Primary NO_2 is the term for direct NO_2 emissions and secondary NO_2 is attributed to the oxidation of Nitrogen oxide (NO) to NO_2 in the atmosphere. By convention, the sum of NO and NO_2 is called Nitrogen oxides (NO_x). During engine combustion processes NO_x is primarily produced at high combustion temperatures and large oxygen compounds [Bielaczyc2011]. In the European Union (EU) road transport is one of the main contributors to local air pollution and made up 39% of the total NO_x emissions in 2015 [EEAreport2016].

In the EU local air quality was improved by introducing emission limits for passenger cars starting with the first Euro standard in 1990. The limits have strictly been tightened until the current Euro-6 legislation with a NO_x limit of 80 mg/km over the New European Driving Cycle (NEDC) for light duty vehicles. Consequently, NO_x emissions decreased for 55% between 1990 and 2014 in the EU [EEAreport2016].

On the other hand, NO_2 concentrations measured at roadside stations did not show a corresponding effect [EEA2015pollutants]. Figure 1.1 shows the annual NO_2 averages since the year 1995 in Germany measured by traffic, rural and urban background stations. Additionally, the bars represent the fraction of traffic related NO_2 stations which exceeded the annual limit value of $40 \mu\text{g}/\text{cm}^{-3}$ since 2001 (data taken from [UBAweb]).

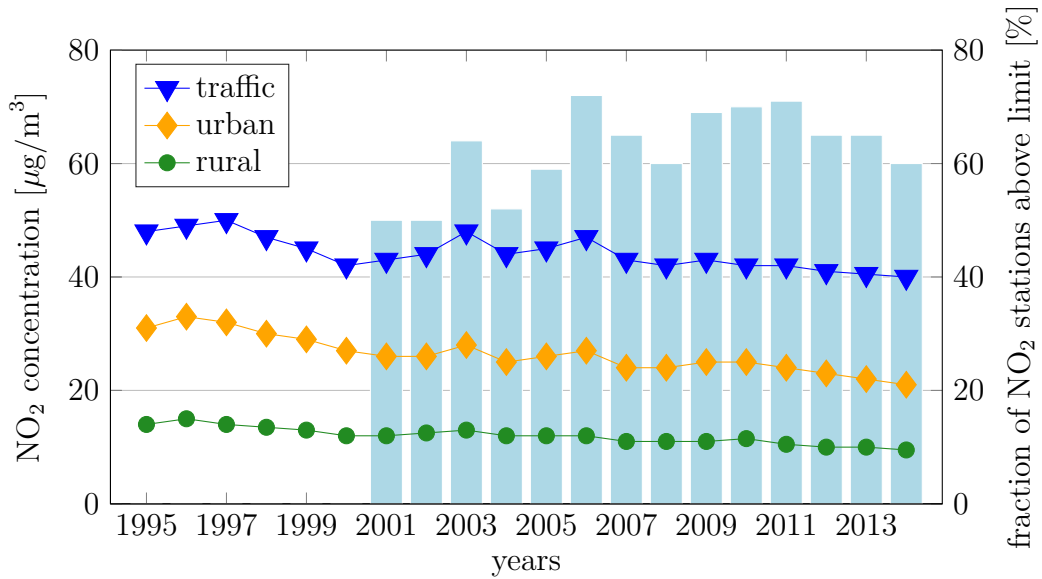


Figure 1.1: Annual mean NO_2 concentrations measured by traffic, urban and rural stations in Germany. The bars represent the fraction of traffic related NO_2 stations which exceeded the limit of $40 \mu\text{g}/\text{cm}^{-3}$ during each year [UBAweb].

There is a small reduction of annual NO_2 values with stations close to traffic roads constantly exceeding the $40 \mu\text{g}/\text{m}^3$ annual limit value. According to the bars shown in figure 1.1, 50 to 70% of the NO_2 stations in Germany exceeded the annual limit value during each year. This trend can be attributed to increasing dieselization and to an on-road NO_x performance of Diesel vehicles strongly diverging from test cycle emission factors [EEA2015pollutants]. In 2014, Diesel passenger vehicles contributed to a fraction of 67% to primary NO_2 emissions in German traffic [UBAweb]. In the UK, the elevated proportion of primary NO_2 emitted from Diesel vehicles led to an increasing NO_2/NO_x emission ratio [Carslaw2005].

PM is generally classified into primary and secondary particles. Primary parti-

cles are directly emitted by natural or anthropogenic sources (e.g. vehicle exhaust), while secondary particles are formed by chemical reactions in the atmosphere [Viana2014]. PM_{10} and $PM_{2.5}$ are defined as particles with diameters $\leq 10\mu m$ and $\leq 2.5\mu m$, respectively. In recent years, nanoparticles with sub-micron size typically $< 100nm$ have gained additional interest. In this regard, Particle Number (PN) concentration became a more significant factor than total mass concentrations. Figure 1.2 shows that Direct Injection (DI) gasoline vehicles are predicted to have an increased contribution to solid PN emissions [Mamakos2011b].

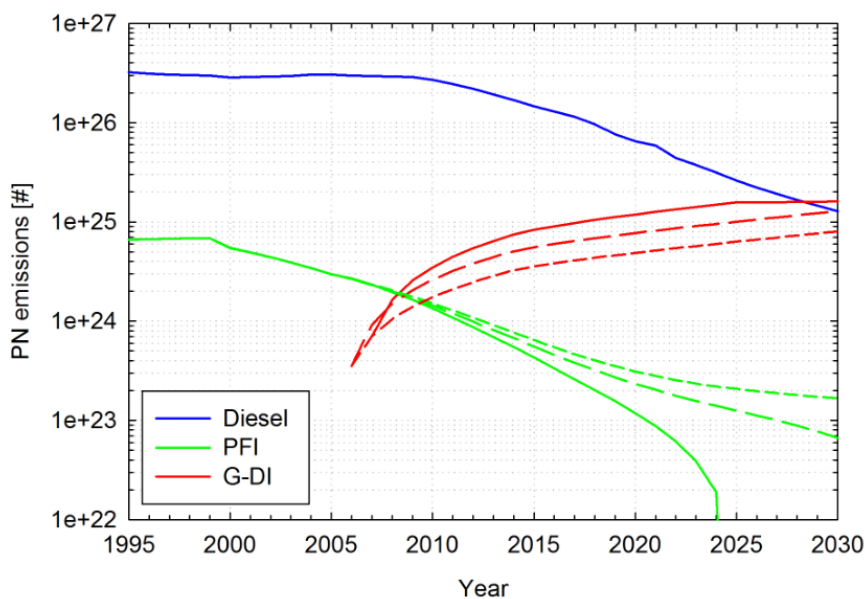


Figure 1.2: Solid PN emissions from passenger cars and light duty vehicles classified into Diesel, port-fuel injection (PFI) and direct injection gasoline (G-DI). The three line types for PFI and G-DI represent different predicted market shares [Mamakos2011b].

In 2011 the EU introduced a solid PN emission limit of $6 \cdot 10^{11} \text{ km}^{-1}$ for Diesel vehicles additionally to total PM mass measured over a filter. Particle regulation tests are conducted over the NEDC and according to the Particle Measurement Program (PMP) [UNECE2011]. The introduction and application of the Diesel Particulate Filter (DPF) enabled Diesel vehicles to meet this emission limit. With the first stage of the Euro-6 regulation (Euro-6b) launched in September 2014, a PN limit of $6 \cdot 10^{12} \text{ km}^{-1}$ was also imposed on DI gasoline vehicles [EU2012] and will be lowered to $6 \cdot 10^{11} \text{ km}^{-1}$ in 2017, as already mandatory for Diesel vehicles.

Chassis dynamometer tests are continued to be applied for type approval under laboratory conditions. However, the NEDC has been recognized as not covering the full spectrum of driving situations that occur during on-road driving. Consequently, there is a discrepancy between emissions obtained from on-road driving and over the NEDC. Figure 1.3 shows the development of Euro-1 to Euro-6 type approval NO_x limits for Diesel passenger cars and corresponding real-world NO_x data collected from TNO [TNO2013]. The pre-Euro-6 data was taken from the first Euro-6 Diesel vehicles on the US market in 2010.

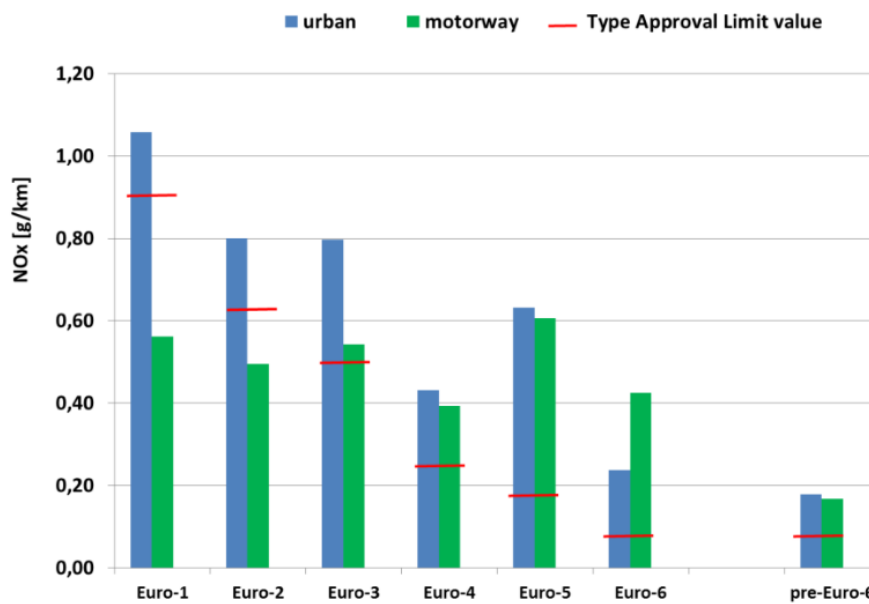


Figure 1.3: Discrepancy between real-world and type approval NO_x emissions from Diesel passenger cars since the Euro-1 legislation [TNO2013].

Since the Euro-1 legislation in 1992/1993 the NO_x type approval limit for Diesel vehicles was periodically tightened from 900 mg/km to 80 mg/km for Euro-6. While the NO_x emission limits were reduced by more than a factor of 10, real-world data did not show a corresponding decrease. Figure 1.3 shows that motorway emissions remained stable between 400 and 600mg and urban traffic NO_x emissions decreased only four times from Euro-1 to Euro-6. The main reason for this increasing gap between type approval and real-world NO_x is an augmented use of external factors that are not considered in the type-approval process, such as air conditioning or media systems.

For Euro-6d both the EU Commission as well as the car manufacturers are working on the development and implementation of Real Driving Emissions (RDE) which includes the regulation of Diesel NO_x and PN. On-road emissions will be measured by mobile measurement devices called Portable Emission Measurement System (PEMS). PN emissions are currently subject of research; corresponding PN PEMS devices are still under development.

For on-road emissions additional boundary conditions need to be defined, e.g. driving style, road grade, ambient temperature [HBEFA2.1], traffic situations [VanMierlo2004] and road type [Huang2013]. Some boundary conditions are already taken into account in the RDE regulation draft (3rd package) [RDE2016], such as the admissible ambient temperature range, basic driving parameters (maximum motorway speed, minimum urban speed, idle fraction) and trip requirements (composition, duration, distance, altitude). However, some boundary conditions still need to be defined in order to exclude non-normal or non-representative driving situations.

Several contemporary studies dealt with the absolute amounts of pollutants by Euro-6 vehicles and related these results with Euro-6 emission limits and test cycle results [ICCT2014; ODriscoll2016; TNO2016a; TNO2016b]. This kind of study required a large fleet of vehicles with lots of test data in order to generate statistically relevant numbers. However, the reasons for the differences between on-road and test cell were hardly investigated, although parameters impacting engine load are recognized to change fuel consumption and especially emissions. In the present study, the impact of driving conditions on on-road exhaust emissions of Diesel and gasoline passenger vehicles is investigated. More specifically, the influence of driving style, the cold start effect and the relevance of road grade is addressed.

Driving style has been characterized by several methods and it was always found to have a significant impact on exhaust emissions [ICCT2014; Fonseca2010]. Standard driving parameters need to be defined in order to characterize different driving styles. Based on repeatability evaluations, the impact of different driving styles on exhaust emissions is investigated.

With reference to chassis dynamometer tests, the cold start effect normally lasts for a few minutes but makes up a major part of CO, HC and PN emissions over the complete trip [Bielaczyc1997; Weilenmann2005; Reiter2016]. According to the RDE regulation, the implementation of the cold start phase is still under discussion. The end of the cold start phase can be defined in different ways while the calculation method of Cold Start Excess Emissions (CSEE) has been developed for test cell conditions and needs to be carried over to on-road operation. Still, a major unknown aspect is the correlation of ambient conditions with the cold start emissions.

Road grade has a significant impact on exhaust emissions [Boriboonsomsin2009; Meccariello2014; Prati2015], however, a consistent methodology to address road grade during on-road driving remains to be determined. The magnitude of road gradients over a test route can be characterized by the parameter Cumulated Altitude Gain (CAG) but the application of data sources, as distinguished from the Global Positioning System (GPS), provides a benefit in accuracy and reproducibility. Based on such data sources, road grade is calculated with a statistically relevant precision and in a next step the correlation with exhaust emissions is evaluated.

Chapter 2

Experimental Methods and Preparation

2.1 Laboratory Chassis Dynamometer

For passenger vehicles, chassis dynamometer tests are applied for emission testing in the EU since the Euro-1 regulation in 1992. The current Euro-6 legislation includes the regulation of CO, NO_x, HC (Diesel: HC + NO_x, gasoline: also Non-Methane Hydrocarbons (NMHC)), PM and PN and separate emission limits are imposed on Diesel and gasoline vehicles. In the test cell, the vehicle is placed on a roller bench which simulates the inertia mass and driving resistances while driving a specified velocity-time pattern (emission test cycle). Road load parameters have to be pre-determined which represent the aerodynamic and inertia friction losses characteristic for each test vehicle [UNECE2011].

In the present study, well-established laboratory measurements were primarily applied for the validation of the on-road measurement devices regarding gaseous and PN emissions (cf. chapter 3). The laboratory tests were conducted on the chassis dynamometers at the Ford research and innovation centre in Aachen and at the development centre in Cologne. Several driving cycles were applied including the NEDC and World harmonized Light-Duty Test Cycle (WLTC) starting with a cold engine after soaking the vehicle for at least eight hours. All laboratory measurements were conducted according to current legislative procedures for type approval including the ambient temperature range (between 20 and 30°C) and absolute humidity in the test cell [UNECE2011].

2.1.1 Emission Test Cycles

Emission test cycles prescribe a specified velocity-time pattern applied on a chassis dynamometer for emission measurements. A number of driving cycles are applied for regulation purposes, such as the NEDC in the EU, the FTP-75 in the United States or the JC08 in Japan [Tutuianu2013]. In the present work, laboratory results of the NEDC and the WLTC are presented. Figure 2.1 shows the velocity-time patterns of the NEDC (top) and the WLTC (bottom).

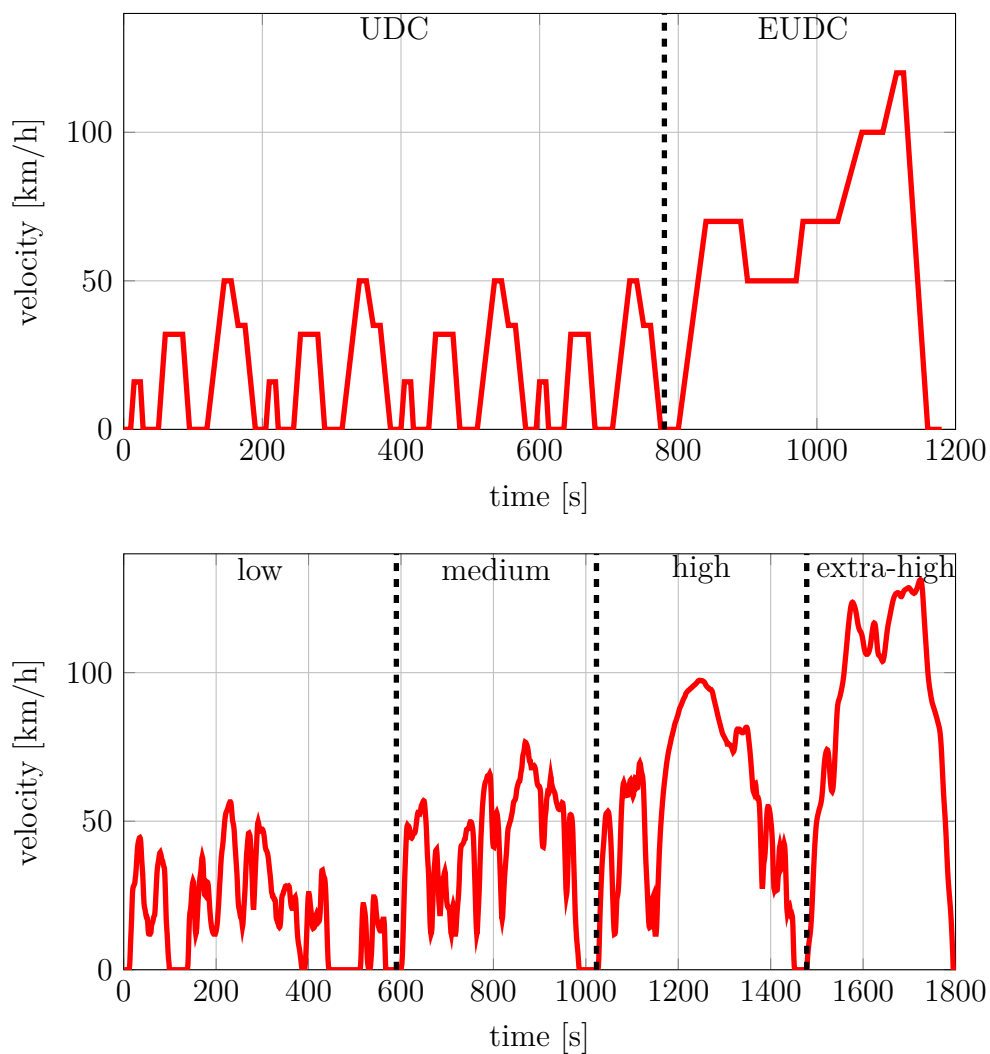


Figure 2.1: Time traces of the emission test cycles NEDC (upper figure) and WLTC (lower figure).

The NEDC is the current legislative cycle in the EU [Samuel2002]. Originally developed for comparing all types of passenger vehicles including also low-powered engines, the NEDC is characterized by moderate accelerations and a small engine power demand. In the first phase, the Urban Driving Cycle (UDC), the same driving pattern is repeated four times and enables the direct comparison of similar driving situations. The second phase is the Extra Urban Driving Cycle (EUDC) which represents motorway driving up to a velocity of 120 km/h (cf. figure 2.1). The tested vehicles are prescribed into NEDC reference mass classes, which is normally the lowest mass available for this vehicle type. Road load parameters are allowed to be determined by road coast down tests under ideal conditions in terms of low resistance tires, best aerodynamic and ambient conditions [UNECE2011]. All these influences normally lead to underestimated emissions in the NEDC compared to on-road measurements [Tutuianu2015; ODriscoll2016].

As part of the World harmonized Light-Duty Test Procedure (WLTP), the WLTC was developed in order to represent a more realistic driving cycle based on real-world traffic data [Demuynck2012; Tutuianu2013]. In the present study, WLTC refers to the latest version 5.3 for light duty vehicles of class 3. Compared to the NEDC, the WLTC includes a more realistic driving profile (cf. figure 2.1) including stronger accelerations, less idling phases and a higher power demand [Tsokolis2016]. Based on the minimum or maximum unladen mass and the best or worst rolling and aerodynamic resistance for each vehicle model, two sets of road load parameters are determined representing the lowest (WLTP-low) and the highest energy demand (WLTP-high) for this vehicle model [Dimaratos2016]. In future EU legislation, the WLTC will replace the NEDC for laboratory regulation purposes, and emissions are regulated in combination with RDE measurements [Tutuianu2013].

2.1.2 Gaseous Emission Analytics

In the EU legislation regulated gaseous emissions are sampled out of a Constant Volume Sampler (CVS) and accumulated over the complete test. In the CVS the exhaust of the vehicle is diluted by filtered ambient air to maintain a constant flow.

The diluted sample is collected in bags and the concentrations of the regulated pollutants are measured after the test using a Non-Dispersive Infra-Red (NDIR) analyser for CO and CO₂, a Flame Ionisation Detector (FID) for total HC and a Non-Dispersive Ultra-Violet (NDUV) or Chemiluminescence Analyzer (CLA) for NO_x. The total mass emissions during the complete test are computed by the sample concentrations inside the bags and the total volume measured during the test [UNECE2011].

The bag method yields robust results, however, emission behaviour is not able to be linked to specific events during the test. Therefore, modal measurements were conducted during the laboratory tests additionally to the bag method. Raw exhaust emission samples were taken on a second-by-second basis and concentrations were recorded by an Fourier Transform Infra-Red spectroscopy (FTIR) analyser as well as a FID for total HC. In this way, driving situations could directly be linked to the corresponding pollutant and emission time traces could be compared to those from the PEMS [TNO2016a].

2.1.3 PMP-Setup

The type approval measurement methodology for solid, non-volatile PN emissions was developed in the framework of the PMP. Since Euro-5.1 and Euro-6 a PN limit is imposed on Diesel and DI gasoline vehicles measured according to the PMP, respectively [EU2012].

A PMP-system samples diluted exhaust directly out of the CVS (cf. figure 3.5). Coarse particles $> 2.5\mu\text{m}$ are removed from the sample by a Pre-Classifier (PCF). The sample is conditioned in the Volatile Particle Remover (VPR) which consists of a Particle Number Diluter (PND) (PND1), an Evaporation Tube (ET) and a second PND (PND2). The VPR ensures that no volatile or semi-volatile particles remain in the sample but evaporate prior to the detector. The focus on solid particles is necessary because droplets of volatile or semi-volatile particles derive from cooling or dilution in the transfer lines and not during combustion in the engine. Their formation is strongly dependent on temperature, humidity and volume flow with a strong test-to-test variability [Kasper2008].

Particle detection is performed in the Particle Number Counter (PNC) which is based on the principle of a Condensation Particle Counter (CPC). The CPC applies a light scattering method and detects particles with a frequency of about 1Hz. Small particles are coated by a liquid in a heated saturation chamber, so that the CPC is able to detect nano-particles that have been enlarged to droplets of around $1\mu\text{m}$ in diameter. However, there is a trade-off between the detection of small particles and the nucleation of droplets without a particle inside. Thus, CPCs are calibrated to have a 50% counting efficiency at 23nm that converges to 100% for particles larger than 100nm [Kasper2008].

In the present study, the laboratory PN measurements were conducted in order to compare the results obtained by the PMP-system with those from the on-road PN measurement system. Both systems are depicted in figure 2.4 and the specifications are compared in table 2.1.

2.2 On-road Emission Measurement Setup

2.2.1 Gaseous Measurements

On-road emission measurements were conducted using a Semtech-DS (Sensors Inc., Saline, Michigan, USA) which measured Carbon monoxide (CO), CO₂, NO, NO₂ and the total amount of Hydrocarbons (HC). The Semtech-DS fulfilled official testing requirements and was designed to match the analytical performance of laboratory grade instrumentation [Sensors2006]. As the utilized PEMS was originally constructed for heavy duty application, the main unit including equipment made up almost 80kg extra weight excluding a necessary battery pack. As an example, a complete PEMS set-up for a passenger vehicle is depicted in figure 2.2.

The device was fixed inside the trunk of the test vehicle and connected close to the tailpipe to an Exhaust Flow Meter (EFM) (Sensors Inc.) The heated sampling line was set to a temperature of 190°C in order to avoid condensation processes of HC. For on-road operation the measurement of HC is not practical due to



Figure 2.2: An example PEMS set-up showing the gas PEMS with accessories.

considerable power consumption and weight as well as the requirement to carry a hydrogen bottle (not visible in figure 2.2) for the operation of the FID. Thus, in the future RDE regulation the measurement of HC will likely not be included. In the present study, HC emissions were measured during all PEMS trips, primarily in order to investigate the cold start behaviour (cf. section 4.2).

A battery pack consisting of three to four lead acid batteries with a capacity of 285 to 380Ah mounted inside the trunk supplied power for the instruments. Several sensors fixed to the roof of the car recorded ambient temperature, relative humidity and GPS data. In addition, Engine Control Unit (ECU) data was recorded directly by the PEMS (On-Board Diagnostic (OBD) data) or using a CANalyzer software and the VN1610 hardware (Vector Informatik GmbH, Stuttgart, Germany). All in all, the measurement equipment depicted in figure 2.2 had a total weight of almost 160kg [Gallus2017].

The working principle of the PEMS and the flow of the collected exhaust are outlined in figure 2.3. For illustration, the analysers are coloured red and additional equipment is coloured green. A more detailed description of the PEMS can be found in the manual [Sensors2006].

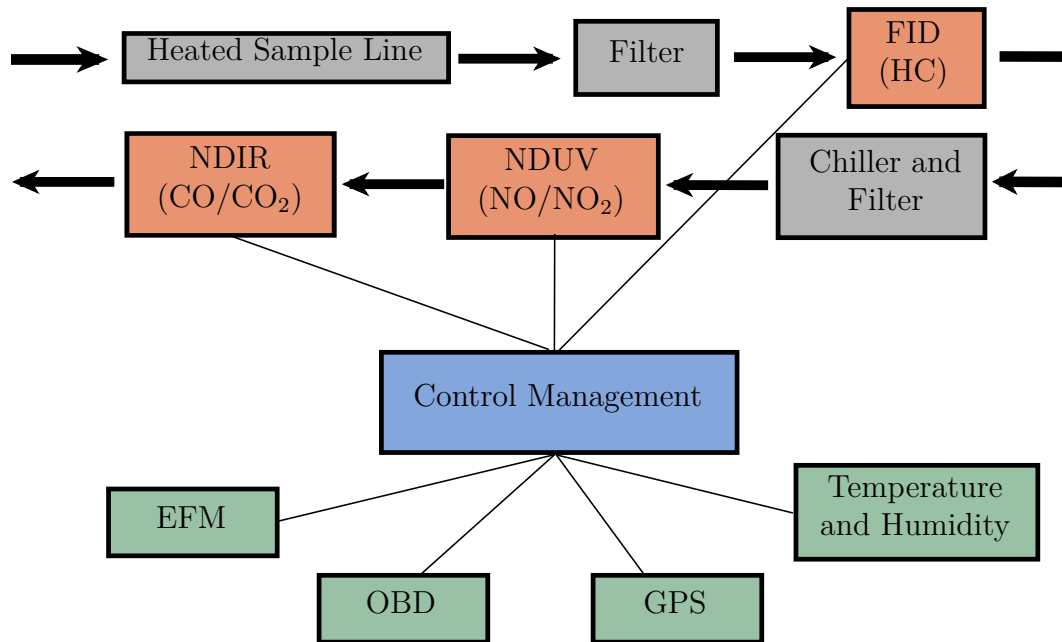


Figure 2.3: Schematic principle of the PEMS. The exhaust flow depicted by the black arrows passes the analyzers FID, NDUV and NDIR detecting CO/CO₂, NO/NO₂ and HC concentrations, respectively. Additionally GPS, OBD and ambient conditions are recorded. This figure is based on [Merkisz2016].

The exhaust was collected with a constant rate of 7 l/min at the tailpipe of the vehicle. It passed the heated sample line (length 3m) and coarse particles were filtered before the sample reached the sensors. A FID measured HC up to a concentration of 40000 ppmC (measured as concentration of carbon-atoms). The FID was followed by a thermoelectric chiller combined with a coalescent filter. At this point, water vapour and heavy HC were removed from the sample that could cause interferences and contamination in the subsequent sensors [Sensors2006].

The NDIR detector measured CO and CO₂ concentrations by an infra-red light source. The maximum range of the CO analyser was up to 8% which is large compared to typical exhaust concentrations of 0.1%. Therefore, the CO analyser was primarily applied to cold start emissions, where such high concentrations were expected. An ultra-violet lamp was applied in the NDUV detector, which measured NO and NO₂ concentrations independently. After the measurements, the PEMS software applied a dry-to-wet correction on the measured CO, CO₂,

NO and NO₂ concentrations due to the water that was removed prior to the concentration measurements [Sensors2006].

Before and after each measurement, a zero test as well as a span gas calibration with known gas concentrations were conducted. If either the zero or span drift over a measurement was not within the admissible range suggested by the RDE regulation [RDE2016], the measurement was not valid and had to be repeated.

An EFM measured the mass flow of the exhaust directly at the tailpipe. Based on the continuity equation the standard volumetric flow at 20°C and 1 atmosphere was calculated by the PEMS software. Instantaneous mass emissions were obtained by the multiplication of the volumetric exhaust flow with the wet concentrations and the corresponding standard density for each constituent [Sensors2006].

The measurement frequency of the PEMS was physically limited by the NDIR analyser at 0.833Hz. For the measurements, the CO and CO₂ data were interpolated to 1Hz, so that all signals were available with the same frequency of 1Hz. The measured concentrations and the exhaust flow required a precise time alignment. Both the exhaust concentration and the exhaust flow were collected at the tailpipe of the vehicle, thus, the length of the heated sample line and the internal distances between the gas analysers had to be considered for the time alignment. Due to the constant sampling rate of the instrument, the residence time in the sample line and in the internal connections of the PEMS could be determined [Sensors2006].

2.2.2 Additional Particulate Equipment

On-road PN measurements were conducted by a pre-series instrument Nanomet3-PS manufactured by Matter Aerosol AG (Testo company, Switzerland). The PN PEMS was designed to be comparable to the current PMP regulation [UNECE2011] regarding the PN measurement on chassis dynamometers in terms of particle conditioning and detection parameters. The main characteristics of both instruments are compared in table 2.1 [Gallus2016].

2.2 On-road Emission Measurement Setup

	PN PEMS (present study)	PMP set-up (Regulation 83)
Sampling position	Raw exhaust	Constant volume sampler
Calibration	Factory calibration with CAST soot particles (80nm), no calibration directly before the measurements	Calibration using a traceable standard within a 12 month period by comparison with a calibrated aerosol electrometer or a second calibrated PNC
Exhaust conditioning method	Hot Dilution and evaporation tube	Hot Dilution and evaporation tube
Dilution	Rotating disk diluter (factors: 10, 100, 300)	PND1 (& PND2) (typical factors: 100 to 20000)
Detection method	Corona charger	Condensation Particle Counter
Concentration range (sensor)	$10 \cdot 10^3$ to $10 \cdot 10^6$ cm^{-3}	0 to $10 \cdot 10^4$ cm^{-3}
Concentration range (diluted)	$3 \cdot 10^3$ to $3 \cdot 10^8$ cm^{-3}	$< 2 \cdot 10^2$ to $> 1 \cdot 10^9$ cm^{-3} (at typical CVS dilution)
Limit of detection counter	1000 cm^{-3}	≤ 0.2 cm^{-3}
Limit of detection system	Typical $1 \cdot 10^4$ to $3 \cdot 10^5$ cm^{-3} (raw exhaust, dependent on dilution)	typical 20 to 400 cm^{-3} (from CVS, dependent on dilution)
Particle Size	10 to 300nm	23 to 2500nm

Table 2.1: Specifications of the PN PEMS [Matter2013] compared to the PMP set-up [UNECE2011]

Figure 2.4 shows a schematic view of the device in comparison to a test cell PMP system. The PN PEMS sampled raw exhaust directly from the tailpipe while the PMP system collected aged particles out of a CVS. Thus, a different shape of the particle peaks was expected for the PN PEMS compared to the PMP results. However, the total PN was supposed to be in the same range, not taking into account coagulation and thermophoretic losses.

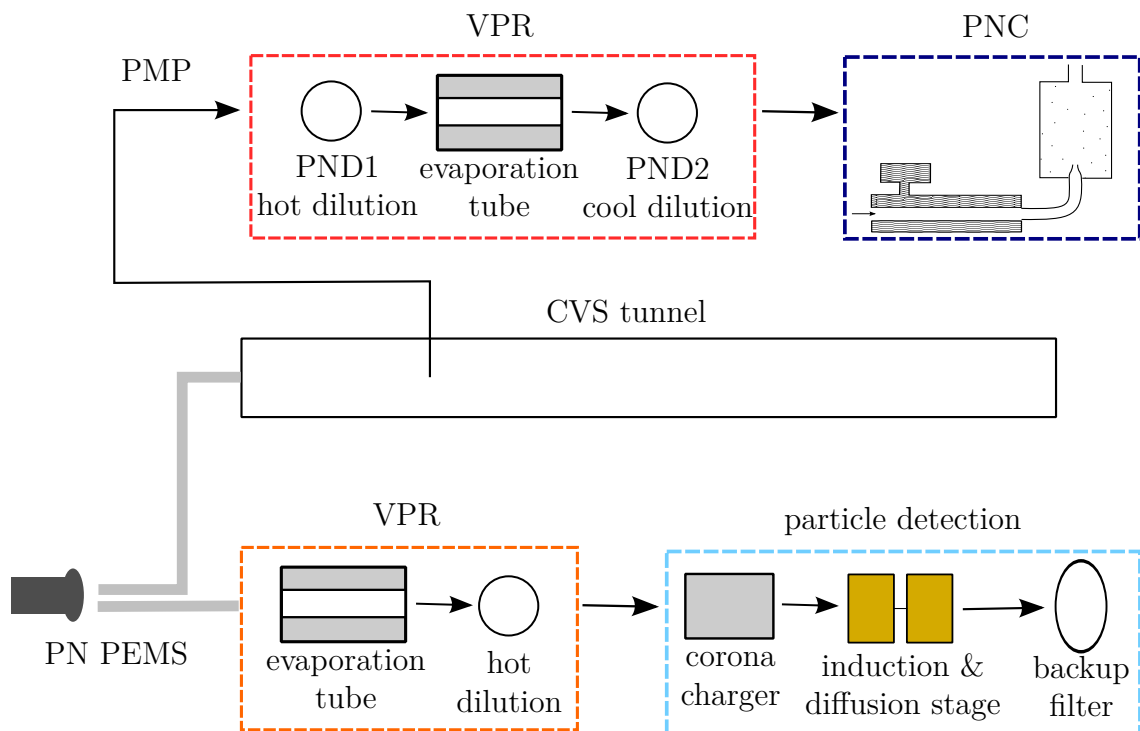


Figure 2.4: Schematics of the PN PEMS that collects the exhaust directly at the tailpipe compared to a test cell PMP system [Gallus2016].

Comparable to the PMP procedure, sample conditioning in the PN PEMS took place in a VPR consisting of a hot diluter and an ET. The sample passed a hot dilution in a rotating disk diluter at 150°C with dilution factors of 10, 100 or 300 and was heated to 300°C in the ET. In the subsequent cooling down zone according to the manufacturer no recondensation occurred because the dilution factor was set to a high enough value, so that the sample did not pass its dew point [Matter2013].

The particle measurement principle of the PN PEMS was completely different compared to the CPCs of PMP systems (table 2.1). In the particle detector the aerosol was charged by a unipolar corona diffusion charger and the resulting current was measured in two stages. In the diffusion stage particles were deposited by diffusion processes while the remaining particles were collected in the filter stage. In both stages the electrical current was measured using two sensitive electrometers. Based on the ratio of both electrometer signals, the mean particle size was able to be estimated [Matter2013].

Diffusion chargers were found to show a non-linear size dependent efficiency curve because larger particles can carry more charges leading to higher currents [Giechaskiel2014]. The efficiency was defined as the ratio of the detected and the true inlet PN concentration. The exponent of the efficiency function for the PN PEMS in other studies was reported as 1.1 [Fierz2008], 1.125 [Fierz2011] and 1.13 [Matter2013]. The PN PEMS was factory calibrated using monodisperse soot particles at 80nm [Matter2013], thus, there was a well-known deviation for particles larger or smaller than 80nm. Figure 2.5 shows experimental data obtained from literature illustrating the difference of the PN PEMS and the PMP system [JR-Creport2014]. In this case, the PN PEMS was calibrated with a monodisperse NaCl aerosol at 90nm and another unknown polydisperse aerosol.

The PN on-road measurements were conducted using gasoline operated Euro-5 passenger vehicles V4 and V5 (cf. table 2.2). Additionally to the gaseous equipment described in the last section, the set-up is augmented by the PN PEMS. The device was also mounted inside the trunk of the car and connected at the tailpipe close to the EFM which was controlled by the gas PEMS (cf. figure 2.6). A fourth lead acid battery was added to the battery pack because of an elevated power demand, compared to the gaseous measurements.

In addition, for some correlation tests the vehicle was equipped with an AVL M.O.V.E. PM PEMS fixed on the back-seat of the vehicle. In parallel to the PN PEMS, the PM PEMS was connected to the EFM and measured soot by applying a photo-acoustic detection method [AVL2012]. The entire measurement equipment consisting of gas PEMS, PN PEMS, PM PEMS and accessories resulted in a total extra weight of roughly 280kg.

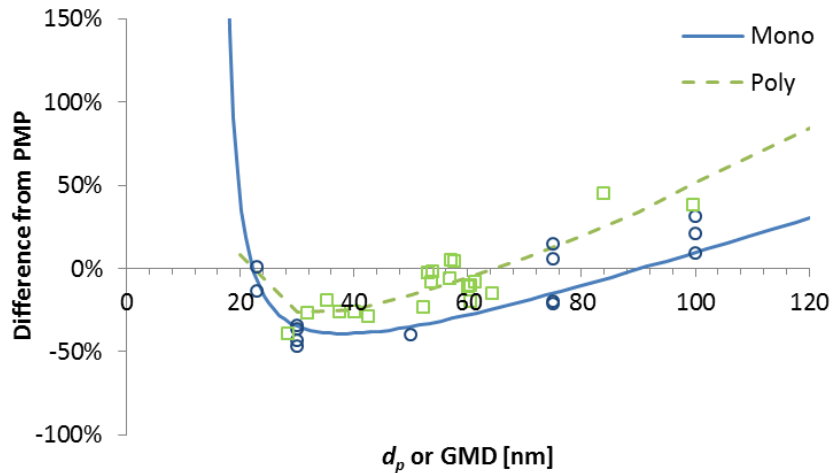


Figure 2.5: Difference of the efficiency curves of the PN PEMS and the PMP system obtained from [JRCreport2014]. Note that in this study the PN PEMS was calibrated with a monodisperse aerosol at 90nm and a polydisperse aerosol.

In order to calculate PN in particles per second, the PN concentration measured by the PN PEMS was multiplied with the exhaust flow measured by the EFM. Similar to the gaseous measurements, the result was very sensitive to offsets between these two signals because of different time bases. The time alignment was realized by adjusting the first increase of the PN concentration signal to the first increase of the CO signal that was provided by the gas PEMS and already time aligned with the exhaust flow. The soot mass in milligrams per second was based on the soot concentration measured by the PM PEMS and was calculated by analogy with the PN data.

2.3 Test Vehicles

Table 2.2 shows a list of the different vehicles used for the gaseous and PN measurements presented in this study. PEMS trips were conducted with three Diesel vehicles V0, V1, V2 that were all equipped with a DPF leading to very low PN emissions. Thus, no Diesel particle measurements were investigated. Vehicle V0 was a Euro-4 light commercial vehicle (class M1G-AF) with elevated emission

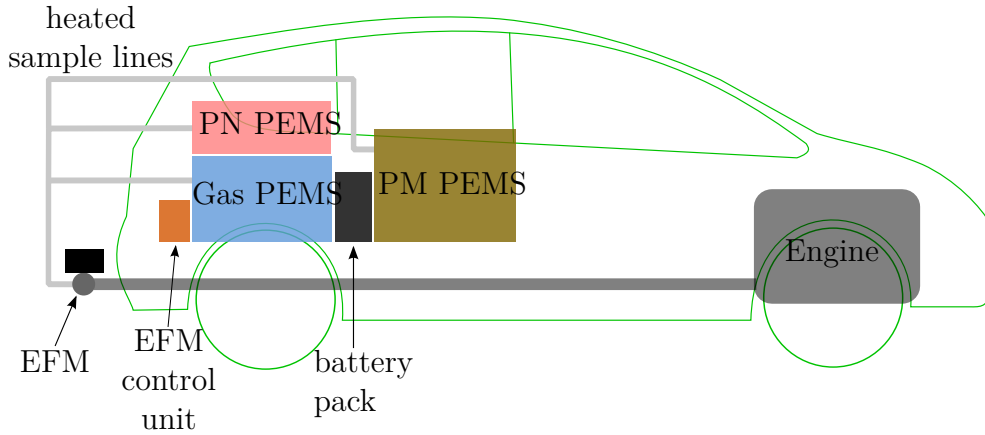


Figure 2.6: PN real world instrumentation consisting of a PN PEMS, a PM PEMS, and an EFM controlled by the gas PEMS [Gallus2016].

limits. Vehicle V2 was a prototype Euro-6 equipped with a NO_x aftertreatment system. The two gasoline vehicles V3, V4 were primarily used for particulate emissions and additionally equipped with the PN PEMS and partly with the PM PEMS for soot measurements.

The measurement equipment led to a distinct increase of the total vehicle mass close to the gross vehicle mass of the vehicles. Due to the elevated total mass of the test vehicles higher fuel consumption as well as a larger amount of gaseous and PN emissions were expected. The equilibrium of forces for a vehicle of mass M with a total acceleration of \vec{v} is given in equation 2.1 [Bae2001].

$$M \cdot \dot{\vec{v}} = \vec{F}_{\text{roll}} + \vec{F}_{\text{air}} + \vec{F}_{\text{downhill}} + \vec{F}_{\text{powertrain}} \quad (2.1)$$

The power that the engine has to provide is the product of the powertrain force and the corresponding velocity of the vehicle (cf. equation 2.2):

$$P_{\text{powertrain}} = \vec{F}_{\text{powertrain}} \cdot \vec{v} \quad (2.2)$$

Based on equations 2.1 and 2.2, figure 2.7 shows the additional power that was provided by the engine of vehicle V1 (mass $\approx 1450\text{kg}$) due to an additional mass of 170kg . The resulting power values were dependent on the current velocity and

	Engine type	Euro norm	Engine displacement	Engine power	Gear shift	Additional PEMS weight	Fraction of gross vehicle weight
V0	Diesel	Euro-4	2.4l	132kW	6-gear manual	170kg	n/a
V1	Diesel	Euro-5	1.6l	77kW	6-gear manual	170kg	89%
V2	Diesel	prototype Euro-6d	2.0l	132kW	6-gear automatic	197kg	97%
V3	DI Gasoline	Euro-5	2.0l	147kW	6-gear automatic	280kg	n/a
V4	DI Gasoline	prototype Euro-6b	1.0l	92kW	6-gear automatic	200kg	n/a

Table 2.2: Basic information about the tested vehicles. The fraction of the gross vehicle weight includes a 75kg driver.

acceleration of the vehicle.

Most of the impact of the additional mass was theoretically found for urban driving (up to 50 km/h) with a contribution of the extra mass of more than 10% to the total engine power. Note that the mean positive acceleration for a normal PEMS trip was around 0.5 m/s^2 (cf. section 4.1). In this study, the impact of driving conditions was primarily investigated by relative and not by absolute increases of emission values.

2.4 Route Selection

Table 2.3 presents the different routes that were chosen for the measurement series in this study. Routes with different characteristics, such as trip composition, location and road grade were used for the emission measurements. Routes R0, R1 and R2 were closed cycles, i.e. with equal start and end points. In the RDE regulation draft a maximum altitude difference between start and end of the route

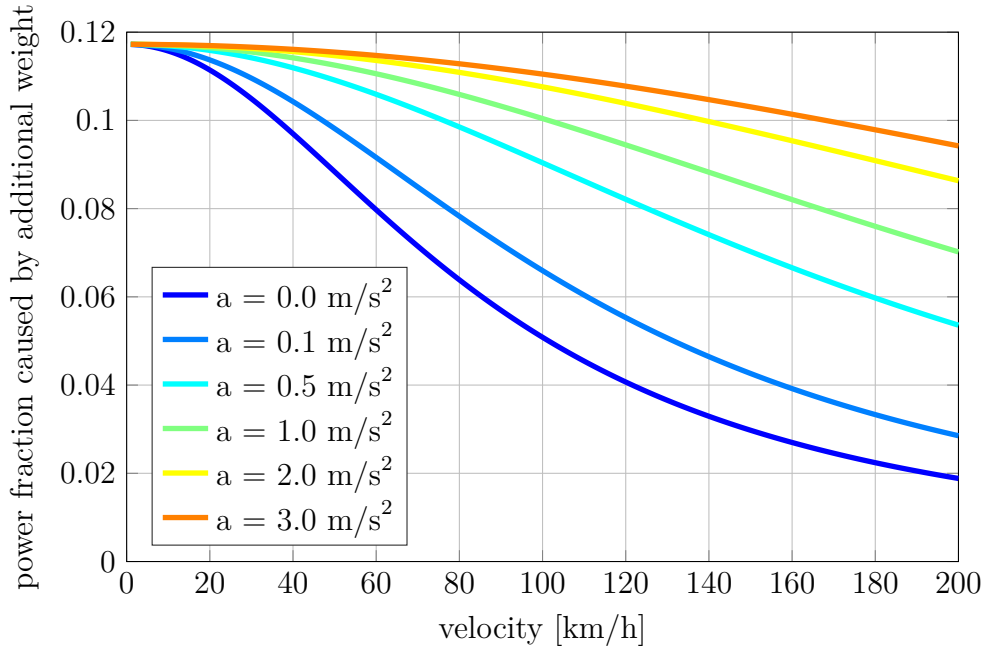


Figure 2.7: Calculation of additional power due to extra mass of the measurement equipment.

is defined as 100m. This restriction is necessary, so that the route is not designed to include a large fraction of downhill segments, leading to an emission benefit on this route. The altitude difference between start and end point of Route R3 accounted for 40m.

Route R0 consisted of an urban section repeated twice and a second section with rural and motorway parts. The urban section was about 15.6km and led through the city centre of Aachen, Germany, mostly with a maximum speed of 50 km/h and some short segments of 70 km/h. The second section of route R0 consisted of a long motorway part and some rural parts in the surroundings of Aachen. The total distance of this section was about 50.5km partly without speed limit. One complete PEMS evaluation run on route R0 resulted to an average run time of about 102 minutes and a total distance of about 81.7km.

Route R0 was mainly designed for cold and warm start comparisons. For this purpose, the urban section was driven at different ambient temperatures ranging from -3 to 28°C and followed by an immediate second urban trip right after

	Location	Average duration	Distance	Distance share of urban/ rural/ motorway
R0	<u>Urban:</u> Aachen (2x) <u>Rural/motorway:</u> Aldenhoven, A4 to Aachen (Germany)	102 min	82km	32/28/40%
R1	<u>Urban:</u> Aachen <u>Rural:</u> Eschweiler, Jülich <u>Motorway:</u> A4 to Aachen (Germany)	103 min	86km	32/35/34%
R2	<u>Urban:</u> Bishop's Stortford <u>Rural:</u> Newport <u>Motorway:</u> M11 to Stansted (UK)	99 min	77km	33/32/34%
R3	<u>Urban:</u> Aachen (Germany), Eupen <u>Rural:</u> N68 to Hockai <u>Motorway:</u> E42 to Herve (Belgium)	107 min	85km	33/32/34%

Table 2.3: Overview of the investigated routes. While routes R0, R1 and R2 show similar characteristics, route R3 was designed with respect to more pronounced road gradients and larger absolute altitudes.

the urban cold start in order to guarantee a real hot engine and similar driving conditions.

The standard route R1 (cf. table 2.3) was designed with respect to the RDE regulation draft [RDE2016]. A specific distance share of urban (34 -5/+10%), rural (33 ± 10%) and motorway (33 ± 10%) was met based on Google map data. The motorway section needed to have at least 10 minutes above 100 km/h and the urban part at most 20% idle fraction.

The total distance of route R1 was about 86km with an equal distance share of urban, rural and motorway parts. The urban part led through the city centre

of Aachen, Germany with a maximum speed of 50 km/h followed by a rural part to the city of Düren with mainly 70 km/h and some 100 km/h maximum speed sections. The motorway part led back to Aachen mostly without speed limit. One complete PEMS trip took between 100 and 110 minutes. All PEMS trips on route R1 were started with a cold engine at ambient temperatures ranging from -1 to 29°C [Gallus2017].

Route R2 was situated close to Stansted in Great Britain. A distinctive feature about this route is the limited maximum velocity on the motorway of 112 km/h (70 mph). Route R3 led partly through Germany but for the most part through Belgium. This route was designed with respect to an elevated amount of hilly sections up to a maximum altitude of almost 700m.

Chapter 3

Validation of PEMS Instrumentation

The chassis dynamometer tests were conducted at the Ford Innovation and Research Centre in Aachen as described earlier in chapter 2. The results of the emission test cycles NEDC and WLTC are presented in this chapter. Both test cycles were characterized by a range of parameters and compared to on-road data (4.1). The driving parameters Mean Positive Acceleration (MPA) and Relative Positive Acceleration (RPA) are defined by the vehicle acceleration which is directly calculated based on the velocity signal of the vehicle. Assuming a velocity signal with n data points, the acceleration is calculated according to equation 3.1.

$$\begin{aligned} a_i &= \frac{v_{i+1} - v_{i-1}}{\Delta t} & \text{where } 1 < i < n & \quad (3.1) \\ a_0 &= 0 \\ a_n &= a_{n-1} \end{aligned}$$

The MPA is a measure for the average accelerations occurring during a specific driving cycle or on-road test. In this study, positive accelerations a_i^+ are defined as accelerations larger than 0.1 m/s^2 . The formula for the MPA is given in equation 3.2 with n^+ as the number of data points with positive acceleration.

$$MPA = \frac{1}{n^+} \sum_i a_i^+ \quad (3.2)$$

The parameter RPA represents the power that is performed by a vehicle during a test run. It is calculated as the sum of the velocity weighted positive acceleration

signal according to equation 3.3.

$$RPA = \frac{1}{d} \sum_i v_i \cdot a_i^+ \cdot \Delta t \quad (3.3)$$

The parameters for the test cycles NEDC and WLTC are summarized in table 3.1. Due to different definitions of the acceleration or thresholds for positive accelerations, some values can partly vary from values found in the literature [Samuel2002; Tutuianu2013].

cycle	dura- tion [s]	dis- tance [km]	mean velo- city [km/h]	max. velo- city [km/h]	idle frac- tion [%]	max. accele- ration [m/s ²]	MPA [m/s ²]	RPA [m ² /s ³]
NEDC	1181	11.0	33.6	120.0	26.0	1.042	0.489	0.110
WLTC	1800	23.3	46.5	131.3	14.3	1.583	0.497	0.145

Table 3.1: NEDC and WLTC driving parameters [Samuel2002; Tutuianu2013].

All measurements were performed according to the current legislative procedures for type approval [UNECE2011]. The model MEXA-2000SPCS from Horiba was used as PMP-conform instrument. Several driving cycles such as NEDC, WLTC and other laboratory cycles representing on-road driving were conducted with different test vehicles (Diesel and gasoline) with emissions over a large range.

3.1 Gaseous Emissions

3.1.1 Repeatability

Figure 3.1 shows the gaseous emissions of NEDC and WLTC tests measured by the test cell devices. The WLTC tests were conducted using WLTC shift points and road load from a similar vehicle. The mean and the standard deviation of several runs are represented by the bar height and the range bar, respectively. The Coefficient of Variance (CoV), which is the ratio of the standard deviation and the mean value, is expressed in percentage at the bottom of every bar.

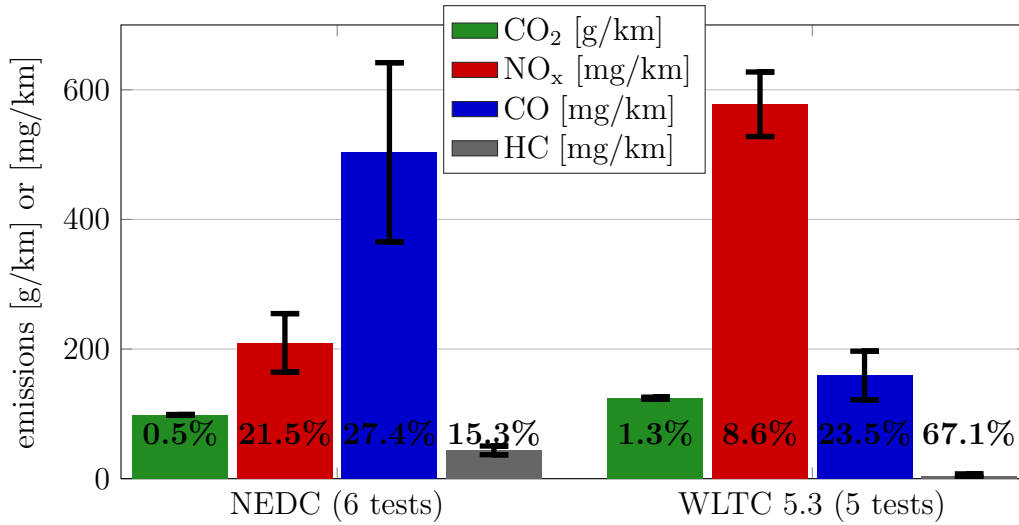


Figure 3.1: Repeatability of several NEDC and WLTC runs.

As expected, the NEDC cycle shows smaller distance specific CO₂ and NO_x emissions, as this cycle is much softer compared to the WLTC (compare table 3.1) and is conducted with lower road load. On the other hand, CO and HC emissions are lower on the WLTC. These types of emissions appear primarily in the cold start phase during the first minutes of the cycles (cf. in more detail chapter 4.2) when the catalyst is not fully warmed-up. Due to an elevated engine load in the WLTC, the catalyst is warmed up more quickly so that the cold start phase takes less time. Additionally, this cold start effect is mitigated in the WLTC due to the total distance being more than double as large compared to the NEDC (cf. table 3.1).

Note that the NEDC tests were not conducted for certification purposes which include many more details specified by the EU, e.g. the best choice of tires or the best preconditioning of the vehicle. For that reason, NEDC emissions partly exceed the Euro-5 limits for NO_x (180 mg/km) and CO (500 mg/km). However, the purpose here is to show the expected repeatability of test cell measurements and set this as a basis for the on-road trips.

The repeatability is different for each of the emission gases. Although the test conditions were similar for all tests, there are non-reproducible testing conditions

as well as inaccuracies of the measurement equipment that cause different emission values.

Figure 3.1 shows the best repeatability for CO₂ emissions with a CoV of 1-3%. Compared to the other emissions, CO₂ was emitted at a much larger concentration and can be measured much more accurately. Additionally, the time delay of the exhaust arriving the analysers is optimized for CO₂ measurements. The CoV for NO_x is on a level of 10% over the WLTC and 20% over the NEDC. The NO_x aftertreatment technology in this vehicle is a Lean NO_x Trap (LNT), which was designed to reduce NO_x emissions at lower engine load. This strongly depended on the history of the LNT at the start of the cycle, thus, different starting points led to different NO_x results. CO and HC emissions showed a poor repeatability of 20 to 30%. The CoV for HC over the WLTC was even higher, however, occurring on a very low emission level.

3.1.2 Correlation of PEMS with Test Cell

Correlation tests were performed between test cell and PEMS equipment. Figure 3.2 shows distance specific CO₂ and NO_x emissions obtained from different test cycles in order to cover a larger range of emissions.

Both CO₂ and NO_x data show a linear correlation with R² values of 0.94 and 0.96, respectively. The slope of the linear regression lines deviate from the 1:1 correlation for 15 and 4% for CO₂ and NO_x, respectively, i.e. PEMS values are generally slightly above test cell values. Note that test cell and PEMS distance specific emissions are calculated based on different exhaust flows measured at different positions. Generally, there is a good agreement between PEMS values and the established test cell equipment.

3.2 Particulate Emissions

The performance of the PN PEMS was investigated by the correlation of experimental data with results obtained with established regulatory test cell equipment.

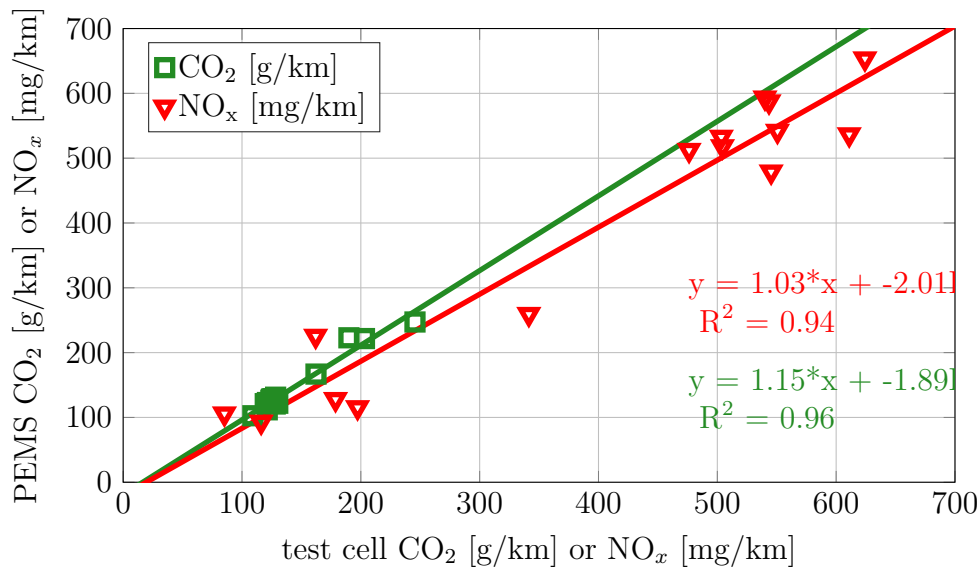


Figure 3.2: Correlation map of distance specific gaseous emissions on different cycles between PEMS and test cell.

The preconditioning stage consisting of a hot diluter and an evaporation tube from the PN PEMS is similar to the PMP equipment, however, the measurement position as well as the detector principle are different (cf. chapter 2).

Second-by-second PN (in particles per second) was obtained by multiplying the PN concentration provided by the PN PEMS with the exhaust volume which was measured at the CVS tunnel. The result is very sensitive to the time alignment between concentration and exhaust volume, a few seconds offset can cause up to 50% PN difference over the complete test cycle. The PN PEMS concentration has a different time basis compared to the PN counts and the exhaust volume provided by the test cell. Therefore, the PN PEMS concentration trace was shifted in steps of 1s relative to the exhaust flow of the test cell. In each step the PN PEMS result in s^{-1} was calculated by multiplying PN concentration with the exhaust volume and the mean quadratic deviation from the PMP PN counts was calculated. The best time alignment between PN PEMS and test cell equipment was then given by the lowest deviation value. This least square method does not determine the best correlation between peaks of concentration and exhaust volume, because the exhaust volume is detected instantaneously after generation in the engine, whereas

particles need some time in the order of seconds to be transported to the tailpipe.

3.2.1 Correlation of PN PEMS with PMP

Figure 3.3 shows two PN time traces visualizing the correlation of the results obtained with the PN PEMS and the PMP set-up in the test cell. The upper graphs show measurements with the gasoline vehicle V4 (cf. table 2.2) on a WLTC 5.3 having PN emissions in the $1 \cdot 10^{12} \text{ km}^{-1}$ range.

The PN PEMS emission data deviate less than 5% from the PMP results. Corresponding peaks from the PN PEMS and the test cell particle counter are at the same positions, however, their shape appears to be different. The test cell peaks are lower and wider, which is mainly due to the sampling position. The Integral over every single peak is within the experimental error identical for both measuring techniques. Particle losses due to thermophoresis or coagulation are accounted for in the calibration of the PN PEMS.

DPF equipped Diesel vehicles emitted significantly lower overall PN emissions (bottom graphs of figure 3.3) in the range of $1 \cdot 10^9 \text{ km}^{-1}$ over the NEDC. The results from the PN PEMS differ for more than one order of magnitude from the corresponding test cell values and also the peak correlation is much worse. At this low emission level the PN PEMS reaches its detection limit: The mean sensor concentration during this run was around 500 cm^{-3} , which is below the detection limit given by the manufacturer (cf. table 2.1). Considering a typical dilution of 10 at this emission level, the mean concentration in the system is 5000 cm^{-3} . This is consistent with a report of the Joint Research Centre (JRC) in Ispra, Italy, in which high measurement uncertainties below particle concentrations of 10000 cm^{-3} were found [Giechaskiel2014].

A more general view on the performance of the PN PEMS is provided in the correlation maps in figure 3.4. Several driving cycles such as NEDC, world harmonized light-duty test cycle (WLTC) 5.3 and other laboratory cycles representing on-road driving were conducted with different test vehicles (Diesel and gasoline operated) producing PN emissions varying over several orders of magnitude.

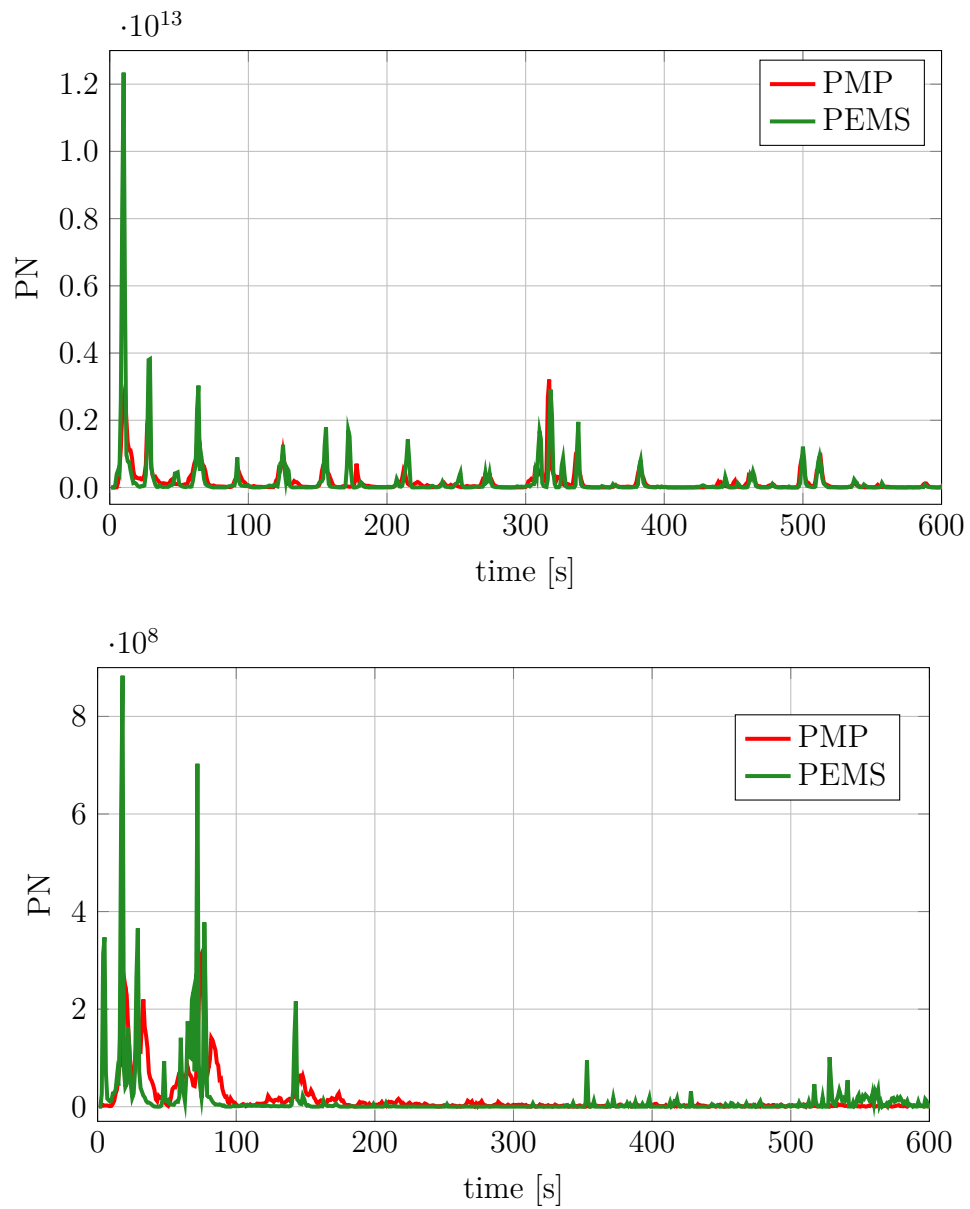


Figure 3.3: Two examples of a correlation measurement of the PN PEMS with the PMP set-up. At large emissions the PN PEMS shows very good performance (upper figure), however, at low-level PN emissions the PN PEMS comes to its detection limit (lower figure).

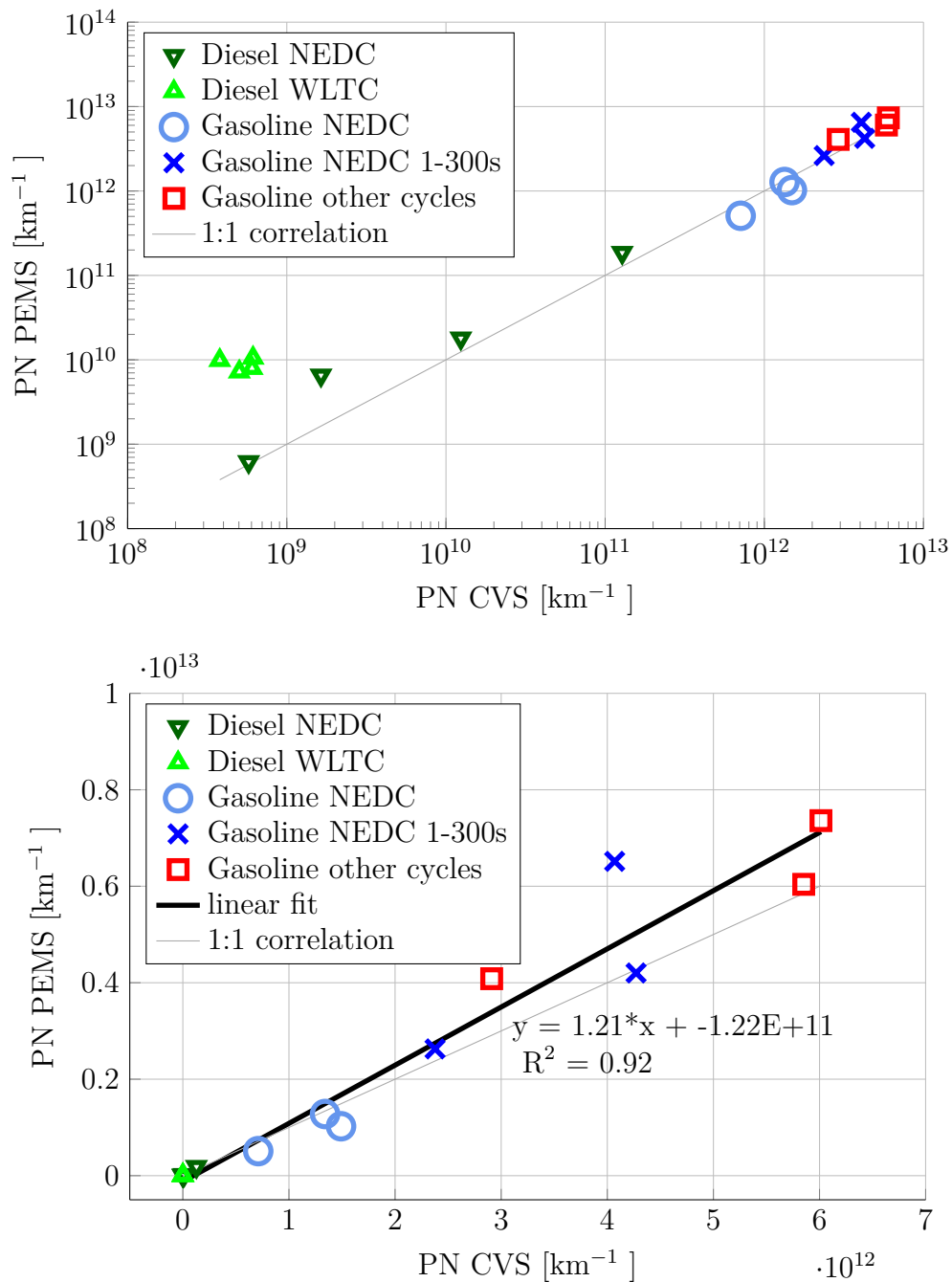


Figure 3.4: Correlation measurement of the PN PEMS with the PMP set-up. At emission levels in the $6 \cdot 10^{12} \text{ km}^{-1}$ range the data show a very good correlation (upper figure), however, at low-level PN emissions ($< 1 \cdot 10^{10} \text{ km}^{-1}$) the PN PEMS reaches its detection limit (lower figure).

Plotting the data in double-logarithmic scale (upper plot), PMP data points in the region $< 1 \cdot 10^{10} \text{ km}^{-1}$ deviate significantly from the 1:1 PN PEMS correlation line. Thus, a limit of detection of the PN PEMS around $1 \cdot 10^{10} \text{ km}^{-1}$ is inferred, which is more than one order of magnitude below the current NEDC Diesel PN emission limit.

The linear scale diagram in Figure 3.4 (lower plot) shows a good linear correlation of the data points with a coefficient of determination R^2 of 0.92. In this calculation all data $< 1 \cdot 10^{10} \text{ km}^{-1}$ were not considered as they are below the detection limit of the PN PEMS. The slope of the regression line is 1.21 ± 0.26 (95% confidence interval) and indicates that the PN PEMS generally records around 20% higher particle counts than the test cell equipment. This deviation probably results from coagulation effects and differences between the detection principles. The PN PEMS is factory calibrated with a PMP device using an 80nm standard aerosol (cf. table 2.1), however, more dynamic test cycles may lead to larger coagulation effects inside the transfer hose from the tailpipe to the CVS entrance and also inside the CVS tunnel. Additionally, particles with sizes differing from 80nm lead to further deviations between the PMP system and the PN PEMS due to the different detection principles. These results are again in-line with the before mentioned study conducted by the JRC which reports differences of -30% to 20% between both instruments [Giechaskiel2014].

Smaller particles with diameters between 10 and 23nm that are detected by the PN PEMS but not completely by the PMP set-up, can only account for a small fraction of the presently observed difference. Figure 3.5 shows a typical unimodal particle size distribution for a gasoline vehicle under real-world conditions with a geometric mean diameter of 45 to 60nm [Khalek2010; Li2013; Maricq1999c]. Assuming a PMP detection efficiency of 50% and 90% at 23 and 41nm, respectively [Giechaskiel2012], as well as a 50% efficiency at 10nm for the PN PEMS, the particle number difference between both systems theoretically accounts for less than 10%.

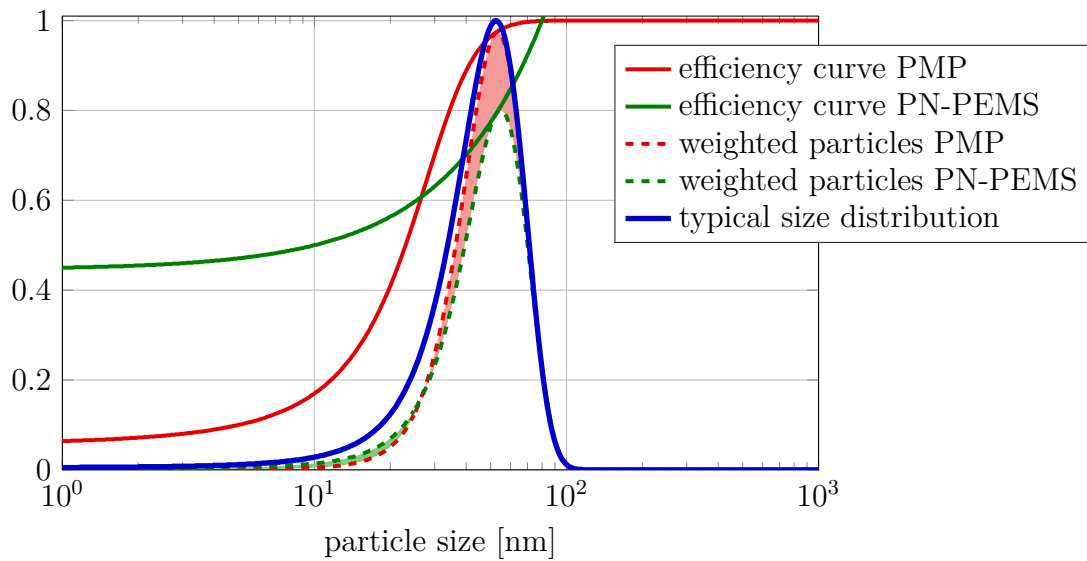


Figure 3.5: The PN difference between PEMS and PMP set-up, assuming a typical unimodal particle size distribution. Due to the different shapes of the efficiency curves, either the PN PEMS (green area) or the PMP set-up (red area) measures higher PN values dependent on the particle size. The difference theoretically makes up less than 10% of all particles.

3.2.2 Soot Measurements

Photo acoustics is an established method for investigating soot mass in vehicle exhaust. Soot measurements were conducted using a Photo Acoustic Soot Sensor (PASS) of an AVL M.O.V.E PM PEMS in parallel with the PN PEMS. The PM PEMS was connected to the tailpipe of the vehicle, as well. Three laboratory tests representing on-road driving were conducted with both instruments in parallel. As an example, figure 3.6 shows the time traces of the PN and soot sensor concentrations for one laboratory test. The time alignment method was based on a discrete cross-correlation method. For every possible offset between both signals, the largest correlation was calculated and the corresponding offset value represented the best time alignment.

Qualitatively, there was a good temporal correlation between PN and soot having a PN-to-soot ratio of $1.3 \cdot 10^{12} \text{ mg}^{-1}$. Three test cycles combined yielded a ratio of $1.3 \cdot 10^{12} \pm 2.8 \cdot 10^{10} \text{ mg}^{-1}$. This appeared to be in good agreement with pre-

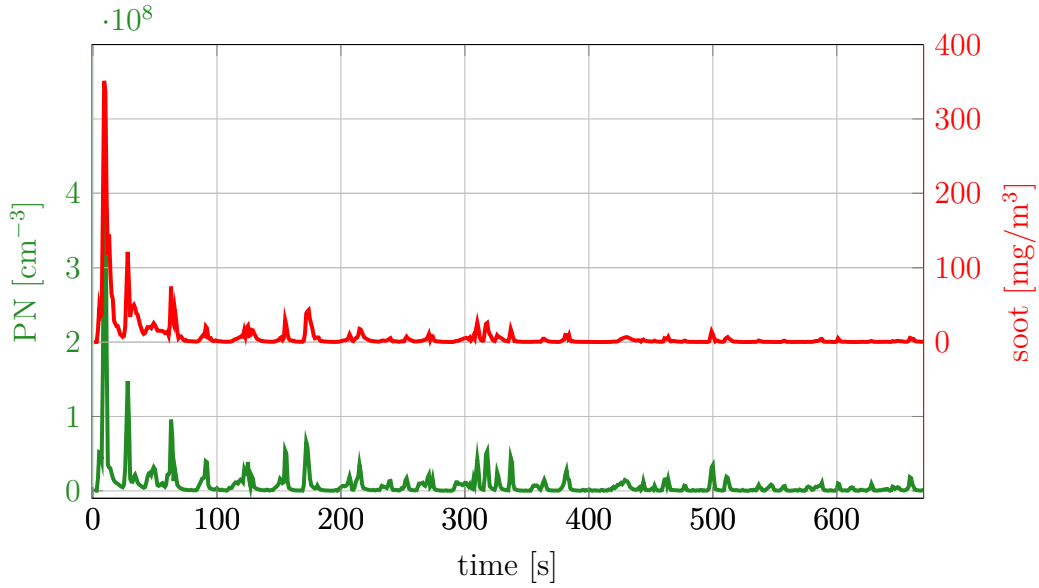


Figure 3.6: PN PEMS and PM PEMS sensor concentrations for a laboratory test representing on-road driving of a DI-gasoline Euro-5 vehicle. The PM PEMS graph is shifted upwards for better visualization. Both signal traces are qualitatively in good agreement, the PN-soot-ratio is $1.5 \cdot 10^{12} \text{ mg}^{-1}$.

vious studies. Kirchner et al. (2010) found a PN-to-soot ratio of $1.8 \cdot 10^{12} \text{ mg}^{-1}$ for a DPF Diesel vehicle [Kirchner2010], Maricq et al. (2011) reported a ratio of $2 \cdot 10^{12} \text{ mg}^{-1}$ for a gasoline direct injection vehicle [Maricq2011] and Khalek et al. (2010) suggested a correlation of $3 \text{ to } 4 \cdot 10^{12} \text{ mg}^{-1}$ [Khalek2010]. In another more extensive study, data from about 50 light duty vehicles were collected and showed that most PN-to-soot ratios ranged between $1 \cdot 10^{12}$ and $6 \cdot 10^{12} \text{ mg}^{-1}$ [Giechaskiel2012].

Chapter 4

Results of On-road Emission Measurements

4.1 Impact of Driving Style and Repeatability

Driving style is known to have a significant impact on fuel consumption and exhaust emissions. Several attempts were published to investigate the impact on exhaust emissions during test cell operation [VanMierlo2004; Berry2007]. First on-road tests addressed the difference of defensive and aggressive driving style on numerous Diesel and gasoline vehicles [DeVlieger2000; Tsirakis2007], but did not characterize the trips by driving parameter and did not choose an RDE compliant test route as stated in [RDE2016].

Three different driving styles were applied in order to investigate the impact of driving dynamics on the measured exhaust emissions. “Normal” trips were supposed to be driven by the drivers’ own estimation, “soft” trips included slower acceleration, longer roll-out times, earlier gear shift and partly smaller maximum speed on the motorway. Some tests were also intentionally driven in a “severe” way representing a clear misuse and non-normal driving. Severe driving was carried out by stronger acceleration, later braking and partly higher maximum speed on the motorway (up to 180 km/h)

Several parameters were introduced in order to characterize and quantify the driving style of the PEMS trips. Additionally to RPA (equation 3.3) and MPA (equation 3.2) that were already introduced in chapter 2, the parameters average velocity and urban idle fraction were calculated and compared to reference data. The average velocity is calculated from second-by-second data over the complete

trip. Urban idle fraction denotes the ratio of idle seconds during a trip, i.e. velocity ≤ 3 km/h, and the total duration of urban driving.

Another relevant driving parameter that is also included in the RDE regulation draft is the parameter $v \cdot a_{pos}$. Similar to RPA, it considers the second-by-second product of velocity and positive acceleration. For $v \cdot a_{pos}$ normally the 95% percentile is considered, i.e. the value where 95% of all values are lower. The parameter $v \cdot a_{pos}95$ was calculated according to equation 4.1 where P_{95} represented the 95% percentile, a_i^+ the positive acceleration at data point i and v_i the corresponding velocity.

$$v \cdot a_{pos}95 = P_{95}(v_i \cdot a_i^+) \quad (4.1)$$

The driving parameters of the PEMS trips were compared to reference values obtained from the test cycle WLTC 5.3 and from FOT databases. Field Operational Test (FOT) data were evaluated from normal people driving their private cars in everyday life. For every trip the validity was checked and driving parameters were calculated. FOT reference values resulted from the mean of the driving parameters for all valid trips.

Based on the classification into the different driving styles, distance specific exhaust emissions were depicted and the repeatability of emissions was evaluated. All the PEMS trips were conducted on working days outside rush hours with moderate traffic volume, thus, the traffic situations could be assumed to be comparable.

4.1.1 Characterization of PEMS Trips

4.1.1.1 RDE Compliant Route

Route R1 was designed for the conformity with the current RDE regulation draft (cf. section 2.4). On this route the driving style was evaluated by PEMS trips with the Diesel vehicles V1 and V2 as well as the gasoline vehicle V4 (cf. table 2.2). The driving parameters RPA, MPA, average velocity and urban idle fraction of the vehicles are shown in figure 4.1 in comparison to WLTC and FOT reference values. The bar height represents the mean of different tests under the same

driving conditions. If more than one test was conducted, the range bar represents the standard deviation for each parameter. The most robust values are given for vehicle V1 because these values are based on totally 17 PEMS trips.

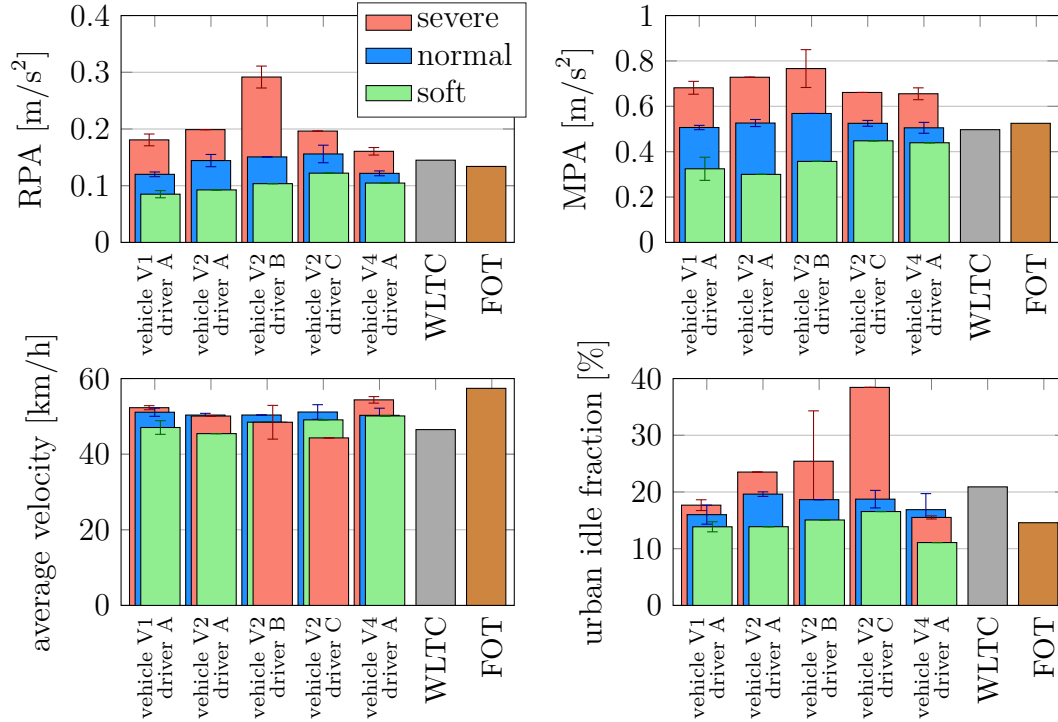


Figure 4.1: Driving Dynamics of the PEMS trips separated for vehicles V1, V2 (both Diesel) and V4 (gasoline) for different drivers on route R1. WLTC and FOT data are given as reference values.

The acceleration based driving parameters RPA and MPA showed a good differentiation of soft, normal and severe trips. In general, severe driving caused a strong increase of 30 to 40% compared to normal driving. Solely the RPA value for driver B almost doubled from normal to severe driving while the MPA value increased for only 40%. This indicated that driver B caused primarily strong accelerations during high velocity sections.

The average velocity shows no clear separation of the driving styles with the trips mostly in the range between 40 to 52 km/h. Although all trips were conducted at the same time of the day, different traffic situations especially in the city centre with numerous traffic lights and other road users lead to deviations

between trips of same driving style represented by the range bars [Gallus2017].

The CoV was calculated for vehicle V1 due to the availability of a sufficient number of trips for each driving style. RPA values ranged from 3.5 (normal) from 7.5% (soft) and MPA values from 1.9 (normal) to 15.7% (soft). Normal driving style was found to be easiest to repeat during different with CoV values of a few percentage. The repeatability of soft and severe driving is limited due to the difference to normal traffic conditions.

The PEMS results are compared to two reference values. The WLTC (version 5.3) is a chassis dynamometer driving cycle that is supposed to represent typical driving conditions (cf. chapter 2). Additionally, FOT values are depicted in figure 4.1 that were evaluated by 1672 trips from eleven vehicles with similar specifications as vehicle V1. For the calculation only PEMS like trips longer than 10km with at least 20% of each urban, rural and motorway part were chosen, leading to a total duration of 821 hours and a distance of 47737 km.

The driving dynamics of the normal PEMS trips are comparable to WLTC data, indicating the PEMS trips to lie in reasonable ranges, especially for the acceleration based parameters RPA and MPA. The FOT reference parameters can directly be compared to the results from vehicle V1. They show similar values compared to PEMS and WLTC results for the normal driving style. The urban idle fraction for vehicle V1 is close to the FOT value, however, the WLTC value is about 30% higher which is similar to vehicle V2, driver A. Thus, urban idle fraction shows a strong dependency on traffic conditions and varies in a normal bandwidth of 15 to 20%. The FOT average velocity is slightly higher than the respective WLTC value. This is probably due to higher velocities on the motorway that are included in the FOT data and not in the WLTC with a maximum velocity of 130 km/h. PEMS values, however, lie in a reasonable range between WLTC and FOT data [Gallus2017].

The driving parameter $v \cdot a_{pos}^{95}$ was calculated according to equation 4.1 and plotted against the average velocity for the different road types (figure 4.2). Urban, rural and motorway parts were determined using second by second velocity limit values of $v \leq 60$ km/h, $60 > v \leq 90$ km/h and $v > 90$ km/h, respectively. This

velocity classification as well as the upper limit separating severe from normal driving were taken from the current RDE regulation draft [RDE2016].

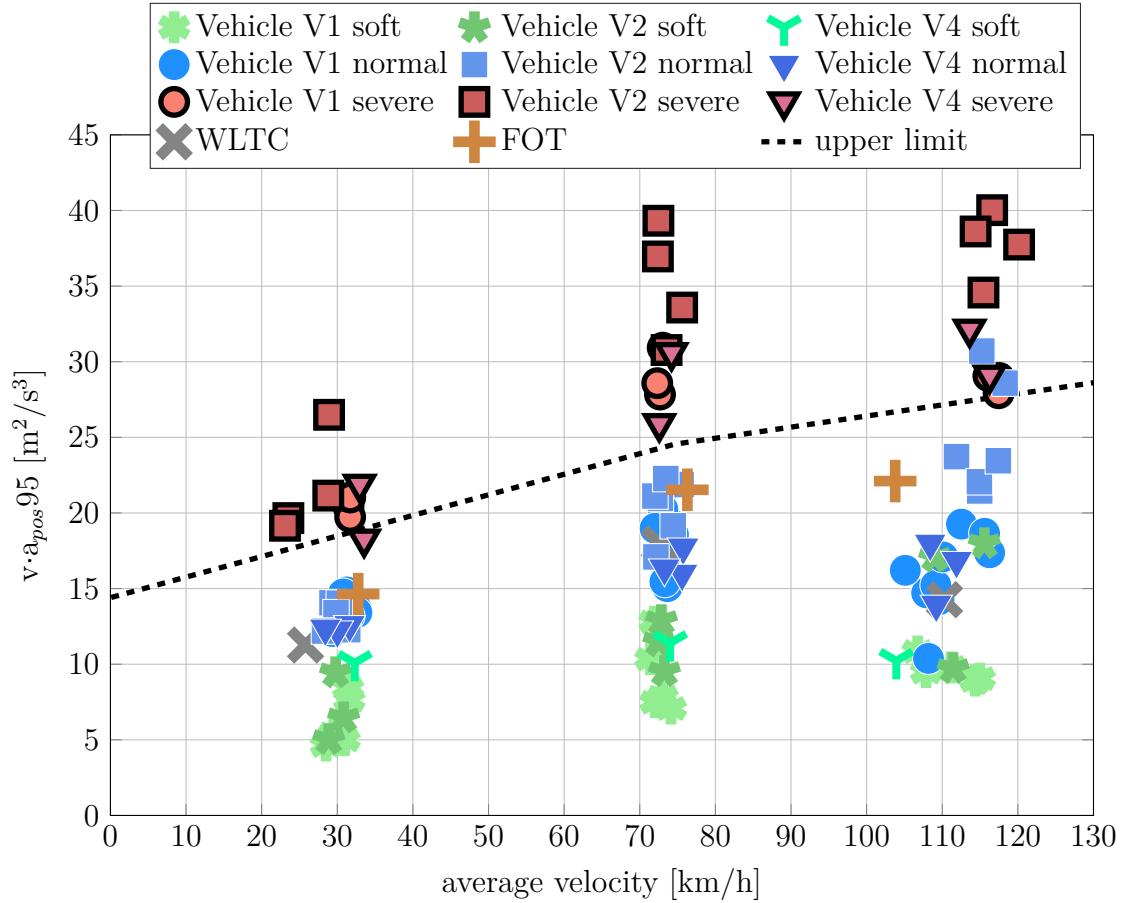


Figure 4.2: The 95th percentile of the parameter $v \cdot a_{pos}$ plotted against the mean velocity. Each trip is divided into urban, rural and motorway sections determined by velocity limits of 60 and 90 km/h . There is a distinct separation of severe tests from normal tests.

The motorway data showed a larger velocity bandwidth due to a strong dependence on non-reproducible traffic conditions. There is also a distinct separation of severe from normal trips given by the upper limit plotted in figure 4.2. All severe tests were above the upper limit confirming that these tests included non-normal driving. Note that two motorway data points from normally driven trips were slightly above the upper limit.

In addition, corresponding $v \cdot a_{pos}$ 95 values of the WLTC and FOT data were

plotted in figure 4.2. The FOT data do not cover all kinds of vehicles and drivers, the inclusion of vehicles with less power would likely lead to lower $v \cdot a_{pos95}$ values. However, both WLTC and FOT data showed similar values below the upper limit and could be attributed to normal driving which has already been concluded for MPA and RPA values. Rural and motorway FOT data showed a higher and lower average velocity, respectively, compared to PEMS and WLTC data. This observation could be attributed to a higher amount of motorway FOT trips conducted during high traffic periods, which led to a decrease of the mean velocities on the motorway and thus contributed to elevated numbers on rural parts. Generally, the PEMS values are in reasonable ranges compared to WLTC and FOT data indicating normal driving in terms of average velocity and $v \cdot a_{pos95}$ values [Gallus2017].

In summary, the acceleration based parameters, i.e. RPA, MPA and $v \cdot a_{pos95}$, appeared to be appropriate for the characterization of PEMS trips, particularly in comparison to WLTC and FOT reference data. This confirmed the normal PEMS trips to be attributable to normal driving.

4.1.1.2 Cold and Hot Start Comparison

The parameters RPA, MPA, average velocity and urban idle fraction were chosen to characterize and quantify different driving styles for vehicles V0 and V3 over the urban part of route R0 (cold and hot start). An overview of the driving dynamics is shown in figure 4.3, the bar height represents the mean and the range bar the standard deviation for each parameter. For better illustration, the normal driving styles of two different drivers were combined for vehicle V0 which did not change the main result.

Both RPA and MPA showed increased values from normal to severe driving. The mean velocity and urban idle fraction were rather similar for all driving styles, probably due to the predominant dependence on traffic situations, especially in the city centre with numerous traffic lights and other road users.

Regarding cold start tests, the vehicle was soaked outside overnight to fully adjust to ambient conditions. In figure 4.3 normal cold and normal hot trips

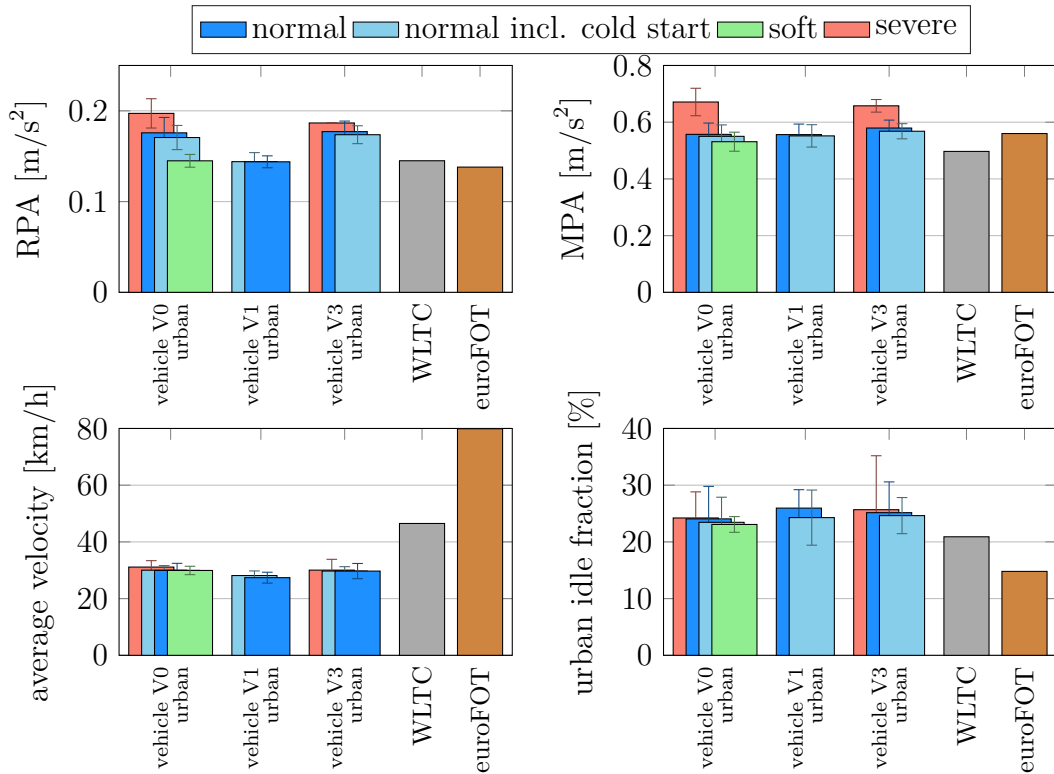


Figure 4.3: Comparison of parameters considering driving dynamics for vehicles V0 and V3. Route R0 was evaluated separately for urban and motorway parts. Severe trips include stronger acceleration, later braking and higher maximum speed on the motorway (up to 180 km/h).

showed equal values for all driving parameters, indicating a similar driving style which was essential for the cold start analysis in chapter 4.2.

RPA, MPA and urban idle fraction values of the WLTC were generally higher than those of the present PEMS trips. The WLTC represents typical driving conditions and includes all urban, rural and motorway driving. Urban only parts were expected to result in higher RPA and MPA values due to an elevated number of stop and start events.

The euroFOT database contains data of numerous trips that were collected in the framework of a large EU research project and that were driven by independent people with their private cars in everyday life [Benmimoun2011]. The bars in figure 4.3 were calculated using a data-subset of trips with the same engine as in

vehicle V3 but with manual transmission. RPA and MPA values are similar to the WLTC data while average velocity and urban idle fraction are different compared to WLTC data. The euroFOT data include a large amount of motorway parts which explains the large average velocity and the small urban idle fraction.

The comparison of RPA and MPA parameters of the PEMS trips to WLTC and euroFOT parameters demonstrated that the present “normal” driving style of the PEMS trips was within reasonable ranges, similar to the Diesel results. As expected, severe driving showed much larger values and was not representative for normal driving. Average velocity and urban idle fraction of the PEMS trips were similar to WLTC values, as well. Differences to euroFOT data could be explained by different driving situations.

4.1.2 Effect on Emissions

4.1.2.1 Gaseous Emissions of Diesel Vehicles

The gaseous emissions CO_2 , NO_x , CO and HC measured by the PEMS for the three Diesel vehicles were evaluated in terms of repeatability and driving style. The emissions were classified into the driving styles soft, normal and severe separately for different vehicles and drivers.

Figure 4.4 shows the distance specific emissions for vehicles V0 and V1 on the urban (cold and hot start) and the motorway part of route R0. The bar height and the range bar represent the mean emission and the corresponding standard deviation, respectively. The emissions were normalized to the corresponding normal trip value for each driver and vehicle. Uncertainties between trips of the same driving style were a superposition of different ambient conditions (temperature range from -3 to 28°C , wind, humidity), non-reproducible traffic situations and small deviations in driving dynamics as described by driving parameters (compare previous section).

In general, the urban soft trips of vehicle V0 had similar or even higher emissions than the corresponding urban normal trips which could not be explained by the driving dynamics (cf. previous section) or other available parameters.

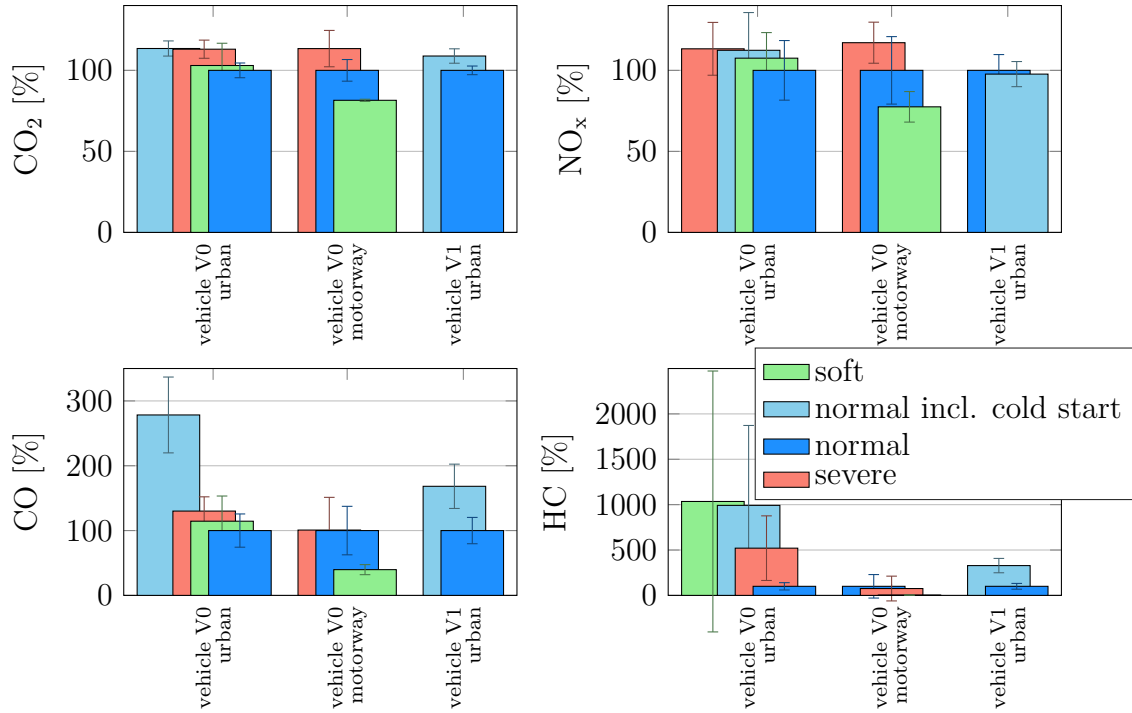


Figure 4.4: Impact of the driving style on gaseous emissions of the PEMS trips for vehicles V0 and V1 on route R0 (urban and motorway part).

CO₂ and NO_x emissions showed similar values for the urban cold start and for the urban severe trip, indicating a similar impact of the driving style and the cold start on these emissions (around 20% larger compared to urban normal trips). Only the NO_x results for vehicle V1 were similar for the cold and hot starts. The motorway emissions for vehicle V0 showed the expected order of severe, normal and soft driving with a repeatability of $\pm 30\%$.

For CO, the urban cold start caused almost three times as much compared to the urban normal trips which is a far larger effect than the driving style (about 30%). For HC emissions, a tendency towards elevated emissions for cold starts and for urban severe driving was observed, however, the range bars are too large to conclude a serious result.

The best repeatability of vehicle V0 was observed for CO₂ emissions (CoV about 4%), NO_x emissions were measured within 20%. Partly, these values could be explained by the variations of the driving dynamics (cf. previous section). The

range bars of CO emissions were comparable to those of NO_x , the largest were observed for the urban cold start with a CoV of about 30%. CO emissions for vehicle V0 showed a larger increase compared to vehicle V1 which is likely due to the different ambient temperature ranges. CO and HC cold start emissions were expected to strongly depend on the ambient temperature (4 to 24°C and -3 to 28°C for vehicles V0 and V1, respectively) but no explanation was found for the large range bars of HC hot start emissions.

Gaseous emissions for vehicles V1 and V2 for the three driving styles and separated for different drivers are depicted in figure 4.5. All trips were conducted on route R1, thus, route effects such as road grade were not relevant. The ambient temperature ranges for vehicles V1 and V2 were 0 to 12°C and 2 to 29°C, respectively.

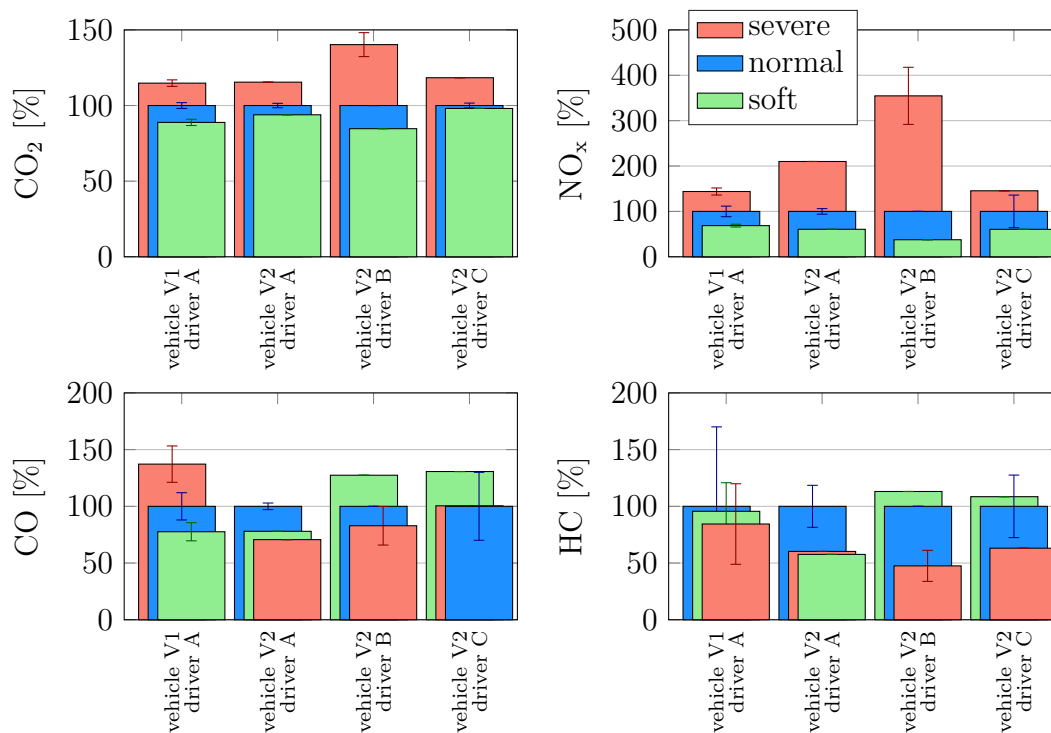


Figure 4.5: Impact of the driving style on gaseous emissions of the PEMS trips separated for different vehicles and drivers. CO_2 and NO_x emissions show good driving style correlation [Gallus2017].

Figure 4.5 shows a strong influence of the driving style on CO_2 and NO_x emis-

sions. Similar to vehicle V0, compared to the normal values, severe driving caused an elevation of 20 to 40% for CO₂, NO_x increased for 50 to 255% depending on the driver and the vehicle. Especially for driver B, elevated CO₂ and NO_x emissions caused by severe driving, were explained by an almost 100% higher RPA value (cf. figure 4.1).

In contrast, there was no distinct separation of the driving style for CO and HC emissions illustrated by larger range bars (except of CO for vehicle V1, driver A). Probably for CO and HC other impacts than driving style were more dominant, e.g. ambient temperature or the cold start.

The effect of the ambient temperature was evaluated by only considering PEMS trips conducted in a small temperature range of 5 to 8°C measured by the in-car intake airflow temperature sensor (not visible in figure 4.5). While CO₂ and NO_x emissions were just slightly different compared to those depicted in figure 4.5, CO and HC showed completely different results, indicating the temperature effect likely to have a higher impact on these emissions than the driving style [Gallus2017].

For comparison, in an ICCT study PEMS data were classified into four different driving situations characterized by the instantaneous product of velocity and acceleration ($v \cdot a$) [ICCT2014]. Distance specific CO₂ and NO_x increased four to five times from low to high $v \cdot a$ values. However, due to the classification of second-by-second data, the results were not directly comparable to those observed in the present study but indicated the same trend. In another study, a performance index for the characterization of the driving style along an urban route was calculated [Fonseca2010]. A group of Euro-2 to Euro-5 Diesel vehicles showed an average CO₂ increase related to aggressive driving of around 40% which was in-line with the results found in the present study.

Figure 4.6 shows the normalized and cumulated NO_x emissions plotted against the parameter $v \cdot a$, which is the product of velocity and acceleration calculated for every second of all PEMS trips. The positive values of this parameter correspond to the previously mentioned parameter $v \cdot a_{pos}$. Three plots are depicted representing the driving styles normal, soft and severe on route R1.

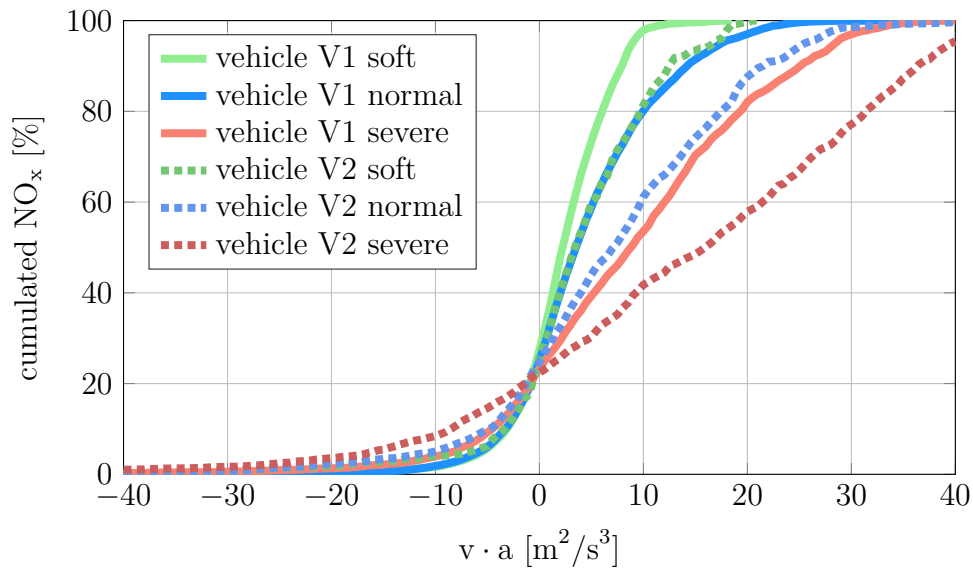


Figure 4.6: Cumulated NO_x plotted against the parameter $v \cdot a$ for vehicles V1 and V2. The three lines in the graph represent soft, normal and severe driving.

Compared to vehicle V1, the NO_x emissions of vehicle V2 occurred at higher $v \cdot a$ values which is likely due to different vehicle characteristics. Both vehicles showed equally for all driving styles at most 25% of NO_x emitted during deceleration or cruising events, i.e. accelerations below or equal to zero. Regarding positive values of the parameter $v \cdot a$, different trends for normal and severe driving were observed. Considering normal trips vehicle V1 emitted 90% of the NO_x at a moderate $v \cdot a$ value of 8 to 13 m^2/s^3 while severe driving showed a much steeper trend towards larger $v \cdot a$, as expected. As a comparison for normal driving, a mean velocity of 50 km/h and an MPA of 0.5 m/s^2 (cf. figure 4.1) led to an average positive $v \cdot a$ value of about 7 m^2/s^3 . This value corresponded to around 70% cumulated NO_x in figure 4.6 and by subtracting the 25% fraction for the non-acceleration part, it was close to the expected 50% [Gallus2017].

4.1.2.2 Gasoline PN Emissions

Several urban (with and without cold start phase) and motorway trips were performed for vehicle V3, partly driven in a severe driving style. An overview of

the PN emissions for the gasoline vehicles V3 and V4 is depicted in figure 4.7 in comparison to chassis dynamometer cycles and other PN data obtained from literature test cell results. In this plot the bar height and the range bar represent the mean PN emission and the standard deviation, respectively.

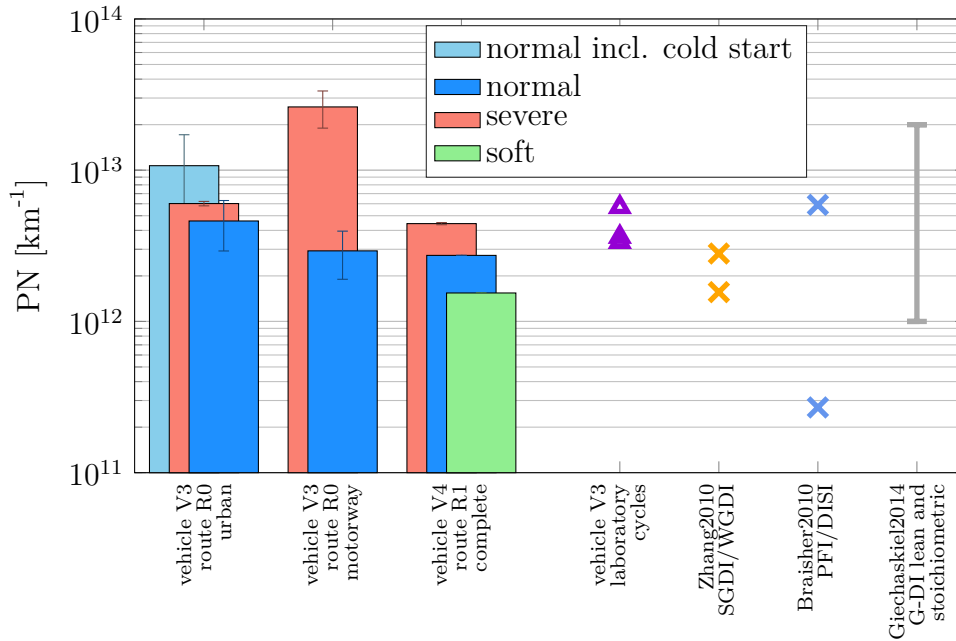


Figure 4.7: PN emissions of several PEMS trips conducted with the gasoline vehicles V3 and V4. The data were classified into driving styles and compared to laboratory cycles and literature values.

Driving style was an important parameter with a strong impact on the PN emission. For vehicle V3 urban tests showed just a small increase of PN from normal to severe style. This was in-line with the similar driving dynamics discussed in the previous section. The motorway trips showed a stronger increase of PN from normal to severe driving due to larger accelerations, higher velocities and higher power demand. The observed PN emissions were almost ten times higher compared to the normal driving style on the same route. Note that this severe driving style was not representative for normal driving.

Figure 4.7 also shows the PN emission data for urban PEMS trips including the cold start phase obtained within an ambient temperature range from 8 to 28°C for vehicle V3. The PN values including the cold start phase were larger than the

“urban normal” data with a large range bar and a coefficient of variance of about 50% indicating a large temperature dependency. The temperature trend of PN emissions is discussed in more detail in section 4.2.

Vehicle V4 was investigated on the RDE compliant route R1 including the complete cold start phase. Similar to vehicle V3 there was a good separation of the different driving styles in terms of the PN emissions. Severe driving led to double the high values for route R1 including urban, rural and motorway driving.

The PN PEMS results for both vehicles were compared to data from laboratory cycles representing on-road driving, and to test cell results from literature [Zhang2010; Braisher2010; Giechaskiel2012]. On-road PN emission data are within the same range as values obtained from test cycles, whereas separate cold start emissions and severe driving style led to elevated emission values, as expected.

Figure 4.8 shows the normalized and cumulated PN emissions plotted against the parameter $v \cdot a$, which is the product of velocity and acceleration for every second of all PEMS trips conducted with vehicles V3 and V4. The positive values of this parameter correspond to the previously mentioned parameter $v \cdot a_{pos}$. Three plots are depicted for each vehicle representing different driving styles as well as cold start emissions.

Similar to the cumulated NO_x emissions (cf. figure 4.6), PN emissions show a clear separation of severe trips from normal and soft driving. The most extreme trend was observed for the severe driving style of vehicle V3 which showed a nearly linear increase up to a $v \cdot a$ value of $60 \text{ m}^2/\text{s}^3$. 90% of the PN were emitted at a $v \cdot a$ value of $50 \text{ m}^2/\text{s}^3$ which was the largest value observed in the available data. Normal and cold start emissions showed 90% values at moderate $20 \text{ m}^2/\text{s}^3$ and $10 \text{ m}^2/\text{s}^3$, respectively. This difference indicated that cold start PN emissions primarily appeared during lower dynamics driving.

Figure 4.8 shows that at most 25% of PN was emitted during deceleration or cruising events, i.e. accelerations below or equal to zero. For vehicle V4, 90% of the PN was emitted at a moderate $v \cdot a$ value of 5 to $8 \text{ m}^2/\text{s}^3$ for soft and normal driving. Severe driving showed a much steeper trend towards larger $v \cdot a$,

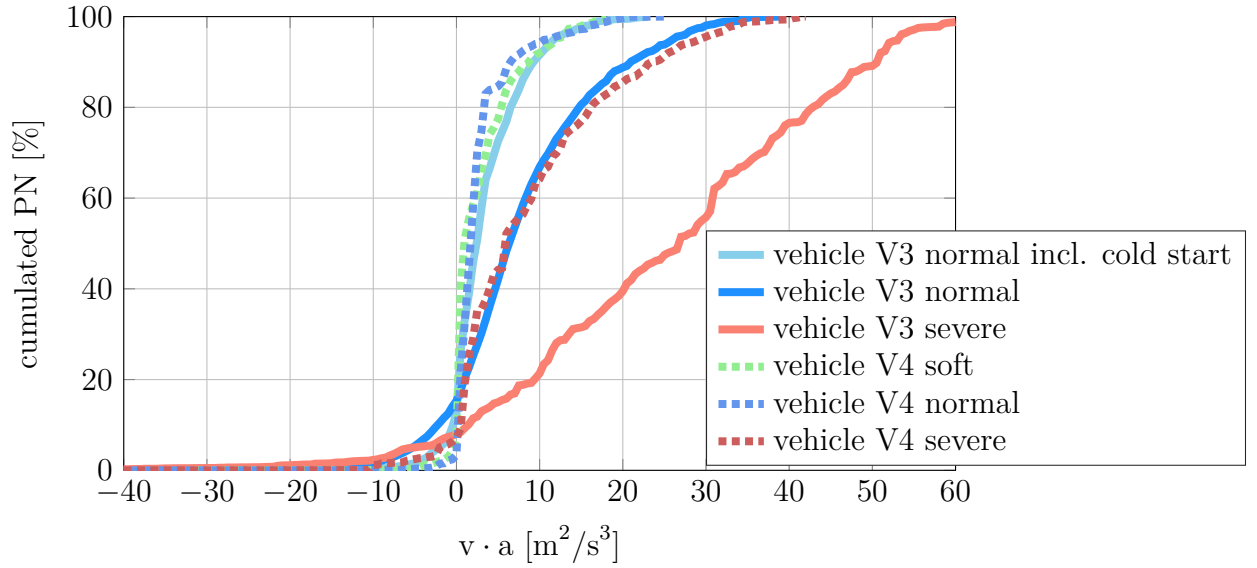


Figure 4.8: Cumulated PN plotted against the parameter $v \cdot a$ for vehicles V3 and V4 and different driving styles.

as expected, and reached the 90% PN at around $24 \text{ m}^2/\text{s}^3$. These results were similar to the cumulated NO_x , indicating a comparable trend of these emissions.

4.1.2.3 PN-PM-Correlation

The on-road performance of the PN PEMS system was investigated with the soot measurement unit of the PM PEMS as an independent particle measurement method running in parallel with the PN PEMS. The target of this experiment was a comparison of the PN-to-soot-ratio, calculated from on-road trips with data from several chassis dynamometer tests (cf. chapter 3).

For the PN-to-soot correlation only trips at ambient temperatures between 15 and 28°C were considered in order to be reasonably comparable with regulated test cell temperatures of approximately 22°C . The resulting correlation is shown in figure 4.9.

The PN PEMS shows good correlation with chassis dynamometer measurements and the PEMS driving style parameters are reasonable. The on-road performance of the PN PEMS was investigated by using the soot measurement unit

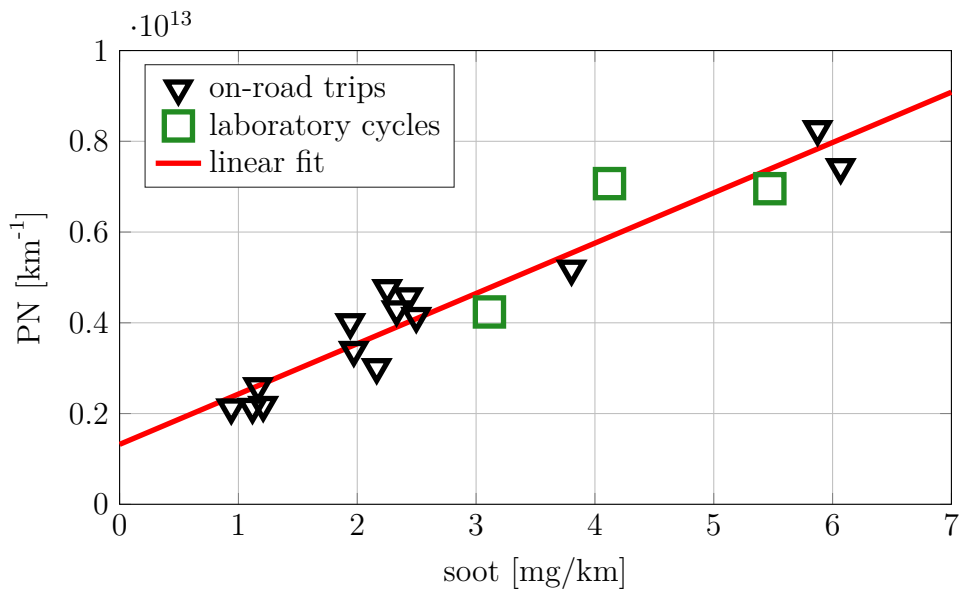


Figure 4.9: Particle emissions from PN PEMS and PM PEMS based on ten PEMS trips at ambient temperatures between 15 and 28°C. The slope of the regression line is $1.1 \cdot 10^{12} \text{ mg}^{-1}$, with a coefficient of determination R^2 of 0.93.

of the PM PEMS as an independent particle measurement method running in parallel with the PN PEMS. The target of this experiment was to compare the PN-to-soot-ratio calculated from real-world trips with that from several chassis dynamometer tests (cf. chapter 3).

For the PN-to-soot correlation only trips between 15 and 28°C ambient temperature were considered in order to be comparable with regulated test cell temperatures around 22°C. The resulting correlation map is shown in figure 4.9.

There is a good linear relation between PN and soot with a coefficient of determination R^2 of 0.93. The slope of the regression line represents the mean PN-to-soot-ratio. For the investigated vehicle a value of $1.1 \cdot 10^{12} \text{ mg}^{-1}$ was determined, which corresponds well to chassis dynamometer cycles (green squares in figure 4.9) as well as to literature values (cf. chapter 3). This result confirms a comparable performance of the PN PEMS operated in the vehicle driving on the road and in the laboratory.

4.2 Cold Start Effect

Cold start emissions of modern Diesel and gasoline passenger vehicles make up a considerable part of the total emissions between 10 and 30%, depending on the pollutant [Reiter2016]. Reduced emissions in the post cold start phase led to a larger share of the cold start to the total emissions [Weilenmann2013]. Cold start emissions are found to depend on numerous factors, such as engine stop time [Favez2009], ambient temperature [HBEFA2.1], the methodology [Andre2005] and the driving dynamics [Weilenmann2009].

CO, HC as well as PN show considerable increased emission values [Badshah2016] due to incomplete combustion and a reduced efficiency of the catalyst or particle filter (catalyst actively working above 200°C) [Favez2009]. The quantification of the cold start phase is represented by the term CSEE normally expressed in g/start or mg/start. Elevated CO₂ emissions are expected due to larger frictions at cylinder walls and a larger oil viscosity in the warming-up engine. The impact on NO_x emissions during the cold start phase is still not completely explained. NO_x formation is strongly triggered by high in-cylinder temperatures. During cold start the fuel-air-mixture is normally enriched in order to overcome the larger friction and oil viscosity. This effect leads to higher in-cylinder temperatures and excess NO_x production during the cold start phase [Bielaczyc2011].

In literature, the cold start effect was investigated on chassis dynamometers, an on-road evaluation based on PEMS measurements is still missing. Therefore the applied test methodologies were based on laboratory conditions and could not be easily transferred to on-road tests. Some studies investigated gaseous cold start emissions under laboratory conditions at different test cell temperatures [HBEFA2.1; Weilenmann2009; Bielaczyc2011; Dardiotis2013].

In the present study, two methods suggested in literature were applied on on-road PEMS tests and the cold start effect at a large range of ambient temperatures was evaluated. In literature, cold, warm and hot starts are controversially defined based on the engine-off time and engine coolant temperature [Reiter2016]. Here, cold start tests were conducted after the test vehicle had soaked overnight, i.e. after more than twelve hours engine-off time. After this duration the engine

coolant temperature was close to the ambient temperature. Ambient temperature was measured during the first few minutes of the PEMS trip. It was either derived from the ECU data or directly noted from the display inside the vehicle. Hot starts in this study refer to trips with a fully warmed up engine, including an engine coolant temperature at normal hot operating level, and actively working catalysts.

4.2.1 Definition of Cold Start Phase

The RDE regulation defines the end of the cold start phase when the engine coolant temperature reaches 70°C or at most 300s [RDE2016]. Based on this definition, for the present study the end of the cold start phase was defined as the engine coolant temperature was reaching 70°C. This criterion was always fulfilled before 300s after engine start. The engine coolant temperature signal was derived from the ECU data of the vehicle. Other limit definitions based on the duration or the covered distance were found not to be suitable to on-road tests. In real-world conditions the duration of the cold start phase strongly depends on the traffic situation and the possibility to heat up the vehicles components by accelerations of the vehicle. As no trip consists of identical driving situations, the end of the cold start needs to be dynamical in terms of distance and durations. The simplest method that considers driving dynamics during the heating up engine was the engine coolant temperature. Normally the catalyst has reached its operating temperature before the engine coolant temperature passes the 70°C marker [Andrews2004], so in most cases the complete cold start was covered by this definition.

As an example, the cold start effect is illustrated for the PN emissions conducted with the gasoline vehicle V3. Figure 4.10 shows the time traces of one cold and one warm start at an ambient temperature of 21°C, both trips have been conducted in a normal driving style.

There were elevated PN emissions during the cold start phase lasting for a maximum travel distance of 2km. After the cold start peak, the PN emissions decreased rapidly to the level of the hot start. In this example, the cold start accounted for about one third of the total PN emissions generated during the

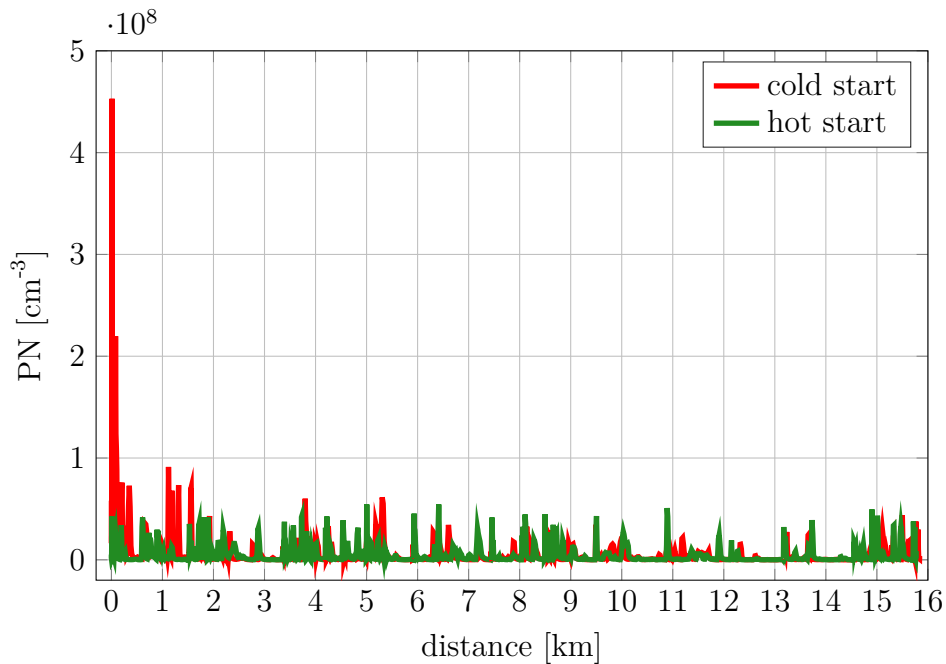


Figure 4.10: Comparison of the PN emissions of one cold start (red trace) and one hot start (green trace) at 21°C ambient temperature conducted with vehicle V3. A PN cold start peak was observed during the first two kilometers [Gallus2016].

entire trip. The engine temperature limit of 70°C was reached after 2.2km. From particle measurements between 20 and 37°C a cold start distance of less than 3.2km was reported [Robinson2010].

Figure 4.11 shows the cold start duration and distance for a large range of ambient temperatures conducted with vehicle V1. The cold start was evaluated with a limit of 70°C engine temperature for soft, normal and severe driving styles.

The cold start duration and distance of normal tests increased with decreasing ambient temperatures due to the lower starting temperature of the engine. Between ambient temperatures of 22 and -1°C both duration and distance doubled. The cold distance ranges between 4 and 8km, which is in-line other studies which reported an average cold start distance of 5.2km at 20°C for a large range of vehicles [Andre2005]. Note that the cold start distance for the Diesel vehicle was much higher than for the gasoline vehicle. This could be explained by a higher

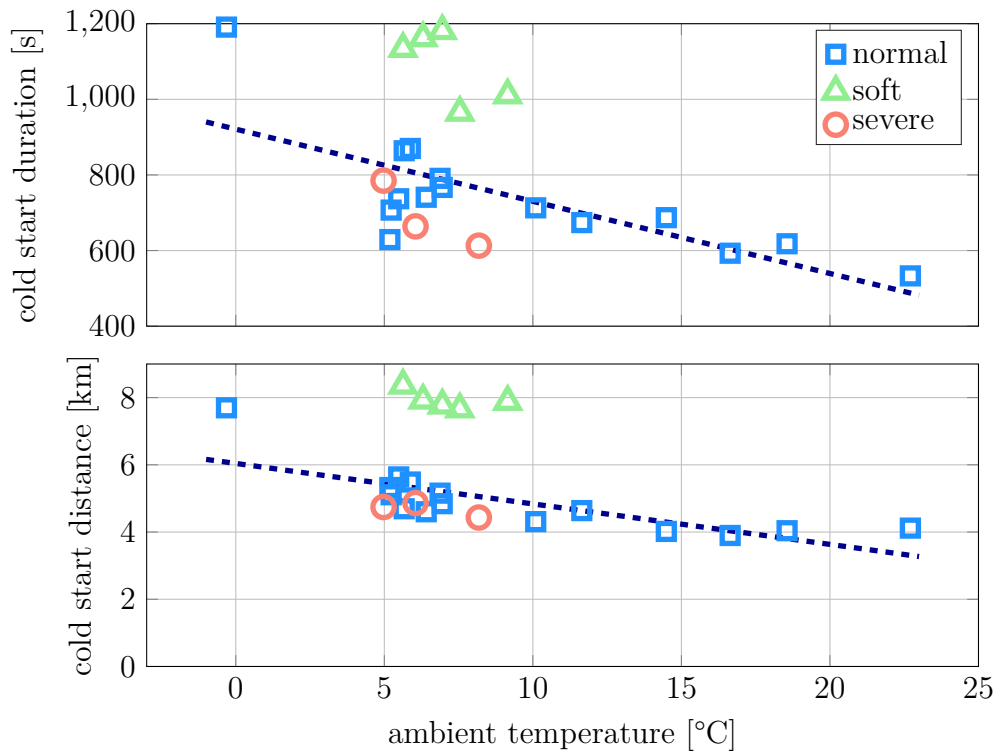


Figure 4.11: The cold start duration and distance plotted against the ambient temperature. The data include normal, soft and severe driving conducted by vehicle V1. The cold start phase was defined to end when the engine temperature reaches 70°C.

engine volume typical for Diesel compared to gasoline engines. The R^2 values for the linear regressions accounted for 0.58 and 0.61 for duration and distance, respectively. The influence of the driving style was also visible, as severe and soft trips lay continuously below or above normal data points. For comparison, the mean covered distance per trip in the EU was reported to be around 12km [EMEP2009], noting that not all trips were started with a cold engine. Thus, the cold start, as presented in figure 4.11, accounts for a significant part, e.g. it would make up almost half the distance at an ambient temperature of 10°C.

4.2.2 Methodology

The evaluation of the on-road cold start emissions was performed by two different methods. Both were adopted from methods presented in literature that were based on test cell measurements. The most accepted method for estimating CSEE is the application of a test cycle consisting of the repetition of one subcycle [Andre2005; Favez2009]. The amount of CSEE was calculated by subtracting the emissions from subcycles with hot engine from those including the complete cold start.

This cold-hot method was transferred to on-road measurements applying test route R0. The route started with an urban part which was repeated subsequently with a hot engine. The direct repetition of this urban part suggests similar ambient and traffic conditions, however, without completely reproducible conditions as in the laboratory. For this method, it was important to apply the same driving style for both cold and hot trips (cf. chapter 4.1). One urban part was around 15.6km and the cold start was included during all tests. The CSEE were calculated by subtracting the emissions obtained during the second urban part from the first urban part including the cold start.

The second method quantified the amount of cold start emissions over a complete driving cycle, such as the NEDC [Dardiotis2013] or the UDC [Bielaczyc2011]. In this context, the cold start emissions are the sum of CSEE and emissions that would occur with a fully warmed-up engine. In most cases, the emissions are presented as cold start and post cold start emissions.

This method was applied for the on-road cold start emissions of route R1. The cold start emissions were defined until an engine temperature of 70°C and the remaining part of the trip was defined as post cold start emissions.

In literature, a linear regression method was presented in order to calculate CSEE values for regulated and unregulated pollutants in the laboratory [Heeb2003; Favez2009]. This method is not presented here because it exhibited poor results for on-road driving. The basis for this method is the assumption that post cold start emissions can be fitted by a linear regression line whereby the y-axis interception represents the CSEE value. However, on-road emission

measurements especially during urban driving are dominated by numerous start-stop and acceleration events, thus, hot emissions normally do not show a linear trend.

4.2.3 Determination of Cold Start Emissions

4.2.3.1 Difference of Cold and Hot Start

The cold-hot method was applied to cold start trips conducted on route R0 with vehicles V0, V1 and V3. Figure 4.12 shows the gaseous CSEE values obtained from the Diesel vehicles for an ambient temperature range of -4 to 24°C. For illustration, the y-axis was normalized at 15°C by dividing the distance specific CSEE values by the corresponding CSEE value at 15°C.

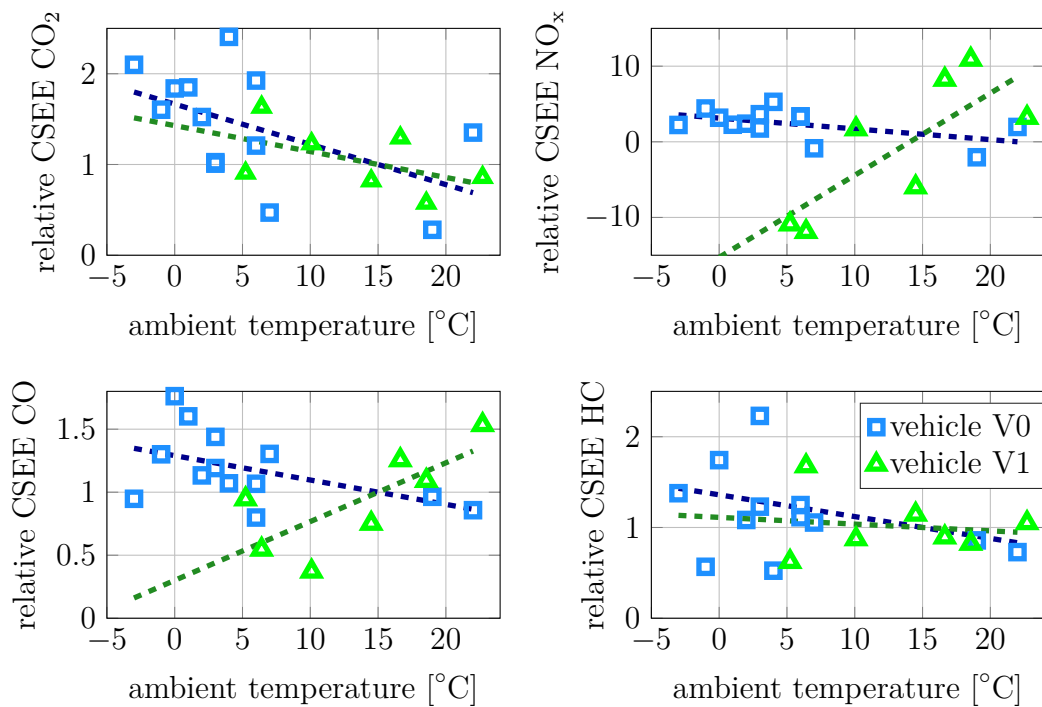


Figure 4.12: Gaseous CSEE values for vehicle V0. CSEE were calculated by subtracting the warm urban from the cold urban trip (route R0). The distance specific emissions were normalized at an ambient temperature of 15°C.

As expected, the gaseous CSEE for vehicle V0 generally showed larger values for lower ambient temperatures. The regression lines suggested a linear trend with poor R^2 values around 0.3, thus, other relationships could not be excluded. However, in another study the temperature dependency of CSEE was also modelled by a linear relationship and additionally confirmed by corresponding measurements [Weilenmann2009]. Especially for NO_x , a linear trend of the CSEE for a Euro-4 Diesel vehicle was found in the laboratory over a temperature range of -20 to 23°C .

Vehicle V1 showed similar results regarding CO_2 and HC emissions. However, an opposite trend was found for NO_x and CO with increasing CSEE values at higher ambient temperatures. NO_x CSEE were even negative below 15°C , indicating hot emissions being higher than cold start emissions. This temperature trend could be explained by too small differences between cold and hot emissions (cf. figure 4.14), leading to a high contribution of noise to the CSEE calculation. For CO, however, no explanation for the temperature trend of CSEE was found, neither in the data nor in the literature. This result is especially unexpected because CO cold start emissions are strongly reduced when the oxidation catalyst has reached the light-off temperature. For lower ambient temperatures this point is reached after a longer time period, leading to larger CO and HC emissions.

An expected linear trend was found for PN CSEE as shown in figure 4.13. Particle measurements with vehicle V3 were conducted over an ambient temperature range of 8 to 28°C . The y-axis was normalized at 15°C by dividing the distance specific CSEE values by the corresponding CSEE value at 15°C .

The R^2 value for the linear regression of PN CSEE was 0.42. The data point at 8°C suggested a non-linear relationship, however, considering this data point as an outlier, the R^2 value was even reduced to almost 0.34. The PN CSEE increased by a factor of 40 from 25 to 8°C . As there was no direct comparison found in literature, this trend needs to be verified by a higher amount of low temperature measurements with several vehicles.

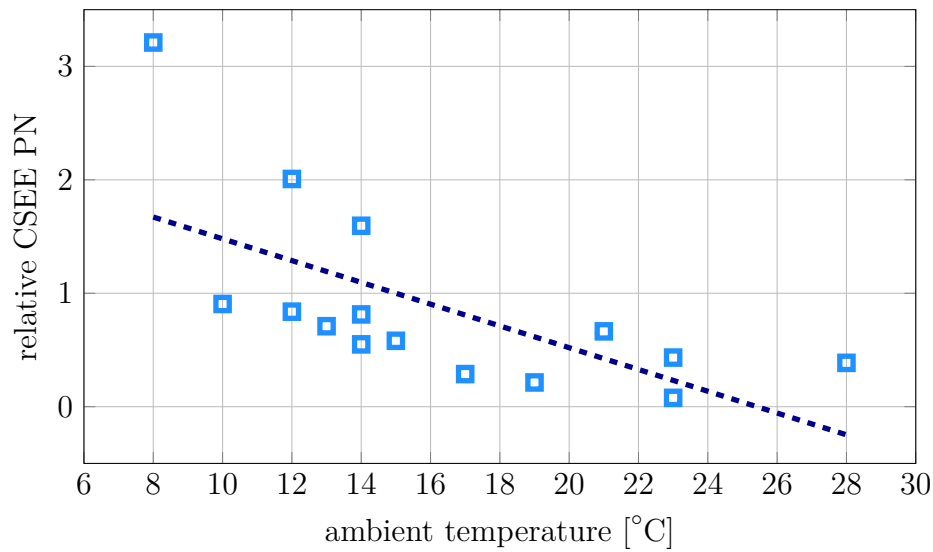


Figure 4.13: Distance specific PN CSEE values for the gasoline vehicle V3. CSEE were calculated by subtracting the warm urban from the cold urban trip (route R0).

4.2.3.2 Comparison of Cold Start and Post Cold Start Phase

In this section the cold start and post cold start phase were evaluated separately. The end of the cold start phase was defined as the engine temperature reached 70°C. The cold start emissions were the sum of the CSEE and the emissions that would occur under hot engine operation. Thus, the cold start emissions were generally higher than the CSEE shown in the previous section. This method was applied to vehicles V1 (Diesel) on route R1 and V3 (gasoline) on route R0 for a large range of ambient temperatures.

Figures 4.14 and 4.15 show the distance specific gaseous and particulate emissions, respectively, during the cold start and the post cold start phase as a function of the ambient temperature. The gaseous emissions were conducted with the Diesel vehicle V1 and normalized at 15°C by dividing the emissions by the corresponding cold start value at 15°C. The PN emission results were investigated with vehicle V3 and were directly compared to the cold-hot method presented in the previous section.

For the investigated vehicles, the emissions showed diverse temperature trends.

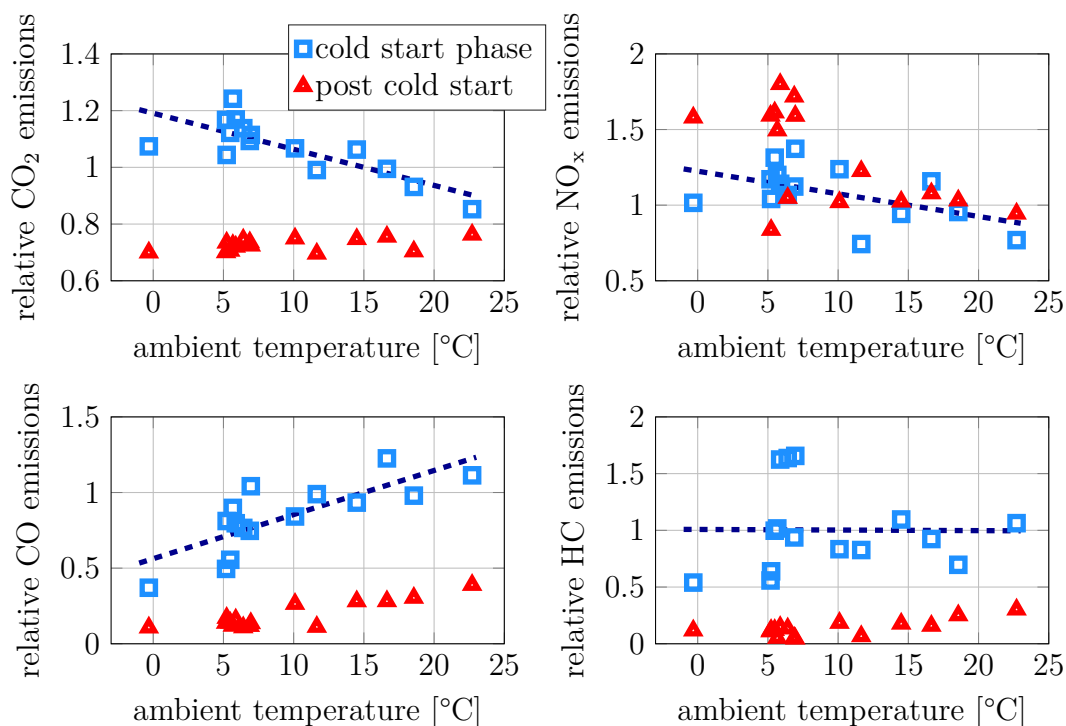


Figure 4.14: Cold start and post cold start emissions depicted for vehicle V1 on route R1. The distance specific emissions were normalized at an ambient temperature of 15°C.

Both CO_2 and NO_x cold start emissions increased linearly for lower ambient temperatures, as expected, with R^2 values of 0.63 and 0.27, respectively. A linear decrease of NO_x emissions for higher temperatures was also suggested in other studies [Bielaczyc2011]. While CO_2 post cold start emissions remained at a constant level about 42 to 22% below corresponding cold start emissions, NO_x hot emissions were at a similar or even higher level compared to the cold start and showed a small temperature trend. This observation emphasized that for this vehicle the NO_x CSEE were very small and confirmed the result obtained from figure 4.12 based on a second independent dataset. Thus, for the NO_x CSEE no temperature trend could be concluded.

CO cold start emissions, however, showed a linearly decreasing trend at low temperatures with a good R^2 value of 0.6 and confirmed the observation found in figure 4.12. This result was unexpected because CO and HC emissions are

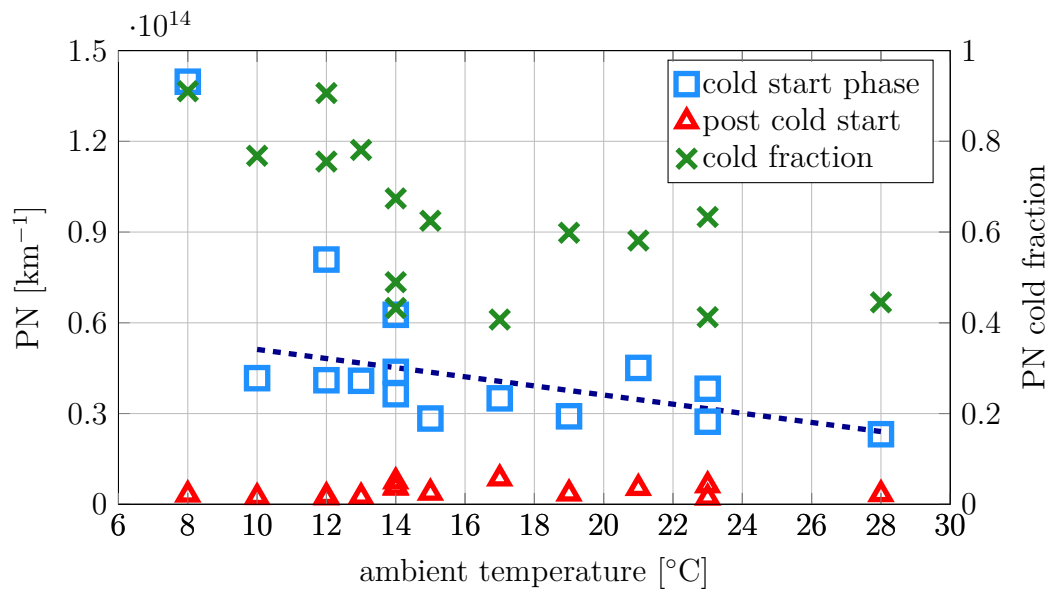


Figure 4.15: Distance specific PN emissions for the cold start and post cold start phase. The PN cold fraction was calculated as the ratio of absolute cold start and post cold start PN. The tests were conducted using vehicle V3 on route R1 [Gallus2016].

very strongly dependent on the oxidation catalyst's efficiency. Regarding HC, no temperature trend was determined, probably due to the large noise of the analyser after the light-off temperature of the oxidation catalyst was reached. However, for both CO and HC, the cold start emissions were significantly higher than corresponding hot emissions (a factor of 2 to 10), indicating the relevance of the cold start for these types of emissions on the road.

The PN cold start emissions presented in figure 4.15 showed a similar trend as a function of the ambient temperatures compared to the CSEE (cf. figure 4.13). This result was most probably caused by the longer warm-up period of the engine (cf. figure 4.11). Compared to the post cold start emissions, which were at a constant level of about $4 \cdot 10^{12} \text{ km}^{-1}$, the cold start effect made up a factor of three higher emission levels at 28°C and more than one order of magnitude at 10°C ambient temperature. Considering the single data point at 8°C as an outlier, a linear regression yields a slope of $-1.5 \cdot 10^{12} \text{ }^\circ\text{C}^{-1}$, with a very poor coefficient of determination R^2 of 0.28.

For comparison, Price and Stone found a strong dependency of PN with the engine coolant temperature of a DI gasoline vehicle, as well [Price2007]. At low temperatures down to -20°C one order of magnitude higher PN emissions were generated compared to 40°C . In another study, the period of 180s after engine start was investigated for several GDI gasoline vehicles in the sub-zero temperature range [Badshah2016]. During the cold start phase around one order of magnitude higher PN emissions was observed compared to the post cold start phase, which is in-line with the results of the present study.

Additionally, the ratio of PN emitted during the cold start phase and during the complete test trip is depicted in figure 4.13. The PN cold fraction increased with lower ambient temperatures, ranging from 0.4 to 0.9. In terms of low ambient temperatures, the cold start was one of the main contributors to the total PN emissions over the complete trip. However, this ratio was strongly dependent on the total trip distance travelled.

The PN cold fraction values were in agreement with literature values derived under laboratory conditions. Over the NEDC, at least 77% of the PN was emitted in the first phase due to the cold start effect [Braisher2010], while in the present study a percentage of about 60% at 22°C was reported (cf. figure 4.13). The lower cold start contribution found in this study was reasonable because the share of particle production from accelerations during the warm-up period of the engine was expected to be larger during on-road driving than over the NEDC.

4.3 Impact of Road Grade

In this chapter the impact of road grade on on-road emissions is evaluated. Road grade was found to have a significant impact on vehicle exhaust emissions [Boriboonsomsin2009; Meccariello2014; Prati2015]. Particularly CO_2 , NO_x and PN emissions show large dependence on positive road grades. As one could expect, uphill and downhill driving do not compensate each other in terms of fuel consumption and emissions [Wyatt2014; Boriboonsomsin2009] due to friction and efficiency losses during downhill driving.

The total force acting on a moving vehicle is a superposition of a number of forces. Air drag and rolling resistance occur opposite to the moving direction of the vehicle. Gravity can have a positive or negative impact on the total acceleration, depending on the angle of the road gradient α . The powertrain force is provided by the engine and has to overcome the other forces to move the vehicle in forward direction. Figure 4.16 shows the forces affecting a vehicle with constant velocity on a road gradient. In this illustration, wind or braking forces are not taken into account.

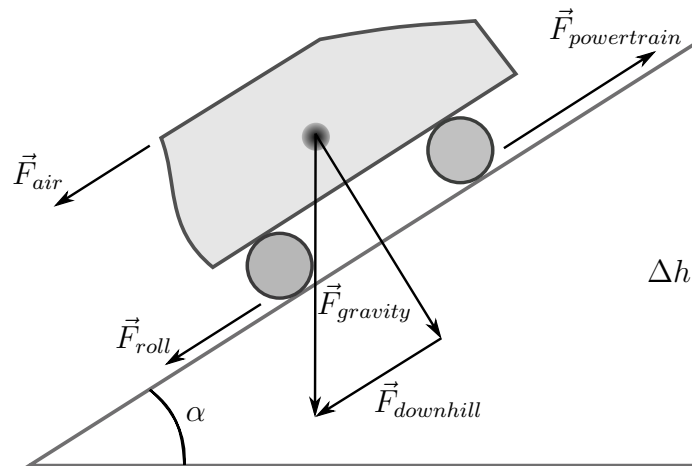


Figure 4.16: Forces affecting a moving vehicle on a road gradient.

The road grade m in % is defined as the height covered over a distance of 100m. It is trigonometrically correlated to the angle of the road gradient α and to the

covered height Δh over a horizontal distance Δs :

$$\begin{aligned}
 m[\%] &= 100 \cdot \tan(\alpha) \\
 &= 100 \cdot \frac{\Delta h}{\Delta s} \\
 &= 100 \cdot \frac{\Delta h}{\sqrt{v^2 \Delta t^2 + \Delta h^2}}
 \end{aligned}
 \tag{4.2}$$

Applying equation 4.2, road grade can be calculated by knowing the altitude difference Δh , the current velocity v and the time interval between two measurement points Δt (typically 1s).

Road grade can be interpreted as an acceleration leading to an additional load on the engine. The downhill acceleration a for a vehicle is given by equation 4.3.

$$\begin{aligned}
 a &= g \cdot \sin(\alpha) \\
 a &= g \cdot \sin(\arctan(m/100))
 \end{aligned}
 \tag{4.3}$$

Presuming the small angle approximation and a gravity acceleration g of 9.81 m/s^2 , 1% of road grade is equivalent to an acceleration of about 0.0981 m/s^2 . Note that the MPA of a typical PEMS trip is around 0.5 m/s^2 (compare figure 4.1).

In literature several approaches have been tried to estimate road grade during on-road driving. Already in 1984 first road grade measurements were started, applying acceleration measurements independently of any exhaust measurement [Rogers1984]. Later Mangan et al. (2002) investigated the potential of an inclinometer under dynamic conditions [Mangan2002]. Other studies performed road grade estimations based on GPS data either with one or two antenna [Bae2001; Sahlholm2010], however due to a limited altitude accuracy GPS data require strong mathematical corrections (low pass filter, Kalman filter). In recent studies, the opportunity of LIDAR signals for road grade estimations were addressed [Zhang2006; Frey2007; Wyatt2014]. LIDAR is an acronym for Light Detection And Ranging and enables the accurate determination of distances via runtime measurements. However, these LIDAR data are only available for few locations on earth.

In this study, altitude data from several sources were consulted and compared in terms of accuracy, quality and practicability of the data. In the upcoming RDE legislation, GPS data are preferred as independent data source. However, due to a lack of accuracy of GPS altitude, road gradients along test routes are accounted for by one more robust value, the CAG (equation 4.10). Here, different routes were characterized by their CAG values obtained from several data sources and correlated with their distance specific emissions.

The goal in this study was to find practical and affordable solutions in order to achieve precise road gradient results. First attempts were made on a test track with predefined road grade values. For PEMS trips, mathematical methods were applied for the purpose of increasing the accuracy of road grade data based on repetitive runs over the same route. The final goal was to experimentally determine a correlation of road grade with engine load and with exhaust emissions measured by the PEMS.

4.3.1 Data Acquisition

The PEMS GPS receiver provided position as well as altitude data during all PEMS trips. The GPS signal was always provided by at least eight GPS satellites without any obvious signal loss. Another parameter provided by the GPS receiver, called dilution of precision, steadily showed good values, indicating a high quality GPS signal.

Additionally, ECU data were recorded using a CAN interface or an INCA box in the trunk of the vehicle. ECU velocity was used as reference signal for the covered distance due to a higher accuracy compared to GPS data. The time alignment was performed by adjusting the ECU velocity to the GPS velocity using a least square method.

4.3.1.1 GPS

Road grade was directly obtained from second-by-second GPS altitude data. Based on the altitude difference Δh of two adjacent altitude data points, the

road grade was calculated according to equation 4.2.

One correction was necessary especially for very small velocities, i.e. the vehicle is driving very slow or even at halt. In this case according to equation 4.2, small values of Δh were divided by small values of the covered distance $v \cdot \Delta t$. Due to the inaccuracy of Δh this partially led to unrealistic road grade results. The correction applied in this case was to define $\Delta h = 0$ for velocities $v < 1m/s$, i.e. no large altitude difference is expected by driving less than one meter per second.

4.3.1.2 Google

Second by second altitude data were acquired from the Google Maps Elevation API (Application Programming Interface) [ElevationAPI] which uses the GPS position to supply the corresponding altitude value. In analogy to GPS data, the altitude difference Δh was determined and road grade was calculated according to equation 4.2. Unfortunately, the accuracy as well as the resolution of the Google altitude data is yet unknown and may vary between different locations. In case Google does not possess exact elevation measurements at the precise location, the service will interpolate and return an averaged value using the four nearest locations.

4.3.1.3 In-car Accelerometer

As a standard feature, all the test vehicles were equipped with an in-car accelerometer which is primarily used as a sensor for the airbag and the hill hold control. The accelerometer is usually positioned in the centre of the vehicle directly below the handbrake. It is fixed to the bodywork of the vehicle and measures the acceleration in longitudinal and transversal direction. This means that a pitch and roll movement of the vehicle will add some noise to the pure vehicle movement which appears parallel to the road.

Theoretically, the accelerometer measures the total acceleration a , which is the sum of the time derivative of the vehicle velocity \dot{v} and the longitudinal part of

the gravitational acceleration g (equation 4.4) [Gustafsson2000].

$$a = \dot{v} + g \cdot \sin(\alpha) \quad (4.4)$$

Based on this equation the road grade m is calculated according to equation 4.5.

$$\begin{aligned} m[\%] &= 100 \cdot \tan(\alpha) \\ &= 100 \cdot \tan\left(\arcsin\left(\frac{a - \dot{v}}{g}\right)\right) \end{aligned} \quad (4.5)$$

The accelerometer was originally designed for the measurement of high acceleration values (up to 10g), therefore some corrections were necessary in order to guarantee good results for highly dynamic road grade measurements. First large, unrealistic accelerations $> 1.5\text{m/s}^2$ were omitted because such values normally do not occur during normal driving situations (not taking into account accidents).

Additionally, during the measurement series the accelerometer showed a non-reproducible drift of the acceleration signal a over each measurement. This drift could be detected by closed cycle tests where the sum over all altitude differences was supposed to be zero. Solving equation 4.4 for $\sin(\alpha)$ and equating the result with the relation $\sin(\alpha) = \frac{\Delta h}{v \cdot \Delta t}$ derived from figure 4.16, the altitude difference Δh was calculated to:

$$\Delta h = v \Delta t \cdot \frac{a - \dot{v}}{g} \quad (4.6)$$

For a closed cycle the drift on the measured acceleration a_i for a data point i was assumed to contribute with an additional term, i.e. $a_i = a'_i + \delta a_i$, with the true value a'_i and the drift δa_i . Inserting this into equation 4.6 and summing up resulted in:

$$\begin{aligned} \sum_i \Delta h_i &= \frac{\Delta t}{g} \cdot \sum_i v_i \cdot (a'_i + \delta a_i - \dot{v}_i) \\ &= \frac{\Delta t}{g} \cdot \left[\underbrace{\sum_i v_i \cdot (a'_i - \dot{v}_i)}_{=0} + \sum_i v_i \delta a_i \right] \end{aligned}$$

In this equation the first term strictly had to be zero because of the assumption of true acceleration values a'_i and ideal values of \dot{v}_i . Considering a constant value

$\delta a_i = \delta a$, the drift could be calculated to:

$$\delta a = \frac{g}{\Delta t} \cdot \frac{\sum_i \Delta h_i}{\sum_i v_i} \quad (4.7)$$

Every acceleration data point was corrected for this drift value. Finally, the road grade obtained over closed cycles was calculated using equation 4.8.

$$m[\%] = 100 \cdot \tan\left(\arcsin\left(\frac{(a - \delta a) \cdot \dot{v}}{g}\right)\right) \quad (4.8)$$

During road grade changes the pitch movements of the vehicle add higher frequency noise to the longitudinal acceleration signal of the accelerometer. Therefore a second order butterworth low pass filter was applied to the drift corrected acceleration signal. According to Bae et al. (2001) the cut-off frequency was set to 0.5Hz [Bae2001].

4.3.1.4 Barometer

The barometer applied in this study was a PAA-33X from Keller. The resolution and accuracy are specified by 0.002% and $\pm 0.013\%$ (full scale), respectively. Assuming a measurement range of 0.8 to 1.2 bar (full scale), the accuracy is estimated to around ± 0.156 mbar.

The altitude was calculated based on the barometric formula for an isothermal atmosphere. The assumption of an isothermal atmosphere is legitimate as only small altitude differences (time interval $\Delta t = 1s$) and no absolute altitudes were considered. Based on the barometric formula, the altitude difference Δh between two adjacent measurement points with ambient pressures p_1 and p_2 was calculated according to equation 4.9, with the gas constant R , the molar mass of the air M and the gravitational acceleration g . The temperature T_0 accounts for the isothermal temperature of the atmosphere and is calculated as the average ambient temperature throughout the measurement.

$$\Delta h = -\frac{RT_0}{Mg} \cdot \left(\ln(p_2) - \ln(p_1)\right) \quad (4.9)$$

Inserting the estimated pressure accuracy of 0.156 mbar into equation 4.9 leads to an estimated altitude accuracy of 1.1 to 1.6m in a pressure bandwidth of 0.8 to 1.2 bar. Note that this value just represents the statistical accuracy of the sensor, not taking into account other influences, such as atmospheric turbulences.

4.3.2 Road Grade Measurements on Test Track

The first measurement approach was on a test track (Ford Proving Ground, Lommel/Belgium) with defined road grade sections between -20 and +30%. The test vehicle already included an in-car accelerometer and was additionally equipped with a barometer, which was fixed on the back seat and a dGPS system on the roof of the vehicle. The dGPS makes use of a reference signal and provides a much higher accuracy compared to ordinary GPS systems. For this measurement series the reference signal was directly received from the test track but was not available for the on-road tests described in the next section. For the test track measurement series, the accuracy in altitude was expected to be about 10cm (ordinary GPS system around 10 to 15m altitude accuracy).

The complete measurement took around 40 minutes. It provides a qualitative analysis about dGPS and accelerometer data and makes sure that calculated road grades are in a correct range. Figure 4.17 shows a small section showing a mixture of cruising, deceleration and acceleration events, representative for the complete series.

The calculated road grade obtained from dGPS data showed good results. In nearly all cases the dGPS matched the predefined road grade values very well and was also not sensible to accelerations. Unfortunately, dGPS could not be used during on-road tests due to the missing reference signal which was not available at all locations.

The barometer road grade was calculated from the pressure differences in the interior of the vehicle. The result was poor as the noise was very large and predefined values were mostly overestimated. In figure 4.17 the barometer data

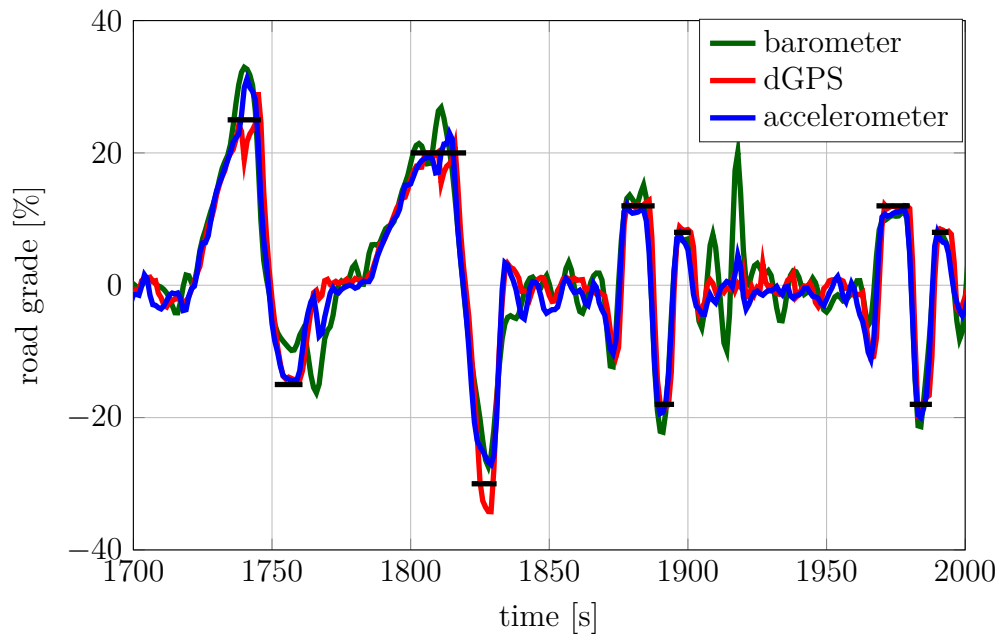


Figure 4.17: Road grade results of the barometer, the dGPS and the accelerometer based on test track measurements. The black horizontal lines indicate the sections with stated road grade values.

were already filtered using a second order butterworth low pass filter at a cut-off frequency of 0.3Hz. In this configuration, the barometer showed no sufficient accuracy for road grade estimation and it is likely that it even becomes worse for dynamic driving situations for on-road tests.

The accelerometer showed good results similar to the dGPS. The road grade calculation model corrects for vehicle accelerations (compare equation 4.9) but the accelerometer intrinsically measures the sum of all accelerations. Therefore the accelerometer signal was treated as described in the previous section. Figure 4.17 shows that one -30% road grade value at 1830s was not matched where the accelerometer probably reaches its detection limit. However, these extreme road grade values are normally not included in on-road measurements, normal road grade values range within $\pm 6\%$ (cf. next section).

4.3.3 On-Road Methodologies

4.3.3.1 Route Comparison

The CAG was calculated for the different data sources according to equation 4.10.

$$CAG = \sum_i \Delta h_i, \Delta h_i > 0 \quad (4.10)$$

Additionally, the suggested CAG calculation method described in the RDE regulation draft [RDE2015] was applied. This method was based on the GPS altitude signal and included the correction of large deviations from corresponding map data and of spikes that may occur during GPS measurements. In a second step the altitude data were interpolated for 1m distance points and finally a linear data smoothing over a distance of $\pm 200\text{m}$ was performed. The CAG value is divided by the complete distance of the trip and multiplied by 100 in order to define the final result relative to a total distance of 100km. The proposed limit in the regulation is defined by the value 1200m/100km, which is strongly correlated to this specific calculation method.

Table 4.1 shows the average CAG values of the investigated routes based on different vehicle data and calculated by several data sources as well as the RDE method. The CAG values are presented relative to a total trip distance of 100km. Additionally, for routes R0 and R1 the standard deviation is given, for routes R2 and R3 the values were based on too few trips to provide a reasonable standard deviation value. The accelerometer values were based on trips with only normal driving style. The CAG values showed a dependence on absolute accelerations during the trip, i.e. severe and soft trips showed elevated and reduced CAG values compared to normal trips, respectively. The barometer was only applied on route R1, thus, for the other routes no CAG value was calculated.

As expected, routes R0, R1 and R2 showed similar CAG values. Route R3 was designed with respect to strong uphill and downhill sections leading to elevated CAG values. Depending on the data source, route R3 showed 48 (GPS) to 162% (RDE method) increased values compared to the other three routes.

	Number of trips (all vehicles)	GPS (RDE method) [m/100km]	GPS [m/100km]	Google [m/100km]	Accelerometer [m/100km]	Barometer [m/100km]
R0	12	609 ± 20	1184 ± 73	906 ± 9	735 ± 4	n/a
R1	40	512 ± 33	1101 ± 77	780 ± 13	670 ± 24	1070 ± 201
R2	2	561	1307	969	848	n/a
R3	3	1339	1934	1832	1347	n/a

Table 4.1: Calculated CAG values for the investigated routes based on different data sources. While routes R0, R1 and R2 show similar characteristics, route R3 was designed with respect to large CAG values. Accelerometer results were calculated from trips with normal driving style only. Barometer results were just available for route R1.

There was a remarkable difference between the CAG values calculated via the different methods and data sources. For routes R0, R1 and R2, the CAG obtained by GPS data were 31 to 41% higher compared to Google values and even 54 to 61% compared to the accelerometer. This could be explained by small, unrealistic spikes that occurred in the normal GPS signal because of a poor altitude accuracy [Wing2005]. Additionally, there was a large standard deviation of the GPS values of about 70 to 80m. Route R3, however, was characterized by larger altitude differences that could be resolved by the GPS leading to similar GPS and Google CAG values. Due to the limitation of a total accelerations of 1.5 m/s², the accelerometer shows a much smaller CAG value for route R3.

Based on GPS altitude data, the RDE method was applied which includes a correction and subsequent filtering algorithm. The altitude gain showed a strong reduction by 31 to 57% compared to uncorrected GPS data which was primarily a result of the strong smoothing process applied in the RDE method. Additionally, the comparison to Google and accelerometer CAG values showed that the RDE method underestimated the CAG of all four routes. Probably due to the high smoothing distance of ±200m the small altitude variations were simply averaged out.

These large CAG deviations between the different methods and data sources confirmed the requirement for a uniform method with directly comparable values. The regulation limit value of 1200m/100km is strictly coupled to the suggested RDE method and route R3 would be invalid. However, for the mean of repeatability and a reliable definition of a CAG limit value, the Google data and for a common driving style also the acceleration data were found to be the best alternatives to the RDE method. In this case the CAG limit is required to be changed to a more realistic value because it is directly related to the calculation method.

The barometer provided a large CAG standard deviation for route R1. In agreement with the test track measurements, the altitudes were filtered with a second order butterworth low-pass filter at a cut-off frequency of 0.3Hz. However, the barometer in this constellation provided no sufficient method to characterize the road gradients along a route.

Instead of a transient analysis, the CAG represents one parameter that characterizes the altitude variation of a route by a robust value. Thus, the CAG of a route represents the impact of the road grade on the emissions of the vehicle. In figure 4.18 the distance specific NO_x emissions of the Diesel vehicles V0, V1 and V2 were plotted against the 95th percentile of the driving parameter $v \cdot a_{pos}$ for each trip on routes R0, R1, R2 and R3. In order to compare the emissions of different vehicles, the NO_x emissions were normalized at a $v \cdot a_{pos95}$ value of $15 \text{ m}^2/\text{s}^3$. Separately for each vehicle the NO_x emissions were divided by the corresponding NO_x value at $15 \text{ m}^2/\text{s}^3$ of route R1 [Gallus2017].

All trips conducted on route R1 showed a rather linear trend with an R^2 value of 0.64 as depicted by the regression line in figure 4.18. Only for trips with very large $v \cdot a_{pos95}$ values $> 30 \text{ m}^2/\text{s}^2$ the data show a strong scattering around the regression line. As expected, the NO_x emissions for routes R2 and R3 followed the trend quite well because of a similar CAG compared to route R1, i.e. similar NO_x emissions were observed for similar driving dynamics (this conclusion was already drawn for the driving style evaluation in chapter 4.1). For route R3 involving much more hilly parts expressed by a larger CAG value, the NO_x emissions occurred explicitly above the regression line (red triangles). For these two trips the distance specific NO_x emissions were nearly twice as large as corresponding values from the

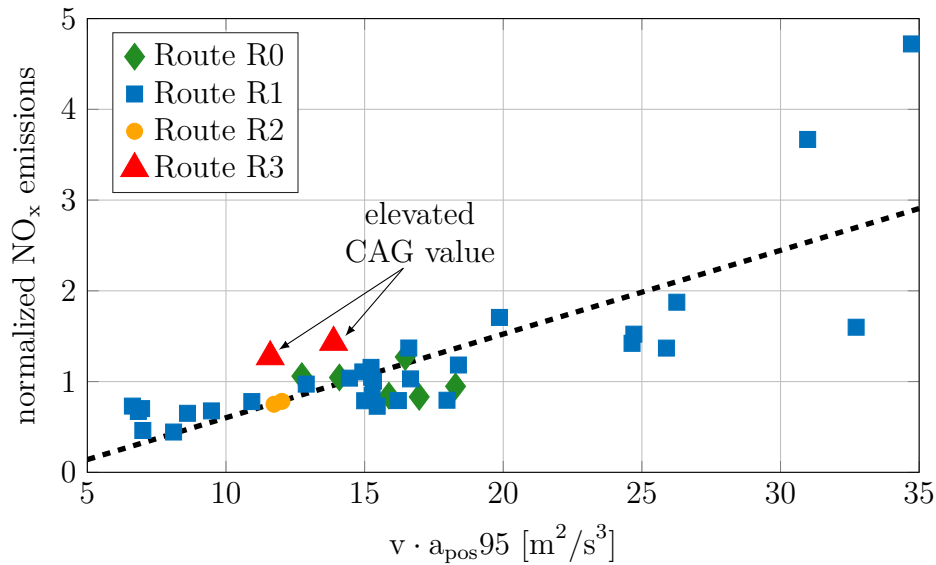


Figure 4.18: NO_x emissions plotted against the 95% percentile of the parameter $v \cdot a_{pos}$ for different test routes. The linear regression was calculated for all data points on route R1. Note that route R3 had a much larger CAG value compared to the other routes. For better illustration, NO_x emissions were normalized at a value of $15 \text{ m}^2/\text{s}^3$ by dividing the NO_x emissions for each vehicle by the corresponding NO_x value at $15 \text{ m}^2/\text{s}^3$ of route R1 [Gallus2017].

other routes. To provide a more robust result, more tests on route R3 have to be conducted with a larger variation of the driving dynamics [Gallus2017].

4.3.3.2 Segment Method

A segment method introduced by [Yazdani2012; Yazdani2014] was applied in order to determine the road grade with a defined accuracy. The basis were altitude data, e.g. obtained from GPS or Google data. Following the method each trip was divided into segments of a constant length. It was important that every trip started from the same position so that segments from different trips provide the largest overlap. However, due to small variations in the trip distance (lane change, inaccuracy of the signal etc.) a reference trip length was calculated by averaging the total distance of all trips on each route. The cumulated distance for each trip was corrected by this reference trip length in order to have a consistent trip

length with the same number of segments. For every segment the road grade was calculated using a linear regression through all collected altitude data. In this way it was possible to combine several trips over the same route in order to increase the statistical accuracy of the calculated road grade in each segment.

In this study, a segment length of 100m was chosen because it was found to offer the best trade-off between the number of points per segment and the segment length. Less data points per segment decreased the reliability of the calculated road grade in each segment and very large segments smoothed out small road grade changes.

The segment method was applied to six PEMS trips conducted by vehicle V3 on route R0 and to 17 trips conducted by vehicle V1 on route R1. Using 100m segments routes R0 and R1 were separated into 818 and 860 segments with at least 14 and 44 data points per segment, respectively. The cumulated distance was calculated based on the velocity obtained from GPS data. In every segment, the standard deviation of the slope parameter obtained from the linear regression was calculated and the average value of all segments was defined as precision [Yazdani2012]. The best precision value was found for the Google data with an average precision of 0.29% (route R0) and 0.12% (route R1) for all segments. As expected, GPS data provided worse precision values with 2.79% (route R0) and 1.57% (route R1). For comparison, in [Yazdani2014] the target precision was 0.5% for a segment length of 80m, calculated from GPS data.

The accelerometer directly provided second-by-second road grade values. In this case, the accelerometer road grade data were classified into the segments and the average road grade per segment was calculated. The standard deviation in each segment was comparable to the precision obtained from Google and GPS data. The precision of the accelerometer resulted in 2.00% and 1.42% for routes R0 and R1, respectively.

The segment method was applied to generate a road grade histogram for routes R0 and R1. Figure 4.19 shows the covered distance (equivalent to the number of segments multiplied by the segment length of 100m) plotted against the road grade separated into 0.5% bins. The four plots represent the complete route as well as each the urban, rural and motorway parts. The basis for the histograms

were the Google altitude data due to the highest precision values. Urban, rural and motorway parts were evaluated by the average velocity in each segment with urban ≤ 60 km/h, rural > 60 km/h and ≤ 90 km/h as well as motorway > 90 km/h [Gallus2017].

Route R1 had a symmetric shape indicating a balanced amount of flat and steep uphill and downhill segments, also for each the urban, rural and motorway part. Note that the histogram did not necessarily need to be symmetrical for a closed cycle but the distance based sum of all road grades for the complete test was supposed to be zero. On the other hand, route R1 showed an elevated shift of the urban and rural parts to positive road grade values, indicating more pronounced uphill segments, which was compensated by downhill segments in the motorway part. For both routes, the urban part makes up the highest amount of covered distance, which is strongly dependent on the urban velocity limit of 60 km/h [Gallus2017].

Figure 4.19 shows that the mean positive road grade of the complete trip is about 1.56% for route R0 and 1.34% for route R1 which is theoretically equivalent to an acceleration of 0.153 m/s^2 and 0.131 m/s^2 , respectively (equation 4.3). For comparison, the mean positive acceleration of all normal PEMS trips was around 0.5 m/s^2 on average. For a rough estimate, road grade contributed to about 20 to 25% of the resulting acceleration of a trip.

4.3.3.3 Correlation with Exhaust Emissions

The segment method as explained above was applied to provide correlations between road grade values and emission data obtained from the PEMS. For a reasonable correlation with the emission data, only cruising parts were considered, i.e. data points with accelerations in the range of $\pm 0.1 \text{ m/s}^2$. This limitation guarantees the emissions not to be influenced by acceleration events derived from uphill or downhill driving.

Figure 4.20 shows the correlation of CO_2 (upper figure) and NO_x (lower figure) emissions for the Diesel vehicle V1 on route R1 with road grade separated by urban, rural and motorway parts. For this calculation, only segments with a

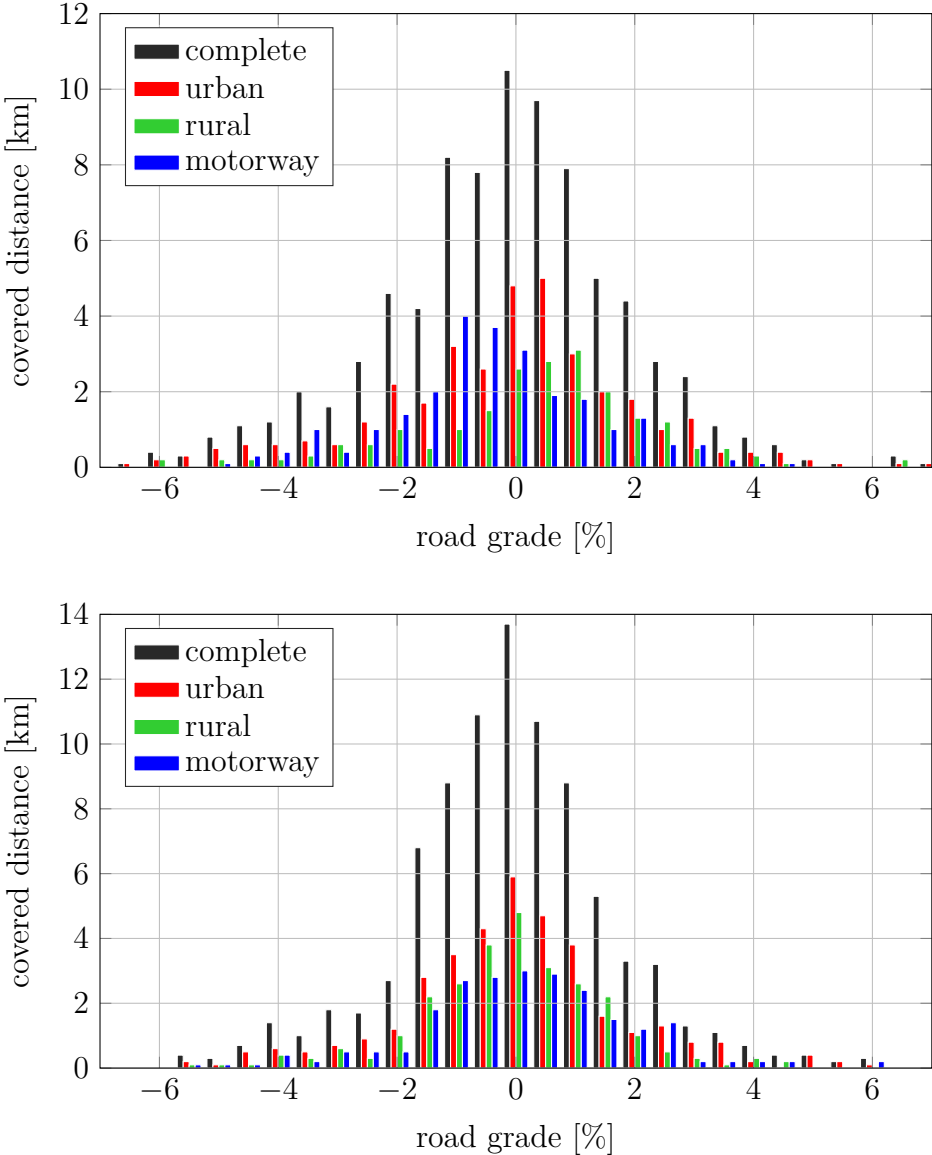


Figure 4.19: Road grade histogram for routes R0 (upper figure) and R1 (lower figure) for the complete route and separated into urban, rural and motorway parts calculated from Google altitude data. The 95% percentile of all positive road grades for route R0 and R1 is at 4.3% and 3.9% road grade, respectively [Gallus2017].

road grade standard deviation of at least 0.5% were considered corresponding to more than 94% of all 863 segments. Cold start emissions were included in this calculation because the cold start effect was not so significant for the CO₂ and NO_x emissions (compare chapter 4.2). Additionally, data binning was performed within 0.5% road grade intervals and was illustrated by the mean and standard deviation of each segment [Gallus2017].

Both CO₂ and NO_x emissions increased with larger road grades for urban, rural and motorway parts. In both cases the motorway emissions were highest based on the condition that only cruising data points were considered. In previous studies, engine power demand was found to be linear with road grade [Yazdani2013; Zhang2006] and fuel consumption was modelled by a linear function of the engine power [Boriboonsomsin2009]. Thus, in this study emissions and road grade were fitted by a linear regression line. Note that the individual test to test variability within each road grade interval is substantial (up to 94% and 156% for CO₂ and NO_x, respectively) as illustrated by the range bars.

The CO₂ data showed a similar slope of the regression line for all three road types. For a road grade change from 0% to 5% CO₂ emissions increased for 81, 77 and 66% for urban, rural and motorway driving, respectively. For all three road types a good coefficient of determination of 0.81, 0.82 and 0.93 was found, respectively [Gallus2017].

In literature a parabolic correlation between fuel consumption and road grade was assumed that showed a larger increase of around 130% between 0 and 5% road grade [Boriboonsomsin2009]. By fitting a linear regression, this increase would have been much closer to the results suggested in the present study. Additionally, the deviation was further enhanced by a different total mass of the tested vehicles. According to [Boriboonsomsin2009], 5% higher total mass led to an increase in fuel consumption of 5 to 20% at 1 to 6% road grade, respectively.

NO_x emissions also showed a clear correlation with road grade, the strongest one was observed on the motorway and the lowest one for the urban part. This result primarily derived from the formation of NO_x under high engine temperature operation during high speed driving on the motorway which was supported by large road grades. As indicated by the linear regression line, the NO_x increase

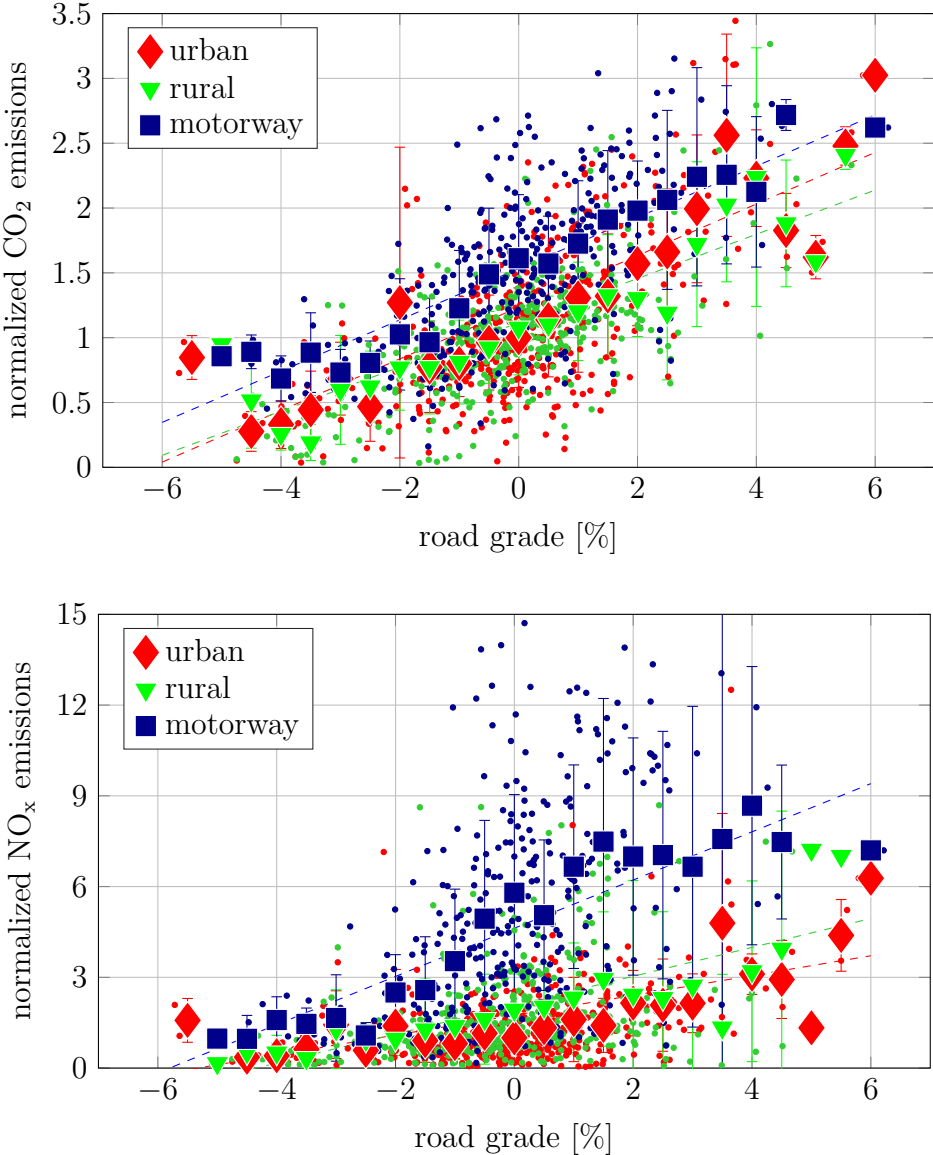


Figure 4.20: Correlation of normalized CO₂ (upper figure) and NO_x (lower figure) emissions of Diesel vehicle V1 on route R1 with road grade separated by urban, rural and motorway parts evaluated only for cruising parts. Data binning was performed within 0.5% road grade intervals and depicted using larger markers and range bars, indicating the mean and standard deviation, respectively [Gallus2017].

from 0 to 5% road grade on the motorway accounted for 86% ($R^2 = 0.87$). Urban and rural driving showed a NO_x increase of 94 and 115% ($R^2 = 0.56$ and 0.69 , respectively) [Gallus2017].

Figure 4.21 shows the correlation of CO_2 (upper figure) and PN (lower figure) emissions for the gasoline vehicle V3 on route R0 with road grade separated by urban, rural and motorway parts. For this calculation, only segments with a road grade standard deviation of at least 0.5% and more than five data points were considered, corresponding to more than 85% of all segments. The cold start was excluded from the road grade analysis because cold start emissions were many times larger than the post cold start emission (compare chapter 4.2). Thus, from route R0 the first urban part that includes the complete cold start phase was omitted. Additionally, in figure 4.21 data binning was performed within 0.5% road grade intervals and was illustrated by the mean and standard deviation of each segment.

Similar to figure 4.20 CO_2 showed an increasing trend for urban, rural and motorway parts with the highest emissions for motorway and followed by the urban part. For a road grade change from 0% to 5% CO_2 emissions increased for 69, 72 and 45% for urban, rural and motorway driving, respectively, which is slightly below Diesel CO_2 results. The coefficient of determination for all three road types with 0.78, 0.96 and 0.85, respectively, were comparable to Diesel values. Note that the individual test to test variability within each road grade interval is again substantial (up to 100%).

PN emissions showed an expected increasing trend of PN with road grade, as well. The type of correlation is still unknown, however assuming a linear PN correlation with road grade all three parts revealed strong outliers with tremendous range bars up to 400%. Especially on the motorway, a large variation was observed leading to a poor linear correlation with an R^2 value of 0.17 (urban 0.54, rural 0.49). Based on the regression lines, the urban, rural and motorway PN increase from 0 to 5% road grade accounted for 60, 92 and 79%, respectively, however, these results only had qualitative expression.

An explanation for the elevated exhaust emissions was the tendency to higher engine loads from flat to uphill driving. Figure 4.22 shows the engine torque

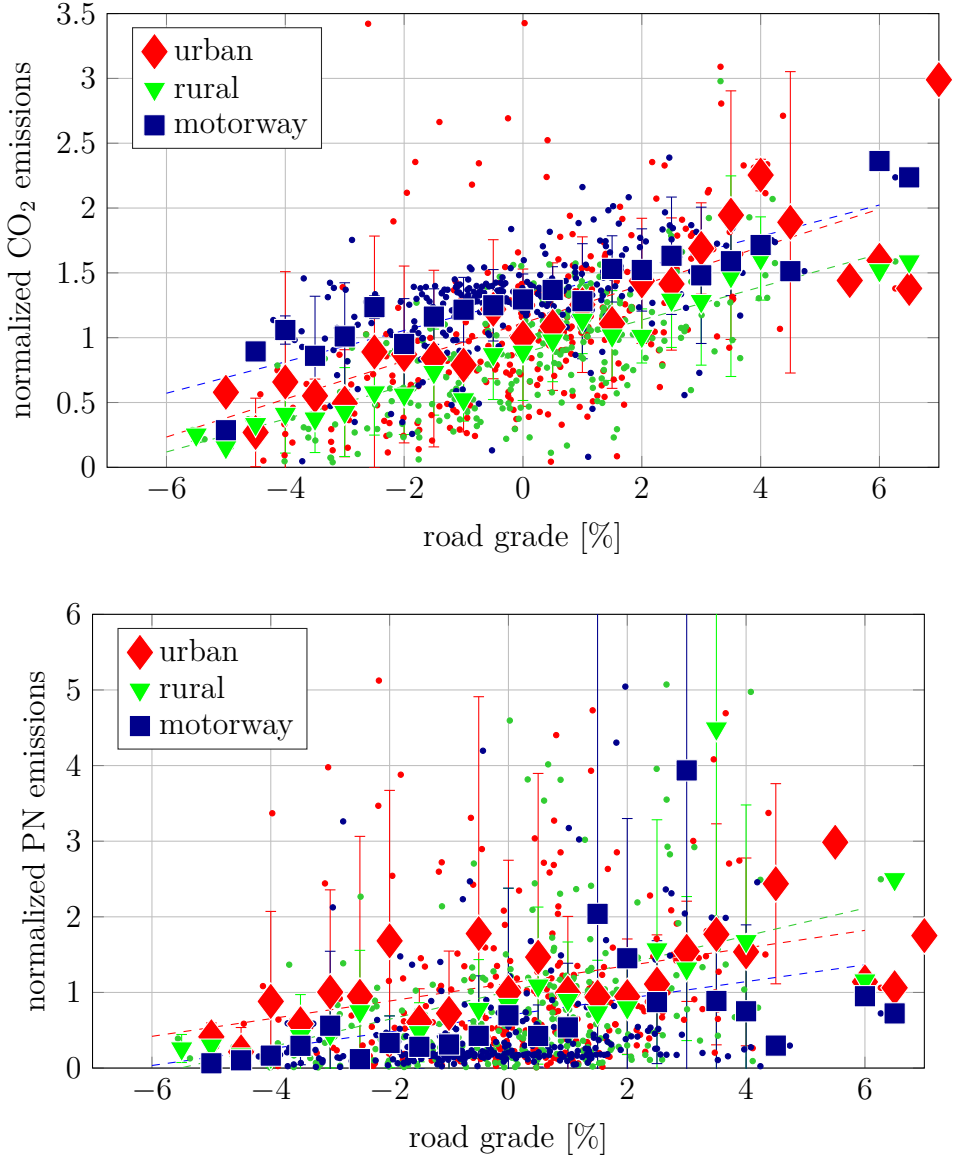


Figure 4.21: Correlation of normalized CO₂ (upper figure) and PN (lower figure) emissions of the gasoline vehicle V3 on route R0 with road grade separated by urban, rural and motorway parts evaluated only for cruising parts. Data binning was performed within 0.5% road grade intervals and depicted using larger markers and range bars, indicating the mean and standard deviation, respectively.

plotted against engine speed for flat segments with road grade between -1 and +1% (upper figure) and for uphill segments (road grade $> 1\%$). This figure is based on results from vehicle V1 but is representative for all vehicles. Only data points with a limited acceleration between -1 and 1 m/s^2 were considered for this evaluation. For both frequency distribution maps, binning was performed with engine speed steps of 50/min and engine torque steps of 5Nm. The frequency of each bin was plotted on the z-axis. Additionally the maximum torque curves that could be provided by the engine were depicted as dashed line [Gallus2017].

The most frequented points for flat segments were concentrated in a small area below 60Nm engine torque and engine speed below 1800/min. For cruising on a flat road only a small amount of engine power ($\approx 3.5\text{kW}$) was required. In this driving condition, the engine has to compensate the rolling resistance and air friction at a constant velocity (cf. equation 2.1). Assuming a standard air density of 1.23 kg/m^3 and an average velocity of 15 m/s (cf. chapter 4.1) the theoretical engine power demand was about 3.83kW which is in-line with the experimental results.

Uphill segments with more than 1% road grade showed a clear shift of the most frequented areas to higher torques. A three times higher torque led to a three times higher power demand of the engine, which was likely the main reason for the elevated emissions at larger road grades [Gallus2017].

Figure 4.23 shows the cumulated NO_x and PN emissions relative to road grade segments separated into urban, rural and motorway parts. Again only data points with a limited amount of acceleration (within $\pm 0.1 \text{ m/s}^2$) were considered. Regarding PN the cold start was excluded by omitting the first urban part that included the cold start phase completely. For better illustration, the road grade was binned into 0.5% steps and depicted as larger symbols. Additionally, the corresponding number of data points within each bin is shown.

The upper plot shows that most Diesel NO_x emissions occurred at moderate road grades. For all urban, rural and motorway parts 60% of the NO_x emissions were observed for rather flat segments between -1 and 1% which also made up around 60% of all segments for route R1 (compare figure 4.19). Note that this result was strongly dependent on the chosen route profile. 90% of the NO_x was

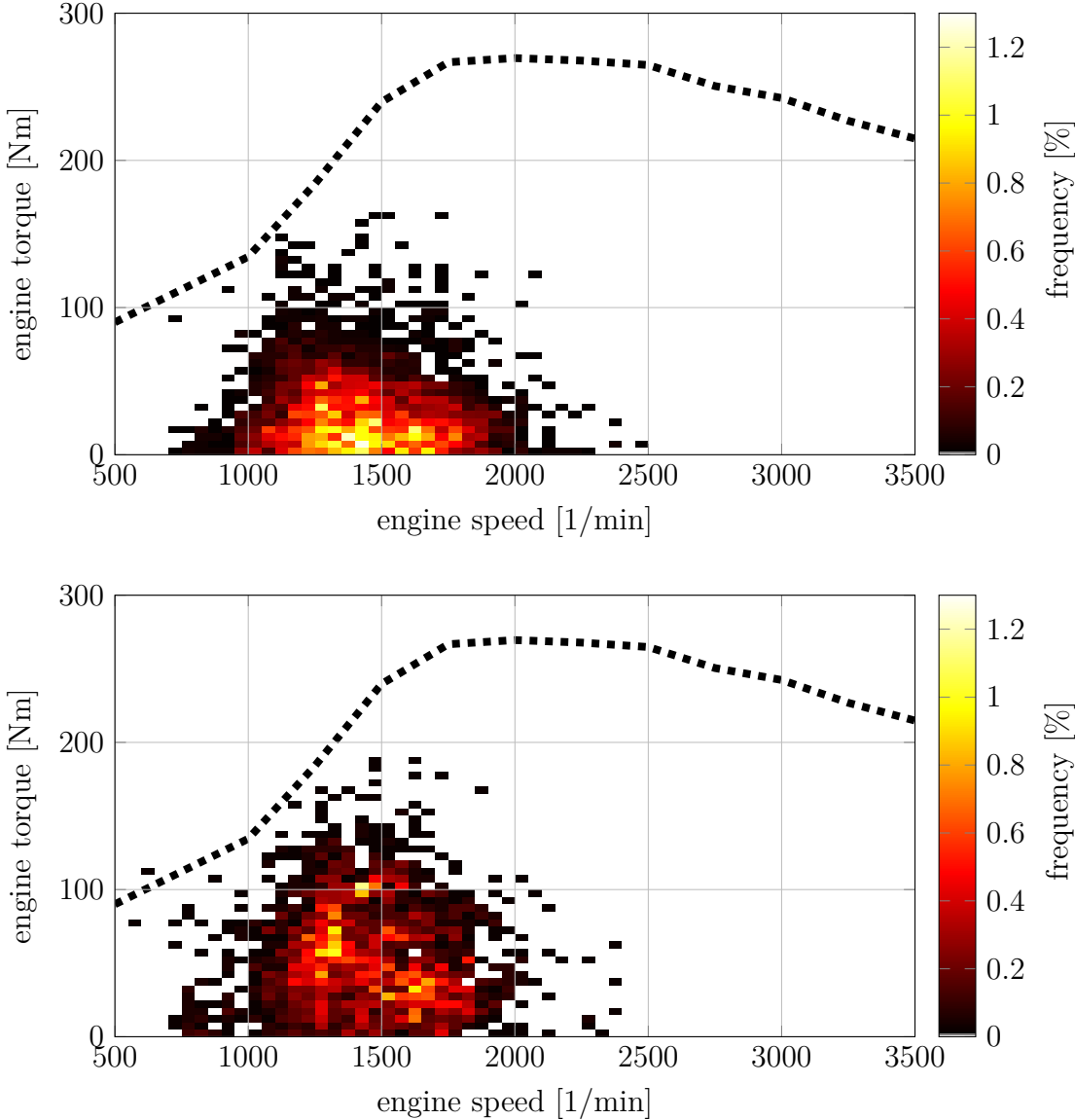


Figure 4.22: Frequency distribution maps for urban cruising and flat segments between -1 and +1% (upper figure) and larger than 1% road grade (lower figure), based on results from vehicle V1. The dashed line indicates the maximum torque curve [Gallus2017].

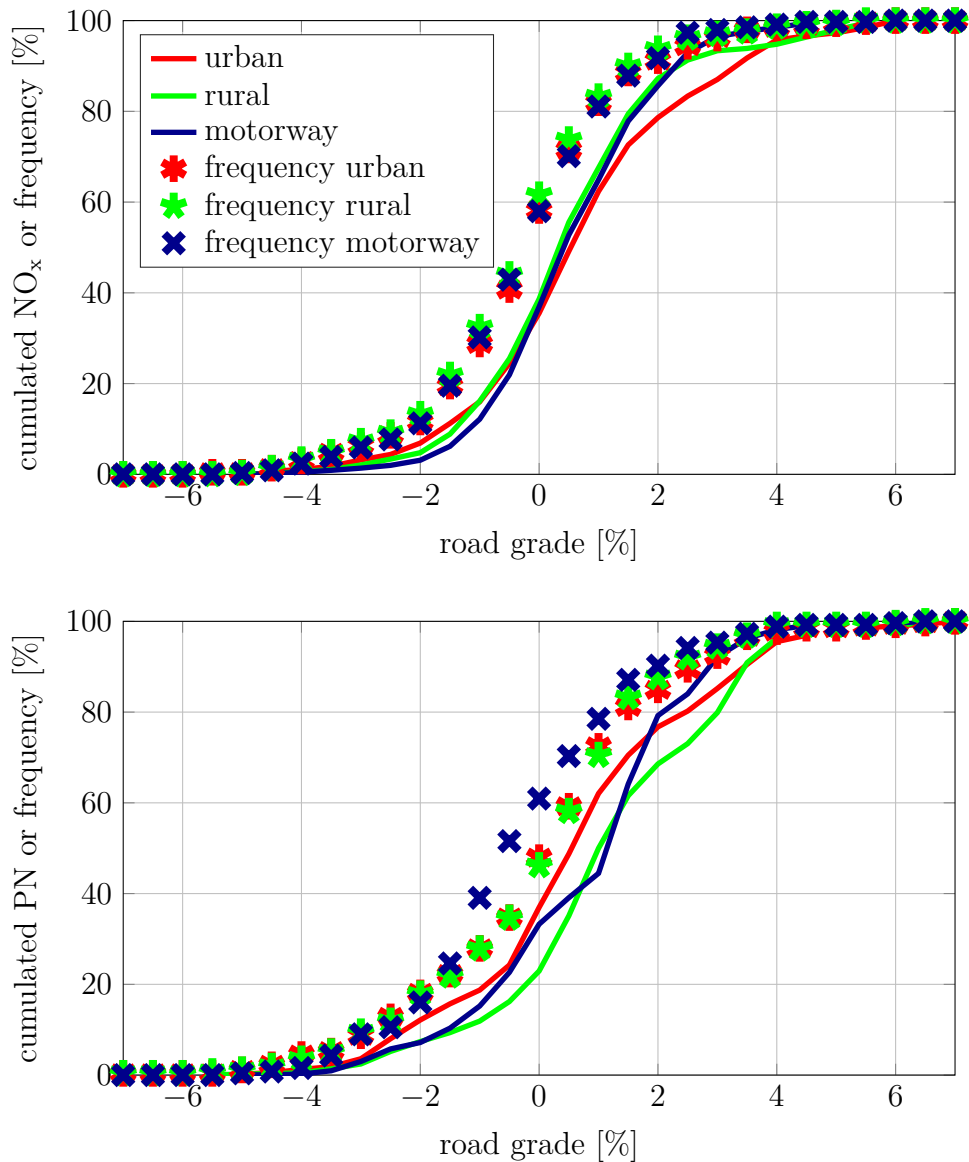


Figure 4.23: Correlation of cumulated NO_x obtained from vehicle V1 on route R1 (upper figure) [Gallus2017] and PN emissions from vehicle V4 on route R0 (lower figure) with road grade separated by urban, rural and motorway parts. The evaluation was performed for cruising only parts and binning was performed within 0.5% road grade. The frequency of every road grade bin is depicted using larger markers.

emitted below 2.8 (urban) and 2% road grade. A fraction of 35 to 38% of all NO_x emissions occurred during downhill driving, i.e. road grade values $< -1\%$ [Gallus2017].

Cumulated PN emissions showed a very similar trend to NO_x , as depicted in the lower plot of figure 4.23. The spreading of urban, rural and motorway data was larger than for NO_x which is a characteristic of route R0 and due to a non-equal share of the different parts (compare table 2.3). However, similar to the NO_x results around 50% of all PN emissions appeared for flat segments while downhill driving contributed between 20 (rural) and 40% (urban) to total PN emissions. The 90% percentile of the PN emissions was observed between 3 and 3.5% road grade.

In summary, the segment method showed a good way to enhance and quantify the accuracy of road grade measurements. The reference Google data as well as results obtained via the accelerometer provided precisions far below 0.5%. As an independent altitude data source, GPS is preferred in the upcoming RDE legislation, however, GPS was found to be limited in its altitude accuracy and probably many more repetitions on the same route are necessary to achieve a precision below 0.5%. Based on Google altitude data, more than half of the NO_x and PN emissions were found for flat segments and 90% below 2 to 2.8% (NO_x) or 3 to 3.5% (PN) road grade. Thus, using this method, a road grade limitation could be proposed as a boundary condition for the RDE regulation. Based on the present results, the introduction of a 3% road grade limit would cover around 90% of the NO_x and PN emissions and thus represent a reasonable boundary for an RDE compliant route.

Chapter 5

Summary and Conclusions

In the Euro-6d legislation RDE will be implemented including the regulation of NO_x and PN emissions measured by a PEMS. On-road emissions were found to depend on a variety of parameters, in the present study the impact of driving style, cold start and road grade on on-road exhaust emissions was investigated.

The validation of the PEMS was conducted on a chassis dynamometer in parallel to laboratory equipment including a variety of vehicles and test cycles. The deviation of CO_2 and NO_x results measured by the PEMS were below 15% compared to corresponding test cell data. The PN PEMS showed a limit of detection of $1 \cdot 10^{10} \text{ km}^{-1}$, which is far below the Euro-6 Diesel PN emissions limits of $6 \cdot 10^{11}$. In the test cell a good correlation was determined with a systematic deviation of around 20% in comparison to a PMP compliant reference set-up. Simultaneous soot measurements were conducted using a PM PEMS both in the test cell and during on-road testing with similar PN-to-soot ratios in the range of $1 \cdot 10^{12}$ to $2 \cdot 10^{12} \text{ mg}^{-1}$. Both PEMS devices demonstrated the suitability and reliability for on-road operation.

Diesel and gasoline test vehicles were equipped with a PEMS set-up and numerous on-road tests were conducted. An RDE compliant test route was created and numerous on-road test trips have been conducted including gaseous and PN measurements. Several driving parameters were chosen in order to characterize different driving styles. The acceleration based parameters RPA, MPA and $v \cdot a_{pos}$ showed a good separation of severe from normal trips. The comparison to reference values obtained from the WLTC and from FOT data proved the normal PEMS trips to be representative for normal driving. In urban districts the repeatability of on-road tests was naturally strongly affected by randomly changing traffic situations.

The driving style had a strong impact on CO₂ and NO_x emissions of Diesel vehicles. Severe trips characterized by larger RPA, MPA and $v \cdot a_{pos95}$ values generated elevated CO₂ and NO_x emissions compared to normal trips. Especially NO_x emissions were sensitive to the driving style, a 100% higher RPA value resulted in an almost four-fold elevation of NO_x. Thus, for the RDE regulation, non-normal driving needs to be excluded by appropriate driving parameter limits, such as $v \cdot a_{pos95}$.

On-road PN emission data were within the range of realistic laboratory cycle and literature values. On the motorway, severe driving resulted in a PN increase of up to one order of magnitude while urban driving was hardly affected. On the RDE compliant route a classification of soft, normal and severe driving was expressed by different PN emission levels with a large contribution of the cold start phase.

The on-road cold start effect was investigated in terms of PN and gaseous emissions for a large range of ambient temperatures. The end of the cold start was defined to be reached at an engine temperature of 70°C and the cold start phase was found to endure significantly longer at low ambient temperatures in terms of duration and travelled distance.

The gaseous emissions showed controversial cold start behaviours for the investigated Diesel vehicles. Euro-4 CSEE and cold start emissions decreased linearly with lower ambient temperatures and the results were generally in-line with literature values. For the Euro-5 vehicle no significant cold start NO_x and HC temperature trends could be determined. Only CO CSEE and cold start emissions decreased for lower ambient temperatures. This result was not explained by the literature and remained unexplained. However, CO₂, CO and HC emissions for both vehicles were significantly higher during the cold start phase compared to the post cold start phase. Especially CO and HC emissions showed two to ten times higher cold start values, which emphasizes the important role of the cold start for these pollutants also for on-road driving.

For a Euro-5 DI gasoline vehicle, a large PN cold start peak was found that was more pronounced for low ambient temperatures, ranging from $5 \cdot 10^{12}$ to $1.5 \cdot 10^{13}$ km⁻¹ within a temperature range of 8 to 28°C. The contribution of PN

emissions during cold engine operation was smaller than in previous NEDC studies which could be explained by longer and stronger acceleration events during on-road driving. Generally, the cold start results were in-line with previous studies reported from laboratory tests and indicated the significance of the cold start, especially for low ambient temperatures. Thus, the cold start is included in the upcoming Euro-6d regulation of on-road PN emissions.

Route characteristics of four different routes were investigated applying the parameter CAG. Routes with a similar CAG value showed NO_x emissions in the same range for constant driving dynamics. One route had a more than double as high cumulated altitude gain value because of many uphill and downhill sections. For similar $v \cdot a_{pos95}$ values, the NO_x emissions nearly doubled compared to the other routes with moderate cumulated altitude gain values. A filtering and a subsequent strong smoothing process as implemented in the RDE regulation draft led to much lower CAG values as compared to the direct calculation method. Based on these test results, the current RDE regulation method for calculating the CAG straightly underestimated the real CAG value for each route due to a too strong smoothing process. The regulated limit value of 1200m/100km is strongly coupled to the RDE calculation method. Thus, for the method presented in this study a different CAG limit value would be required.

Based on Google altitude data, road grade was calculated utilizing a segment method with an average precision of 0.13%. CO_2 and NO_x emissions showed a linear correlation with road grade for all urban, rural and motorway parts. The step from 0 to 5% road grade led to a CO_2 increase of 65 to 81% and a NO_x increase of 85 to 115%, depending on the road type. Larger emissions at higher road grades could be explained by more frequent high engine load points. The results showed the strong dependency of exhaust emissions on road gradients for on-road driving. Based on the presented segment method, road grade is able to be implemented as a boundary condition in the RDE regulation. However, the suggested GPS data need to be substituted by a more precise data source, such as external reference data or an accelerometer. Otherwise the necessary accuracy for road grade determination is likely not possible.

List of Figures

1.1	Annual mean NO ₂ concentrations measured by traffic, urban and rural stations in Germany. The bars represent the fraction of traffic related NO ₂ stations which exceeded the limit of 40 μg/cm ⁻³ during each year [UBAweb].	2
1.2	Solid PN emissions from passenger cars and light duty vehicles classified into Diesel, port-fuel injection (PFI) and direct injection gasoline (G-DI). The three line types for PFI and G-DI represent different predicted market shares [Mamakos2011b].	3
1.3	Discrepancy between real-world and type approval NO _x emissions from Diesel passenger cars since the Euro-1 legislation [TNO2013].	4
2.1	Time traces of the emission test cycles NEDC (upper figure) and WLTC (lower figure).	8
2.2	An example PEMS set-up showing the gas PEMS with accessories.	12
2.3	Schematic principle of the PEMS. The exhaust flow depicted by the black arrows passes the analyzers FID, NDUV and NDIR detecting CO/CO ₂ , NO/NO ₂ and HC concentrations, respectively. Additionally GPS, OBD and ambient conditions are recorded. This figure is based on [Merkisz2016].	13
2.4	Schematics of the PN PEMS that collects the exhaust directly at the tailpipe compared to a test cell PMP system [Gallus2016]. . .	16
2.5	Difference of the efficiency curves of the PN PEMS and the PMP system obtained from [JRCreport2014]. Note that in this study the PN PEMS was calibrated with a monodisperse aerosol at 90nm and a polydisperse aerosol.	18
2.6	PN real world instrumentation consisting of a PN PEMS, a PM PEMS, and an EFM controlled by the gas PEMS [Gallus2016]. . .	19
2.7	Calculation of additional power due to extra mass of the measurement equipment.	21

3.1	Repeatability of several NEDC and WLTC runs.	27
3.2	Correlation map of distance specific gaseous emissions on different cycles between PEMS and test cell.	29
3.3	Two examples of a correlation measurement of the PN PEMS with the PMP set-up. At large emissions the PN PEMS shows very good performance (upper figure), however, at low-level PN emissions the PN PEMS comes to its detection limit (lower figure).	31
3.4	Correlation measurement of the PN PEMS with the PMP set-up. At emission levels in the $6 \cdot 10^{12} \text{ km}^{-1}$ range the data show a very good correlation (upper figure), however, at low-level PN emissions ($< 1 \cdot 10^{10} \text{ km}^{-1}$) the PN PEMS reaches its detection limit (lower figure).	32
3.5	The PN difference between PEMS and PMP set-up, assuming a typical unimodal particle size distribution. Due to the different shapes of the efficiency curves, either the PN PEMS (green area) or the PMP set-up (red area) measures higher PN values dependent on the particle size. The difference theoretically makes up less than 10% of all particles.	34
3.6	PN PEMS and PM PEMS sensor concentrations for a laboratory test representing on-road driving of a DI-gasoline Euro-5 vehicle. The PM PEMS graph is shifted upwards for better visualization. Both signal traces are qualitatively in good agreement, the PN-soot-ratio is $1.5 \cdot 10^{12} \text{ mg}^{-1}$	35
4.1	Driving Dynamics of the PEMS trips separated for vehicles V1, V2 (both Diesel) and V4 (gasoline) for different drivers on route R1. WLTC and FOT data are given as reference values.	39
4.2	The 95th percentile of the parameter $v \cdot a_{pos}$ plotted against the mean velocity. Each trip is divided into urban, rural and motorway sections determined by velocity limits of 60 and 90 km/h. There is a distinct separation of severe tests from normal tests.	41

4.3	Comparison of parameters considering driving dynamics for vehicles V0 and V3. Route R0 was evaluated separately for urban and motorway parts. Severe trips include stronger acceleration, later braking and higher maximum speed on the motorway (up to 180 km/h).	43
4.4	Impact of the driving style on gaseous emissions of the PEMS trips for vehicles V0 and V1 on route R0 (urban and motorway part). .	45
4.5	Impact of the driving style on gaseous emissions of the PEMS trips separated for different vehicles and drivers. CO ₂ and NO _x emissions show good driving style correlation [Gallus2017].	46
4.6	Cumulated NO _x plotted against the parameter v·a for vehicles V1 and V2. The three lines in the graph represent soft, normal and severe driving.	48
4.7	PN emissions of several PEMS trips conducted with the gasoline vehicles V3 and V4. The data were classified into driving styles and compared to laboratory cycles and literature values.	49
4.8	Cumulated PN plotted against the parameter v·a for vehicles V3 and V4 and different driving styles.	51
4.9	Particle emissions from PN PEMS and PM PEMS based on ten PEMS trips at ambient temperatures between 15 and 28°C. The slope of the regression line is 1.1·10 ¹² mg ⁻¹ , with a coefficient of determination R ² of 0.93.	52
4.10	Comparison of the PN emissions of one cold start (red trace) and one hot start (green trace) at 21°C ambient temperature conducted with vehicle V3. A PN cold start peak was observed during the first two kilometers [Gallus2016].	55
4.11	The cold start duration and distance plotted against the ambient temperature. The data include normal, soft and severe driving conducted by vehicle V1. The cold start phase was defined to end when the engine temperature reaches 70°C.	56
4.12	Gaseous CSEE values for vehicle V0. CSEE were calculated by subtracting the warm urban from the cold urban trip (route R0). The distance specific emissions were normalized at an ambient temperature of 15°C.	58

4.13	Distance specific PN CSEE values for the gasoline vehicle V3. CSEE were calculated by subtracting the warm urban from the cold urban trip (route R0).	60
4.14	Cold start and post cold start emissions depicted for vehicle V1 on route R1. The distance specific emissions were normalized at an ambient temperature of 15°C.	61
4.15	Distance specific PN emissions for the cold start and post cold start phase. The PN cold fraction was calculated as the ratio of absolute cold start and post cold start PN. The tests were conducted using vehicle V3 on route R1 [Gallus2016].	62
4.16	Forces affecting a moving vehicle on a road gradient.	65
4.17	Road grade results of the barometer, the dGPS and the accelerometer based on test track measurements. The black horizontal lines indicate the sections with stated road grade values.	72
4.18	NO _x emissions plotted against the 95% percentile of the parameter $v \cdot a_{pos}$ for different test routes. The linear regression was calculated for all data points on route R1. Note that route R3 had a much larger CAG value compared to the other routes. For better illustration, NO _x emissions were normalized at a value of 15 m ² /s ³ by dividing the NO _x emissions for each vehicle by the corresponding NO _x value at 15 m ² /s ³ of route R1 [Gallus2017].	76
4.19	Road grade histogram for routes R0 (upper figure) and R1 (lower figure) for the complete route and separated into urban, rural and motorway parts calculated from Google altitude data. The 95% percentile of all positive road grades for route R0 and R1 is at 4.3% and 3.9% road grade, respectively [Gallus2017].	79
4.20	Correlation of normalized CO ₂ (upper figure) and NO _x (lower figure) emissions of Diesel vehicle V1 on route R1 with road grade separated by urban, rural and motorway parts evaluated only for cruising parts. Data binning was performed within 0.5% road grade intervals and depicted using larger markers and range bars, indicating the mean and standard deviation, respectively [Gallus2017].	81

4.21 Correlation of normalized CO ₂ (upper figure) and PN (lower figure) emissions of the gasoline vehicle V3 on route R0 with road grade separated by urban, rural and motorway parts evaluated only for cruising parts. Data binning was performed within 0.5% road grade intervals and depicted using larger markers and range bars, indicating the mean and standard deviation, respectively.	83
4.22 Frequency distribution maps for urban cruising and flat segments between -1 and +1% (upper figure) and larger than 1% road grade (lower figure), based on results from vehicle V1. The dashed line indicates the maximum torque curve [Gallus2017].	85
4.23 Correlation of cumulated NO _x obtained from vehicle V1 on route R1 (upper figure) [Gallus2017] and PN emissions from vehicle V4 on route R0 (lower figure) with road grade separated by urban, rural and motorway parts. The evaluation was performed for cruising only parts and binning was performed within 0.5% road grade. The frequency of every road grade bin is depicted using larger markers.	86

List of Tables

2.1	Specifications of the PN PEMS [Matter2013] compared to the PMP set-up [UNECE2011]	15
2.2	Basic information about the tested vehicles. The fraction of the gross vehicle weight includes a 75kg driver.	20
2.3	Overview of the investigated routes. While routes R0, R1 and R2 show similar characteristics, route R3 was designed with respect to more pronounced road gradients and larger absolute altitudes. . .	22
3.1	NEDC and WLTC driving parameters [Samuel2002; Tutuianu2013].	26
4.1	Calculated CAG values for the investigated routes based on different data sources. While routes R0, R1 and R2 show similar characteristics, route R3 was designed with respect to large CAG values. Accelerometer results were calculated from trips with normal driving style only. Barometer results were just available for route R1.	74

Bibliography

- [Andre2005] André and Joumard, “Modelling of cold start excess emissions for passenger cars”, URL: https://hal-sde.archives-ouvertes.fr/file/index/docid/917071/filename/AndreI_cold_start_LTE0509.pdf.
- [Andrews2004] Andrews et al., “The Effect of Ambient Temperature on Cold Start Urban Traffic Emissions for a Real World SI Car”, Proceedings of SAE 2004 Powertrain, Fluid Systems Conference, and Exhibition, DOI: [10.4271/2004-01-2903](https://doi.org/10.4271/2004-01-2903).
- [AVL2012] AVL List GmbH, “AVL PM PEMS - Product Guide”, URL: <https://www.avl.com/-/avl-m-o-v-e-pm-pems-portable-soot-and-pm-measurement-device-on-board-a-vehicle>.
- [Badshah2016] Badshah, Kittelson, and Northrop, “Particle Emissions from Light-Duty Vehicles during Cold-Cold Start”, *SAE Int. J. Engines* 9, DOI: [10.4271/2016-01-0997](https://doi.org/10.4271/2016-01-0997).
- [Bae2001] Bae, Ryu, and Gerdes, “Road grade and vehicle parameter estimation for longitudinal control using GPS”, Center for Design Research, Stanford University, URL: https://ddl.stanford.edu/sites/default/files/bae_ieee_its2001.pdf.
- [Benmimoun2011] Benmimoun, Kessler, and Zlocki, “euroFOT: Field operational test and impact assessment of advanced driver assistance systems – First results”, *20. Aachener Kolloquium Fahrzeug - und Motorentechnik 2011*, DOI: [10.1007/978-3-642-33805-2_43](https://doi.org/10.1007/978-3-642-33805-2_43), URL: http://www.eurofot-ip.eu/en/library/presentations/eurofot_fot_and_impact_assessment_of_adas_%96_first_results.htm.
- [Berry2007] Berry, “The Effects of Driving Style and Vehicle Performance on the Real-World Fuel Consumption of U.S. Light-Duty Vehicles”, Vir-

ginia Polytechnic Institute and State University, URL: web.mit.edu/sloan-auto-lab/research/beforeh2/files/IreneBerry_Thesis_February2010.pdf.

[Bielaczyc1997] Bielaczyc and Merkisz, “Exhaust Emission from Passenger Cars During Engine Cold Start and Warm-Up”, *SAE International*, DOI: [10.4271/970740](https://doi.org/10.4271/970740).

[Bielaczyc2011] Bielaczyc, Szczotka, and Woodburn, “The effect of a low ambient temperature on the cold-start emissions and fuel consumption of passenger cars”, *Proceedings of the Institution of Mechanical Engineers, Part D: Journal of Automobile Engineering* 225, pp. 1253–1264, DOI: [10.1177/0954407011406613](https://doi.org/10.1177/0954407011406613), URL: <http://pid.sagepub.com/content/225/9/1253.abstract>.

[Boriboonsomsin2009] Boriboonsomsin and Barth, “Impacts of road grade on fuel consumption and carbon dioxide emissions evidenced by use of advanced navigation systems”, *Transportation Research Record: Journal of the Transportation Research Board* 2139, pp. 21–30, DOI: [10.3141/2139-03](https://doi.org/10.3141/2139-03), URL: <http://trrjournalonline.trb.org/doi/abs/10.3141/2139-03>.

[Braisher2010] Braisher, Stone, and Price, “Particle Number Emissions from a Range of European Vehicles”, *SAE Technical Paper* 01, p. 0786, DOI: [10.4271/2010-01-0786](https://doi.org/10.4271/2010-01-0786).

[Carslaw2005] Carslaw, “Evidence of an increasing NO₂/NO_X emissions ratio from road traffic emissions”, *Atmospheric Environment* 39, pp. 4793–4802, DOI: [10.1016/j.atmosenv.2005.06.023](https://doi.org/10.1016/j.atmosenv.2005.06.023).

[Dardiotis2013] Dardiotis et al., “Low-temperature cold-start gaseous emissions of late technology passenger cars”, *Applied Energy* 111, pp. 468–478, DOI: [10.1016/j.apenergy.2013.04.093](https://doi.org/10.1016/j.apenergy.2013.04.093).

[Demuynck2012] Demuynck et al., “Recommendations for the new WLTP cycle based on an analysis of vehicle emission measurements on NEDC and

- CADC”, *Energy Policy* 49, pp. 234–242, DOI: [10.1016/j.enpol.2012.05.081](https://doi.org/10.1016/j.enpol.2012.05.081).
- [DeVlieger2000] De Vlieger, Keukeleere, and Kretzschmar, “Environmental effects of driving behaviour and congestion related to passenger cars”, *Atmospheric Environment* 34, pp. 4649–4655, DOI: [10.1016/S1352-2310\(00\)00217-X](https://doi.org/10.1016/S1352-2310(00)00217-X).
- [Dimaratos2016] Dimaratos et al., “Comparative Evaluation of the Effect of Various Technologies on Light-duty Vehicle {CO₂} Emissions over {NEDC} and {WLTP}”, *Transportation Research Procedia* 14, pp. 3169–3178, DOI: [10.1016/j.trpro.2016.05.257](https://doi.org/10.1016/j.trpro.2016.05.257).
- [EEA2015AQ] European Environment Agency, “Air quality in Europe — 2015 report”, DOI: [10.2800/62459](https://doi.org/10.2800/62459), URL: <http://www.eea.europa.eu/publications/air-quality-in-europe-2015>.
- [EEA2015pollutants] European Environment Agency, “Emissions of the main air pollutants in Europe”, URL: <http://www.eea.europa.eu/data-and-maps/indicators/main-anthropogenic-air-pollutant-emissions/assessment-3>.
- [EEAreport2016] European Environment Agency, “European Union emission inventory report 1990–2014 under the UNECE Convention on Long-range Transboundary Air Pollution (LRTAP)”, DOI: [10.2800/628267](https://doi.org/10.2800/628267), URL: <http://www.eea.europa.eu/publications/lrtap-emission-inventory-report-2016#tab-data-references>.
- [ElevationAPI] URL: <https://developers.google.com/maps/documentation/elevation/intro>, Google.
- [EMEP2009] European Environment Agency, “EMEP/EEA air pollutant emission inventory guidebook - 2009”, URL: <http://www.eea.europa.eu/publications/emep-eea-emission-inventory-guidebook-2009/>.
- [EU2012] European Commission, “Commission Regulation (EU) No 459/2012 of 29 May 2012 amending Regulation (EC) No 715/2007 of the European

Parliament and of the Council and Commission Regulation (EC) No 692/2008 as regards emissions from light passenger and commercial vehicles (Euro 6)”, URL: <http://www.eur-lex.europa.eu/legal-content/EN/TXT/PDF/>.

[Favez2009] Favez, Weilenmann, and Stilli, “Cold start extra emissions as a function of engine stop time: Evolution over the last 10 years”, *Atmospheric Environment* 43, pp. 996–1007, DOI: [10.1016/j.atmosenv.2008.03.037](https://doi.org/10.1016/j.atmosenv.2008.03.037).

[Fierz2008] Fierz et al., “Field Measurement of Particle Size and Number Concentration with the Diffusion Size Classifier (Disc)”, *SAE Technical Paper* 01, DOI: [10.4271/2008-01-1179](https://doi.org/10.4271/2008-01-1179).

[Fierz2011] Fierz et al., “Design, Calibration, and Field Performance of a Miniature Diffusion Size Classifier”, *Aerosol Science and Technology* 45, pp. 1–10, DOI: [10.1080/02786826.2010.516283](https://doi.org/10.1080/02786826.2010.516283).

[Fonseca2010] Fonseca Gonzalez, Kindelán, and Zapata, “Influence of driving style on fuel consumption and Emissions in diesel-powered passenger car”, Proceedings 18th International Symposium Transport and Air Pollution, URL: <https://www.mysciencework.com/publication/show/cd3e89c800187a7ef6a0b886c37be7df>.

[Frey2007] Frey and Zhang, “Implications of measured in-use light duty gasoline vehicle emissions for emission inventory development at high spatial and temporal resolution”, URL: http://www.epa.gov/ttnchie1/conference/ei16/session4/h.c.frey_pres.pdf.

[Gallus2016] Gallus et al., “On-road particle number measurements using a portable emission measurement system (PEMS)”, *Atmospheric Environment* 124, Part A, pp. 37–45, DOI: [10.1016/j.atmosenv.2015.11.012](https://doi.org/10.1016/j.atmosenv.2015.11.012), URL: <http://www.sciencedirect.com/science/article/pii/S1352231015305203>.

[Gallus2017] Gallus et al., “Impact of Driving Style and Road Grade on Gaseous Exhaust Emissions of Passenger Vehicles Measured by a Portable

- Emission Measurement System (PEMS)”, *Transportation Research Part D*, DOI: [10.1016/j.trd.2017.03.011](https://doi.org/10.1016/j.trd.2017.03.011).
- [Giechaskiel2012] Giechaskiel et al., “Sampling of Non-Volatile Vehicle Exhaust Particles: A Simplified Guide”, *SAE International Journal of Engines* 5, pp. 379–399, DOI: [10.4271/2012-01-0443](https://doi.org/10.4271/2012-01-0443).
- [Giechaskiel2014] Giechaskiel et al., “Review of motor vehicle particulate emissions sampling and measurement: From smoke and filter mass to particle number”, *Journal of Aerosol Science* 67, pp. 48–86, DOI: [10.1016/j.jaerosci.2013.09.003](https://doi.org/10.1016/j.jaerosci.2013.09.003).
- [Gustafsson2000] Gustafsson, “Adaptive filtering and change detection” 1, DOI: [10.1002/0470841613](https://doi.org/10.1002/0470841613).
- [HBEFA2.1] Keller and Haan, “Handbuch Emissionsfaktoren des Strassenverkehrs 2.1”, URL: <http://www.hbefa.net/e/documents/reports.html>.
- [Heeb2003] Heeb et al., “Methane, benzene and alkyl benzene cold start emission data of gasoline-driven passenger cars representing the vehicle technology of the last two decades”, *Atmospheric Environment* 37, pp. 5185–5195, DOI: [10.1016/j.atmosenv.2003.04.001](https://doi.org/10.1016/j.atmosenv.2003.04.001).
- [Huang2013] Huang et al., “A PEMS study of the emissions of gaseous pollutants and ultrafine particles from gasoline- and diesel-fueled vehicles”, *Atmospheric Environment* 77, pp. 703–710, DOI: [10.1016/j.atmosenv.2013.05.059](https://doi.org/10.1016/j.atmosenv.2013.05.059).
- [ICCT2014] Franco et al., “Real-World Exhaust Emissions from modern Diesel Cars - A meta-analysis of PEMS Emissions Data from EU (Euro-6) and US (Tier 2 bin 5 ULEV II) Diesel Passenger Cars”, URL: <http://www.theicct.org/real-world-exhaust-emissions-modern-diesel-cars>.
- [JRCreport2014] Giechaskiel, Riccobono, and Bonnel, “Feasibility study on the extension of the Real Driving Emissions (RDE) procedure to Particle Number (PN) - Experimental evaluation of portable emission mea-

- surement systems (PEMS) with diffusion chargers (DCs) to measure particle number (PN) concentration”, DOI: [10.2790/326943](https://doi.org/10.2790/326943).
- [Kasper2008] Kasper, “Characterisation of the Second Generation PMP “Golden Instrument””, *SAE Technical Paper* 01, p. 1177, DOI: [10.4271/2008-01-1177](https://doi.org/10.4271/2008-01-1177).
- [Khalek2010] Khalek, Bougher, and Jetter, “Particle emissions from a 2009 gasoline direct injection engine using different commercially available fuels”, *SAE International Journal of Fuels and Lubricants* 3, pp. 623–637, DOI: [10.4271/2010-01-2117](https://doi.org/10.4271/2010-01-2117).
- [Kirchner2010] Kirchner, Vogt, and Maricq, “Investigation of EURO-5/6 level particle number emissions of European diesel light duty vehicles”, *SAE Technical Paper* 01, p. 0789, DOI: [10.4271/2010-01-0789](https://doi.org/10.4271/2010-01-0789).
- [Li2013] Li, Chen, and Yan, “Comparison of fine particles emissions of light-duty gasoline vehicles from chassis dynamometer tests and on-road measurements”, *Atmospheric Environment* 68, pp. 82–91, DOI: [10.1016/j.atmosenv.2012.11.031](https://doi.org/10.1016/j.atmosenv.2012.11.031).
- [Mamakos2011b] Mamakos, “Feasibility of Introducing Particulate Filters on gasoline direct injection vehicles”, URL: <http://publications.jrc.ec.europa.eu/repository/handle/JRC68675>.
- [Mangan2002] Mangan, Wang, and Wu, “Measurement of the road gradient using an inclinometer mounted on a moving vehicle”, *IEEE International Symposium on Computer Aided Control System Design*, DOI: [10.1109/CACSD.2002.1036933](https://doi.org/10.1109/CACSD.2002.1036933).
- [Maricq1999c] Maricq et al., “Particulate Emissions from a Direct-Injection Spark-Ignition (DISI) Engine”, *SAE Technical Paper* 1999-01-1530, p. 11, DOI: [10.4271/1999-01-1530](https://doi.org/10.4271/1999-01-1530).
- [Maricq2011] Maricq et al., “Motor vehicle PM emissions measurement at LEV III levels”, *SAE International Journal of Engines* 4, pp. 597–609, DOI: [10.4271/2011-01-0623](https://doi.org/10.4271/2011-01-0623).

- [Matter2013] Matter Aerosol AG, “NANOMET 3-PS User Manual”.
- [Meccariello2014] Meccariello and Della Ragione, “Slope Effect in Emission Evaluation to Assess Real Pollutant Factors”, *International Journal of Chemical, Molecular, Nuclear, Materials and Metallurgical Engineering* 8(10), URL: <https://waset.org/Publication/slope-effect-in-emission-evaluation-to-assess-real-pollutant-factors/9999997>.
- [Merkisz2016] Merkisz et al., “Rapeseed Oil Methyl Esters (RME) as Fuel for Urban Transport”, DOI: [10.5772/62218](https://doi.org/10.5772/62218), URL: <http://www.intechopen.com/books/alternative-fuels-technical-and-environmental-conditions/rapeseed-oil-methyl-esters-rme-as-fuel-for-urban-transport>.
- [ODriscoll2016] O’Driscoll et al., “A Portable Emissions Measurement System (PEMS) study of NOx and primary NO2 emissions from Euro 6 diesel passenger cars and comparison with COPERT emission factors”, *Atmospheric Environment* 145, pp. 81–91, DOI: [10.1016/j.atmosenv.2016.09.021](https://doi.org/10.1016/j.atmosenv.2016.09.021), URL: <http://www.sciencedirect.com/science/article/pii/S135223101630721X>.
- [Prati2015] Prati et al., “Real Driving Emissions of a Light-Duty Vehicle in Naples. Influence of Road Grade”, *SAE Technical Paper* 2015-24-2509, DOI: [10.4271/2015-24-2509](https://doi.org/10.4271/2015-24-2509).
- [Price2007] Price et al., “Cold start particulate emissions from a second generation DI gasoline engine”, DOI: [10.4271/2007-01-1931](https://doi.org/10.4271/2007-01-1931).
- [RDE2015] European Commission, “RDE 2nd package (2015) regulation draft amending Regulation (EC) No 692/2008 as regards emissions from light passenger and commercial vehicles (Euro 6)”, URL: http://eur-lex.europa.eu/legal-content/EN/TXT/?uri=uriserv:OJ.L_.2016.109.01.0001.01.ENG.
- [RDE2016] European Commission, “Real-Driving Emissions in the EURO 6 regulation on emissions from light passenger and commercial vehicles

- (RDE3)”, URL: https://ec.europa.eu/info/law/better-regulation/initiatives/ares-2016-6339064_en.
- [Reiter2016] Reiter and Kockelman, “The problem of cold starts: A closer look at mobile source emissions levels”, *Transportation Research Part D: Transport and Environment* 43, pp. 123–132, DOI: [10.1016/j.trd.2015.12.012](https://doi.org/10.1016/j.trd.2015.12.012).
- [Robinson2010] Robinson, Sentoff, and Holmén, “Particle Number and Size Distribution of Emissions During Light-Duty Vehicle Cold Start”, *Transportation Research Record: Journal of the Transportation Research Board* 2158, pp. 86–94, DOI: [10.3141/2158-11](https://doi.org/10.3141/2158-11).
- [Rogers1984] Rogers and Trayford, “Grade measurement with an instrumented car”, *Transportation Research Part B: Methodological* 18, pp. 247–254, DOI: [10.1016/0191-2615\(84\)90035-3](https://doi.org/10.1016/0191-2615(84)90035-3).
- [Sahlholm2010] Sahlholm and Johansson, “Road grade estimation for look-ahead vehicle control using multiple measurement runs”, *Control Engineering Practice* 18, pp. 1328–1341, DOI: [10.1016/j.conengprac.2009.09.007](https://doi.org/10.1016/j.conengprac.2009.09.007).
- [Samuel2002] Samuel, Austin, and Morrey, “Automotive test drive cycles for emission measurement and real-world emission levels—a review”, *Proceedings of the Institution of Mechanical Engineers, Part D: Journal of Automobile Engineering* 216, pp. 555–564, DOI: [10.1243/095440702760178587](https://doi.org/10.1243/095440702760178587), URL: <http://pid.sagepub.com/content/216/7/555.abstract>.
- [Sehlstedt2007] Sehlstedt et al., “The Role of Particle Size and Chemical Composition for Health Risks of Exposure to Traffic-Related Aerosols—A Review of the Current Literature”, *Umeå University och Stockholm University*, URL: https://www.researchgate.net/publication/242083990_The_Role_of_Particle_Size_and_Chemical_Composition_for_Health_Risks_of_Exposure_to_Traffic_Related_Aerosols_-_A_Review_of_the_Current_Literature.

- [Sensors2006] Shahinian, “On-Vehicle Diesel Emission Analyzer Semtech-DS - User Manual Revision 1.09”.
- [TNO2013] Ligterink et al., “Investigations and real world emission performance of Euro 6 light-duty vehicles”, *TNO Report*, R11891, URL: https://www.tno.nl/media/1969/investigations_emission_factors_euro_6_ld_vehicles_tno_2013.pdf.
- [TNO2016a] Kadijk et al., “NOx Emissions of Euro 5 and Euro 6 diesel passenger cars - test results in the lab and on the road”, *TNO Report*, R11891, DOI: [10.13140/RG.2.2.30386.61126](https://doi.org/10.13140/RG.2.2.30386.61126).
- [TNO2016b] Heijne et al., “NOx emissions of fifteen Euro 6 diesel cars: Results of the Dutch LD road vehicle emission testing programme 2016”, *TNO Report*, R11891, URL: <https://www.rijksoverheid.nl/documenten/rapporten/2016/10/14/tno-2016-r11177-nox-emissions-of-fifteen-euro-6-diesel-cars-results-of-the-dutch-ld-road-vehicle-emission-testing-programme-2016>.
- [Tsirakis2007] Tsirakis, Zannikos, and Stournas, “Impact of driving style on fuel consumption and exhaust emissions: defensive and aggressive driving style”, Proceedings of the 10 th International Conference on Environmental Science and Technology, URL: https://www.researchgate.net/publication/258149928_Impact_of_driving_style_on_fuel_consumption_and_exhaust_emissions_defensive_and_aggressive_driving_style.
- [Tsokolis2016] Tsokolis et al., “Fuel consumption and CO2 emissions of passenger cars over the New Worldwide Harmonized Test Protocol”, *Applied Energy* 179, pp. 1152–1165, DOI: [10.1016/j.apenergy.2016.07.091](https://doi.org/10.1016/j.apenergy.2016.07.091).
- [Tutuianu2013] Tutuianu et al., “Development of a World-wide Worldwide harmonized Light duty driving Test Cycle (WLTC)”, URL: <http://www.unece.org/fileadmin/DAM/trans/doc/2014/wp29grpe/GRPE-68-03e.pdf>.

- [Tutuianu2015] Tutuianu et al., “Development of the World-wide harmonized Light duty Test Cycle (WLTC) and a possible pathway for its introduction in the European legislation”, *Transportation Research Part D* 40, pp. 61–75, DOI: [10.1016/j.trd.2015.07.011](https://doi.org/10.1016/j.trd.2015.07.011).
- [UBAweb] URL: <http://www.umweltbundesamt.de/daten/luftbelastung/>, Umweltbundesamt.
- [UNECE2011] European Commission, “Regulation No 83 of the Economic Commission for Europe of the United Nations (UN/ECE) - Uniform provisions concerning the approval of vehicles with regard to the emission of pollutants according to engine fuel requirements”, *Official Journal of the European Union*, URL: [http://eur-lex.europa.eu/legal-content/EN/TXT/?uri=CELEX:42012X0215\(01\)](http://eur-lex.europa.eu/legal-content/EN/TXT/?uri=CELEX:42012X0215(01)).
- [VanMierlo2004] Van Mierlo et al., “Driving style and traffic measures-influence on vehicle emissions and fuel consumption”, Institution of Mechanical Engineers, Part D: Journal of Automobile Engineering, DOI: [10.1243/095440704322829155](https://doi.org/10.1243/095440704322829155), URL: <http://pid.sagepub.com/content/218/1/43.abstract>.
- [Viana2014] Viana, “Urban Air Quality in Europe” 26, DOI: [10.1007/978-3-642-38451-6](https://doi.org/10.1007/978-3-642-38451-6).
- [Weilenmann2005] Weilenmann et al., “Regulated and nonregulated diesel and gasoline cold start emissions at different temperatures”, *Atmospheric Environment* 39, pp. 2433–2441, DOI: [10.1016/j.atmosenv.2004.03.081](https://doi.org/10.1016/j.atmosenv.2004.03.081).
- [Weilenmann2009] Weilenmann, Favez, and Alvarez, “Cold-start emissions of modern passenger cars at different low ambient temperatures and their evolution over vehicle legislation categories”, *Atmospheric Environment* 43, pp. 2419–2429, DOI: [10.1016/j.atmosenv.2009.02.005](https://doi.org/10.1016/j.atmosenv.2009.02.005).
- [Weilenmann2013] Weilenmann, Soltic, and Hausberger, “The cold start emissions of light-duty-vehicle fleets: A simplified physics-based model for the es-

- timation of {CO₂} and pollutants”, *Science of The Total Environment* 444, pp. 161–176, DOI: [10.1016/j.scitotenv.2012.11.024](https://doi.org/10.1016/j.scitotenv.2012.11.024).
- [WHO2013] World Health Organization, “Review of evidence on health aspects of air pollution – REVIHAAP project: final technical report”, URL: <http://www.euro.who.int/en/health-topics/environment-and-health/air-quality/publications/2013/review-of-evidence-on-health-aspects-of-air-pollution-revihaap-project-final-technical-report>.
- [WHO2013PM] World Health Organization, “Health effects of particulate matter”, URL: http://www.euro.who.int/__data/assets/pdf_file/0006/189051/Health-effects-of-particulate-matter-final-Eng.pdf.
- [Wing2005] Wing, Eklund, and Kellogg, “Consumer-Grade Global Positioning System (GPS) Accuracy and Reliability”, *Journal of Forestry* 103, pp. 169–173, URL: <http://www.ingentaconnect.com/content/saf/jof/2005/00000103/00000004/art00004>.
- [Wyatt2014] Wyatt, Li, and Tate, “The impact of road grade on carbon dioxide (CO₂) emission of a passenger vehicle in real-world driving”, *Transportation Research Part D: Transport and Environment* 32, pp. 160–170, DOI: [10.1016/j.trd.2014.07.015](https://doi.org/10.1016/j.trd.2014.07.015).
- [Yazdani2012] Boroujeni, “Road Grade Quantification UsinMeasurementsBoard Vehicle Emission Measurements”, North Carolina State University, DOI: [10.1016/j.atmosenv.2013.12.025](https://doi.org/10.1016/j.atmosenv.2013.12.025).
- [Yazdani2013] Boroujeni, Frey, and Sandhu, “Road Grade Measurement Using In-Vehicle, Stand-Alone GPS with Barometric Altimeter”, *Journal of Transportation Engineering* 139, pp. 605–611, DOI: [10.1061/\(ASCE\)TE.1943-5436.0000545](https://doi.org/10.1061/(ASCE)TE.1943-5436.0000545).
- [Yazdani2014] Boroujeni and Frey, “Road grade quantification based on global positioning system data obtained from real-world vehicle fuel use and

emissions measurements”, *Atmospheric Environment* 85, pp. 179–186, DOI: [10.1016/j.atmosenv.2013.12.025](https://doi.org/10.1016/j.atmosenv.2013.12.025).

[Zhang2006] Zhang and Frey, “Road Grade Estimation for On-Road Vehicle Emissions Modeling Using Light Detection and Ranging Data”, *Journal of the Air & Waste Management Association* 56, pp. 777–788, DOI: [10.1080/10473289.2006.10464500](https://doi.org/10.1080/10473289.2006.10464500).

[Zhang2010] Zhang et al., “Particulate Mass and Number Emissions from Light-duty Low Emission Gasoline Vehicles”, *SAE International* 2011, pp. 07–29, DOI: [10.4271/2010-01-0795](https://doi.org/10.4271/2010-01-0795).

Erklärung

Hiermit versichere ich, dass ich die vorliegende Arbeit selbstständig verfasst und keine anderen als die angegebenen Quellen und Hilfsmittel benutzt habe, dass alle Stellen der Arbeit, die wörtlich oder sinngemäß aus anderen Quellen übernommen wurden, als solche kenntlich gemacht sind und dass die Arbeit in gleicher oder ähnlicher Form noch keiner Prüfungsbehörde vorgelegt wurde.

Wuppertal, 18.03.2017